Chaos in systems with many degrees of freedom

Chaos in systems with many degrees of freedom

Chaos in systemen met veel vrijheidsgraden

(met een samenvatting in het Nederlands)

Proefschrift

ter verkrijging van de graad van Doctor aan de Universiteit Utrecht op gezag van de Rector Magnificus, Prof. Dr. W. H. Gispen, ingevolge het besluit van het College voor Promoties in het openbaar te verdedigen op maandag 22 november 2004 des middags te 12.45 uur

door

Astrid Silvia de Wijn

geboren op 28 september 1979 te De Bilt

Promotor: Prof. Dr. Henk van Beijeren

Instituut voor Theoretische Fysica
Faculteit Natuur- en Sterrenkunde
Universiteit Utrecht

Dit werk maakt deel uit van het onderzoeksprogramma van de Stichting voor Fundamenteel Onderzoek der Materie (FOM), die financieel wordt gesteund door de Nederlandse Organisatie voor Wetenschappelijk Onderzoek (NWO).

ISBN 90-393-3868-X

Contents

1 General introduction **1**
- 1.1 Non-equilibrium statistical mechanics . . . 1
- 1.2 Dynamical systems, chaos, and Lyapunov exponents . . . 2
- 1.3 Many-particle systems and other systems with many degrees of freedom . . . 6

2 Hard spheres in phase space and tangent space **9**
- 2.1 Introduction . . . 9
- 2.2 Dynamics in phase space . . . 10
- 2.3 Tangent space . . . 11
- 2.4 Boltzmann and Enskog equations . . . 13

3 Goldstone modes in Lyapunov spectra of hard disks **19**
- 3.1 Introduction . . . 19
- 3.2 Simulations . . . 20
- 3.3 Symmetries and Goldstone modes . . . 22
- 3.4 Boltzmann and Enskog equations . . . 25
- 3.5 Solutions . . . 28
- 3.6 Results and discussion . . . 31
- 3.7 Ring collisions . . . 35
- 3.8 Conclusions . . . 39

4 The Kolmogorov-Sinai entropy of dilute hard spheres **41**
- 4.1 Introduction . . . 41
- 4.2 Kolmogorov-Sinai entropy . . . 42
- 4.3 Distribution functions . . . 45
- 4.4 Results and discussion . . . 54
- 4.5 Conclusions . . . 56

5 The dilute d-dimensional Lorentz gas **57**
- 5.1 Introduction . . . 57

5.2 Dynamics of the Lorentz gas 58
5.3 The largest Lyapunov exponent at low densities 60
5.4 Partial stretching factors 61
5.5 The spectrum 64
5.6 Discussion 67
5.7 Conclusions 69

6 Hard disks versus isotropically distributed cylinders 71
6.1 Introduction 71
6.2 Scatterer configurations 72
6.3 Simulations of the spectrum of isotropically distributed cylinders . 73
6.4 Isotropic-cylinder approximations for the hard-disk system 76
6.5 Conclusions 82

A Polynomial expansion of the generalised Enskog equation 85
A.1 Expansion in Hermite polynomials of the tangent-space collision operators 85
A.2 Solutions to the generalised Boltzmann equation 87

Bibliography 88

Samenvatting 93

Dankwoord 99

Curriculum Vitae 101

Chapter 1

General introduction

1.1 Non-equilibrium statistical mechanics

Statistical mechanics is the branch of theoretical physics in which the macroscopic behaviour of systems consisting of many particles is derived from microscopic properties. At the end of the nineteenth century, Maxwell, Boltzmann, Gibbs, and others already laid the foundations of the statistical mechanics of systems in equilibrium. A fundamental concept introduced is the Boltzmann factor, which assigns a probability to any equilibrium state. Nowadays, many methods exist to carry out practical calculations for a great variety of equilibrium many-particle systems. The statistical mechanics of non-equilibrium systems, on the other hand, is far less developed.

The second law of thermodynamics states that entropy, a measure for the disorder of the system, increases. In a system out of equilibrium, entropy is produced irreversibly as the system relaxes toward equilibrium. Quantities such as the particle number, energy, or momentum are transported through diffusion or other irreversible means. The classical dynamics of a system of many particles, on the other hand, is deterministic and reversible. One may conclude that time-reversible dynamics, under most initial conditions, lead to irreversible macroscopic behaviour.

A substantial development to the understanding of this apparent paradox was made at the end of the nineteenth century, when Ludwig Boltzmann derived the

equation now known as the Boltzmann equation, which can be seen as describing the behaviour of a system with typical initial conditions after course graining. Despite the reversible underlying dynamics, the Boltzmann equation predicts irreversible macroscopic behaviour. In the derivation of his equation, Boltzmann made use of a statistical assumption about the underlying dynamical system, the Stoßzahlansatz, which requires a certain amount of randomness.

A deeper mathematical understanding of the dynamical properties such as chaoticity, ergodicity, and mixing, which are connected to macroscopic irreversibility is provided by dynamical-systems theory. The precise nature of the connections between dynamical systems and irreversible behaviour of non-equilibrium systems is a source of much heated discussion. Systems exist which are chaotic, but not mixing or ergodic. But systems can also be constructed which are mixing, but not chaotic. An example of such a system is the wind-tree model [1]. None of these systems, however, are particularly physical. Gallavotti and Cohen [2, 3] put forward a chaotic hypothesis, conjecturing that many-particle systems as studied by statistical mechanics behave, in general, strongly chaotic. An introduction to chaos and non-equilibrium statistical mechanics can be found in Dorfman's book on the subject [4].

Often, for understanding the effects of non-equilibrium conditions, relatively simple systems are studied with few degrees of freedom. Many-particle systems in equilibrium, however, have chaotic properties that are different from those of systems with fewer degrees of freedom. For understanding the chaotic properties of many-particle systems under non-equilibrium conditions, first those of the equilibrium systems must be comprehended fully. In this thesis, therefore, several classical dynamical systems with many degrees of freedom are considered in equilibrium.

1.2 Dynamical systems, chaos, and Lyapunov exponents

A central role in the study of chaotic properties is played by the Lyapunov exponents, which describe the exponential separation or convergence of nearby trajectories in phase space. They quantify the rates at which infinitesimal perturbations in initial conditions grow or decrease, and are a measure of the sensitivity of the system to changes in the initial conditions. For a more elaborate introduction into dynamical systems and chaos, see reference [5].

1.2.1 Lyapunov exponents

Consider a dynamical system with an $\mathcal{N}$-dimensional phase space Γ. The time evolution of the system may be discrete, or continuous. At time $t = 0$ the system is assumed to be at an initial point γ_0 in this phase space, evolving with time

according to $\gamma(\gamma_0, t)$. If the system is perturbed by an infinitesimal shift $\delta\gamma_0$ in initial conditions, it evolves along an infinitesimally different path $\gamma + \delta\gamma$, where $\delta\gamma$ is in the tangent space $\delta\Gamma$. The evolution in tangent space is described by

$$\gamma(\gamma_0 + \delta\gamma_0, 0) = \gamma_0 + \delta\gamma_0 \ , \tag{1.1}$$
$$\gamma(\gamma_0 + \delta\gamma_0, t) = \gamma(\gamma_0, t) + \delta\gamma(\gamma_0, \delta\gamma_0, t) \ , \tag{1.2}$$
$$\delta\gamma(\gamma_0, t) = \mathsf{M}_{\gamma_0}(t) \cdot \delta\gamma_0 \ , \tag{1.3}$$

where $\mathsf{M}_{\gamma_0}(t)$ is an $\mathcal{N}$-dimensional matrix, defined by

$$\mathsf{M}_{\gamma_0}(t) = \frac{d\gamma(\gamma_0, t)}{d\gamma_0} \ . \tag{1.4}$$

The Lyapunov exponents are the average rates of growth or shrinkage of such infinitesimal changes that are eigenvectors of M_{γ_0},

$$\lambda_i = \lim_{t\to\infty} \frac{\log \mu_i(t)}{t} \ , \tag{1.5}$$

where $\mu_i(t)$ is the i-th eigenvalue of $\mathsf{M}_{\gamma_0}(t)$. There are as many Lyapunov exponents as there are dimensions of the phase space. In systems which are ergodic, almost every trajectory comes infinitesimally close to any point in phase space. This means that the Lyapunov exponents are (almost) independent of the initial conditions. Often the Lyapunov exponents are defined by using not $\mathsf{M}_{\gamma_0}(t)$, but rather $[\mathsf{M}_{\gamma_0}(t) \cdot \mathsf{M}_{\gamma_0}(t)^\dagger]^{1/2}$. In the latter definition the exponents are real and equal to the real components of the exponents in the former definition. The imaginary components of the Lyapunov exponents, as they are defined here, are also referred to as winding numbers. The subset of phase space onto which the system ultimately converges for almost all initial conditions is called the attractor. If (the real component of) the largest Lyapunov exponent is positive, the system is considered chaotic.

For Hamiltonian systems, such as hard spheres with only hard-core interaction, the dynamics are completely invariant under time reversal. For such systems, the attractors are invariant under time reversal. The spectrum of Lyapunov exponents therefore remains the same as well. Each tangent-space eigenvector which grows exponentially in forward time decreases exponentially under time reversal. Under time reversal it is mapped onto an eigenvector with opposite exponent. For every Lyapunov exponent there is a corresponding Lyapunov exponent with opposite sign. This is known as the conjugate pairing rule. In systems which are reversible, but for which the attractor is not invariant under time reversal, the conditions for and the form of the conjugate pairing rule are somewhat different [6].

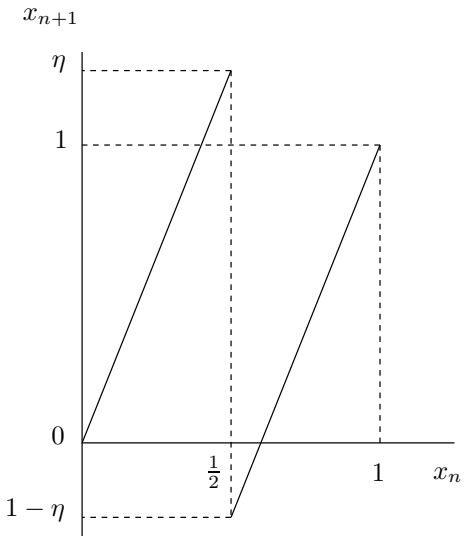

Figure 1.1: A saw-tooth map of the unit interval, as expressed in equation (1.6), displayed for $\eta > 1$. At every iteration some of the points escape from the system, in this parameter range.

An example: a saw-tooth map

Consider as an example of a dynamical system, the following map of the unit interval,

$$x_{i+1} = f(x_i) = \begin{cases} 2\eta x_i & \text{if } \ 0 \le x_i < \frac{1}{2} \ , \\ 2\eta(x_i - 1) + 1 & \text{if } \ \frac{1}{2} \le x_i < 1 \ , \end{cases} \tag{1.6}$$

with positive η. This saw-tooth map is displayed in figure 1.1 for $\eta > 1$. From an initial x_0, a sequence of $x_i = f^i(x_0)$ follows, which defines the time evolution of the system.

As a function of η, three regimes may be distinguished. If η is between 0 and $\frac{1}{2}$, the unit interval is mapped onto a subset of the unit interval, which is mapped onto an even smaller subset in the next iteration, and so on. The attractor consists of the points 0 and 1. If η is between $\frac{1}{2}$ and 1, the unit interval is mapped exactly onto the unit interval. In this case, the attractor is a subset of the unit interval. If η is larger than 1, part of the unit interval is mapped outside the unit interval, and almost all points escape from the system.

The system has a one-dimensional phase space, and therefore the matrix M

reduces to a scalar. It can be calculated from the map,

$$\delta x_{i+1} = f(x_i + \delta x_i) - f(x_i) \ . \tag{1.7}$$

If δx_i is infinitesimal, the discontinuity at $x_i = \frac{1}{2}$ is, with probability 1, not between x_i and $x_i + \delta x_i$, and the tangent-space transformation for any x_i is found to be

$$\delta x_{i+1} = 2\eta \delta x_i \ , \tag{1.8}$$

for any x_i. The system has one Lyapunov exponent which can be calculated from equation (1.8),

$$\lambda = \lim_{i\to\infty} \frac{1}{i} \log \frac{\delta x_i}{\delta x_0} = \lim_{i\to\infty} \frac{1}{i} \log[(2\eta)^i] = \log(2\eta) \ . \tag{1.9}$$

For $\eta > \frac{1}{2}$, the Lyapunov exponent is positive and the system is chaotic.

1.2.2 Kolmogorov-Sinai entropy

If the measurements on a system have only a finite resolution, the Lyapunov exponents quantify how quickly the error in the measurements makes it impossible to make accurate predictions of the future phase-space path. They also indicate how fast extra information can be gained about the original state of the system. If the system is chaotic, two points in phase space which could, originally, not be distinguished separate exponentially. Eventually, the separation becomes larger than the resolution of the measurements and new information can be extracted about the initial conditions. The maximal rate at which information on the system is gained is called the Kolmogorov-Sinai entropy. In closed systems, such as the systems described in this thesis, the Kolmogorov-Sinai entropy equals the sum of all positive Lyapunov exponents.

In systems with escape, such as the saw-tooth map for $\eta > 2$, the points which have escaped from the system can no longer provide information about their initial conditions, and so the Kolmogorov-Sinai entropy in such systems is smaller. The escape rate formalism of Gaspard and Nicolis [7] formalises this. In this formalism, the rate of escape of particles from an open system is expressed in terms of the sum of the positive Lyapunov exponents and the Kolmogorov-Sinai entropy on the repeller. Macroscopically, the escape rate can often be expressed in terms of a diffusion constant or some other transport property. More on the connection between the Kolmogorov-Sinai entropy and transport coefficients can be found in references [8–10].

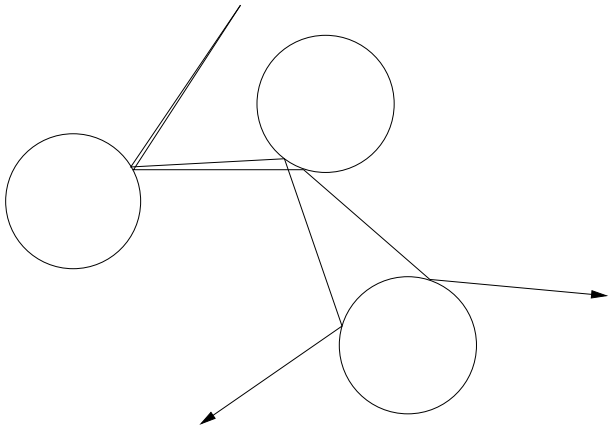

Figure 1.2: Part of a random Lorentz gas in two dimensions without external fields. Two diverging trajectories of the point particle are drawn.

1.3 Many-particle systems and other systems with many degrees of freedom

1.3.1 Lorentz gases

Many studies have been done on the chaotic properties of the Lorentz gas in different forms (see, for example, references [11–20]). It is a simple model which consists of a single point particle moving freely between elastic, spherical scatterers. The scatterers can either be placed at random or in a lattice configuration, overlapping or not. The Lorentz gas provides a physical system, yet is still simple enough to allow for exact calculations of many properties. This simplicity is partially due to the fact that the Lorentz gas contains only one moving particle, and therefore does not have many dynamical degrees of freedom. Due to the shape of the scatterers, the Lorentz gas is chaotic. In figure 1.2, a part of a random Lorentz gas is shown with two exponentially diverging trajectories.

The simplicity of the Lorentz gas makes it possible to examine its properties under a variety of conditions. For example, the scatterers can be replaced by a repulsive potential [21]. The Lorentz gas can also be investigated under non-equilibrium conditions. For example, calculations can be done on systems with external fields [11, 15–17]. In such systems, energy is added to the system by the field, and therefore must be removed by other means. This is done with thermostats. Thermostats are fiercely debated, as many commonly used thermostats are of somewhat unphysical nature.

The Lorentz gas may be defined in an arbitrary number of dimensions d, but has mostly been studied in two or three dimensions. It is possible to study the Lorentz gas with large d. This is of interest, as the phase space of a hard-sphere system can also be described as a high-dimensional space with fixed scatterers. In chapter 5 of this thesis, the Lyapunov spectrum of the high-dimensional Lorentz gas is studied in equilibrium.

1.3.2 Many degrees of freedom

Systems which consist of many particles have many Lyapunov exponents. They behave differently from systems which have only a few degrees of freedom, such as the two- or three-dimensional Lorentz gas. The Lyapunov spectra of such systems show some interesting features, which are specific to systems consisting of many particles, or at least systems with many degrees of freedom. Understanding the chaotic properties of systems of many particles starts with understanding the chaotic properties of equilibrium systems.

In this thesis, three systems with many degrees of freedom are considered in equilibrium. Firstly, the system consisting of freely moving hard spheres or disks is discussed in chapters 3 and 4. The second system, in chapter 5, is the high-dimensional Lorentz gas. In chapter 6, a system is described which is similar to the Lorentz gas, but contains cylindrical scatterers instead of spherical ones. This system is far more similar to many-particle systems than the high-dimensional Lorentz gas.

1.3.3 Hard disks and spheres

The simplest many-particle systems to do calculations on are systems of hard particles. Molecular dynamics simulations for the entire Lyapunov spectrum of such systems have been done by Posch, Dellago, and Hirschl [22, 23]. Calculations have been done for the largest exponents of systems of many freely moving, elastically colliding hard disks [6, 24–26].

The smallest positive and corresponding negative exponents found in these simulations have received a lot of attention because of their surprising behaviour. For large enough systems, their values are inversely proportional to the system length. The tangent-space eigenvectors associated with these exponents show a wave-like behaviour. These kind of properties have not been observed in systems with few degrees of freedom.

Eckmann and Gat [27] as well as Taniguchi, Dettmann, and Morriss [28, 29], have made attempts to approach these exponents by using random-matrix theory. Another approach, based on kinetic theory has been taken by McNamara and Mareschal [30]. Our own calculations of these exponents, also based on kinetic theory, are described in chapter 3.

In chapter 4, the Kolmogorov-Sinai entropy is estimated for hard disks/spheres at low densities. The next to leading order is found to be larger than in earlier calculations [31], and is in better agreement with simulation results.

Chapter 2

Hard spheres in phase space and tangent space

2.1 Introduction

This chapter and chapters 3, 4, and 6, are devoted to the study of classical systems consisting of large numbers of disks or spheres, moving freely between elastic collisions described by hard-core interaction. The two other systems considered in this thesis, the high-dimensional Lorentz gas and the system with a point particle moving among high-dimensional cylindrical scatterers, are similar in their phase-space and tangent-space dynamics. This chapter serves to provide an introduction to the dynamics of systems of hard spheres, as well as to their statistical properties.

Due to the convex curvature of hard disks or spheres, the systems are strongly chaotic. At low densities systems with hard-core interaction or with soft potentials behave nearly the same. However, the hard-core interaction makes the calculations of the dynamics much simpler, because the collision rules are simple and, in addition, there is no typical energy scale. Also, only two particles can interact at a time.

In chapter 1, the concept of chaos was introduced, and it was discussed how chaos can be characterised using Lyapunov exponents, the exponential rates of divergence of infinitesimally perturbed trajectories in phase space. For this description the space of such infinitesimal perturbations, the tangent space, was

introduced. In order to calculate the Lyapunov exponents for a system, it is necessary to understand the dynamics in phase space, from which the dynamics in tangent space can be derived.

2.2 Dynamics in phase space

Consider a gas of N identical, hard spheres of diameter a and mass m, freely moving in d dimensions. The number of dimensions is, usually, equal to 2 or 3. The phase space of this system is characterised by the positions $\mathbf{r}_i$ and velocities $\mathbf{v}_i$ of the particles,

$$\gamma = (\gamma_i) \ , \tag{2.1}$$
$$\gamma_i = (\mathbf{r}_i, \mathbf{v}_i) \ . \tag{2.2}$$

The space of vectors γ_i is called μ space. The tangent space of this space may be described by the infinitesimal perturbations $\delta\mathbf{r}_i$ and $\delta\mathbf{v}_i$ of the positions and velocities. Together they span the tangent space to phase space,

$$\delta\gamma = (\delta\gamma_i) \ , \tag{2.3}$$
$$\delta\gamma_i = (\delta\mathbf{r}_i, \delta\mathbf{v}_i) \ . \tag{2.4}$$

The dynamics in phase space of this system consist of an alternating sequence of free flights and collisions. During free flights the particles do not interact. At a collision the positions of the particles remain the same, but the velocities are changed instantaneously. During a free flight, the velocity of a particle is constant and the position of a particle grows linearly with its velocity,

$$\mathbf{v}_i(t) = \mathbf{v}_i(t_0) \ , \tag{2.5}$$
$$\mathbf{r}_i(t) = \mathbf{r}_i(t_0) + (t - t_0)\mathbf{v}_i(t_0) \ . \tag{2.6}$$

At a collision between particles i and j, the positions of the particles remain the same, but the momenta are exchanged. The dynamics of a collision are shown in figure 2.1 in relative coordinates. Note that in these coordinates the dynamics are the same as those of a point particle colliding with a cylinder.

Define the collision normal $\hat{\sigma}$ as the unit vector that indicates the relative positions of the two particles at the instant of collision,

$$\hat{\sigma} = \frac{1}{a}(\mathbf{r}_i - \mathbf{r}_j) \ . \tag{2.7}$$

During the collision, momentum is exchanged between the colliding particles along the collision normal. None of the other particles interact. Using primes to denote

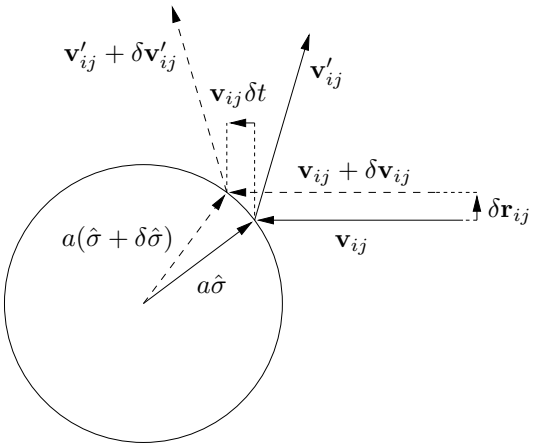

Figure 2.1: Two particles at a collision in relative phase space. The collision normal $\hat{\sigma}$ is the unit vector pointing from the centre of one particle to the centre of the other.

the coordinates in phase space after the collision, one finds

$$\mathbf{r}'_i = \mathbf{r}_i \ , \tag{2.8}$$
$$\mathbf{r}'_j = \mathbf{r}_j \ , \tag{2.9}$$
$$\mathbf{v}'_i = \mathbf{v}_i - \hat{\sigma}(\hat{\sigma} \cdot \mathbf{v}_{ij}) \ , \tag{2.10}$$
$$\mathbf{v}'_j = \mathbf{v}_j + \hat{\sigma}(\hat{\sigma} \cdot \mathbf{v}_{ij}) \ , \tag{2.11}$$

where $\mathbf{v}_{ij} = \mathbf{v}_i - \mathbf{v}_j$ is the relative velocity. The positions and velocities of the other particles remain unchanged.

2.3 Tangent space

From equations (1.4) and the dynamics in phase space, equations (2.5)–(2.11), the dynamics in tangent space can be derived [6]. During free flights there is no interaction between particles in phase space, and therefore also not in tangent space. The dynamics in tangent space are similar to the dynamics in phase space. The perturbation in position grows linearly with the perturbation in the velocity, while the perturbation in velocity remains unchanged. This can be written in

matrix form as

$$\begin{pmatrix} \delta\mathbf{r}_i(t) \\ \delta\mathbf{v}_i(t) \end{pmatrix} = \mathcal{Z}(t-t_0)\cdot \begin{pmatrix} \delta\mathbf{r}_i(t_0) \\ \delta\mathbf{v}_i(t_0) \end{pmatrix} , \tag{2.12}$$

$$\mathcal{Z}(t-t_0) = \begin{pmatrix} \mathbf{1} & (t-t_0)\mathbf{1} \\ 0 & \mathbf{1} \end{pmatrix} , \tag{2.13}$$

in which $\mathbf{1}$ is the $d \times d$ identity matrix.

At a collision between particles i and j, there is only interaction between the two colliding particles. Only the tangent-space vectors of the colliding particles are changed [25]. By applying equation (1.3) to the dynamics described in equations (2.8)–(2.11) the collision dynamics in tangent space can be found. In figure 2.1 an example of the phase-space and tangent-space dynamics is shown.

It is important to realise that an infinitesimal difference in the positions of the colliding particles produces an infinitesimal difference in the collision time,

$$\delta t = -\frac{\hat{\sigma}\cdot(\delta\mathbf{r}_i - \delta\mathbf{r}_j)}{\hat{\sigma}\cdot\mathbf{v}_{ij}} . \tag{2.14}$$

This, in turn, leads to an infinitesimal change in the collision normal, proportional to the component of the relative velocity which is perpendicular to the collision normal,

$$\delta\hat{\sigma} = \frac{1}{a}\left[(\delta\mathbf{r}_i - \delta\mathbf{r}_j) + \mathbf{v}_{ij}\delta t\right] = \frac{(\hat{\sigma}\cdot\mathbf{v}_{ij})\mathbf{1} - \mathbf{v}_{ij}\hat{\sigma}}{a\hat{\sigma}\cdot\mathbf{v}_{ij}}\cdot(\delta\mathbf{r}_i - \delta\mathbf{r}_j) . \tag{2.15}$$

Here the notation $\mathbf{ab}$ denotes the standard tensor product of vectors $\mathbf{a}$ and $\mathbf{b}$.

The perturbed momenta $\mathbf{v}+\delta\mathbf{v}$ are exchanged along the perturbed collision normal $\hat{\sigma}+\delta\hat{\sigma}$ according to equations (2.10) and (2.11), instead of along $\hat{\sigma}$. This produces an infinitesimal perturbation in the post-collisional positions and velocities of the particles involved in the collision, leading to infinitesimal changes in both positions and velocities right after the collision.

For convenience, we switch to relative and centre-of-mass coordinates, and infinitesimal perturbations of them, $\delta\mathbf{r}_{ij} = \delta\mathbf{r}_i - \delta\mathbf{r}_j, \delta\mathbf{R}_{ij} = (\delta\mathbf{r}_i + \delta\mathbf{r}_j)/2, \delta\mathbf{v}_{ij} = \delta\mathbf{v}_i - \delta\mathbf{v}_j$, and $\delta\mathbf{V}_{ij} = (\delta\mathbf{v}_i + \delta\mathbf{v}_j)/2$. These can be found from equations (2.10) and (2.11) to transform as

$$\delta\mathbf{r}'_{ij} = \delta\mathbf{r}_{ij} - 2\mathsf{S}\cdot\delta\mathbf{r}_{ij} , \tag{2.16}$$

$$\delta\mathbf{R}'_{ij} = \delta\mathbf{R}_{ij} , \tag{2.17}$$

$$\delta\mathbf{v}'_{ij} = \delta\mathbf{v}_{ij} - 2\mathsf{S}\cdot\delta\mathbf{v}_{ij} - 2\mathsf{Q}\cdot\delta\mathbf{r}_{ij} , \tag{2.18}$$

$$\delta\mathbf{V}'_{ij} = \delta\mathbf{V}_{ij} , \tag{2.19}$$

in which S and Q are the $d \times d$ matrices,

$$\mathsf{S} = \hat{\sigma}\hat{\sigma} \ , \tag{2.20}$$

$$\mathsf{Q} = \frac{[(\hat{\sigma}\cdot\mathbf{v}_{ij})\,\mathbf{1} + \hat{\sigma}\mathbf{v}_{ij}]\cdot[(\hat{\sigma}\cdot\mathbf{v}_{ij})\,\mathbf{1} - \mathbf{v}_{ij}\hat{\sigma}]}{a(\hat{\sigma}\cdot\mathbf{v}_{ij})} \ . \tag{2.21}$$

In the tangent space of particles i and j, this may be written as

$$\begin{pmatrix} \delta\mathbf{r}_i' \\ \delta\mathbf{r}_j' \\ \delta\mathbf{v}_i' \\ \delta\mathbf{v}_j' \end{pmatrix} = \left(\begin{array}{cc|cc} \mathbf{1}-\mathsf{S} & \mathsf{S} & 0 & 0 \\ \mathsf{S} & \mathbf{1}-\mathsf{S} & 0 & 0 \\ \hline -\mathsf{Q} & \mathsf{Q} & \mathbf{1}-\mathsf{S} & \mathsf{S} \\ \mathsf{Q} & -\mathsf{Q} & \mathsf{S} & \mathbf{1}-\mathsf{S} \end{array}\right) \cdot \begin{pmatrix} \delta\mathbf{r}_i \\ \delta\mathbf{r}_j \\ \delta\mathbf{v}_i \\ \delta\mathbf{v}_j \end{pmatrix} \ . \tag{2.22}$$

The presence of the matrix Q in the tangent-space collision dynamics is essential for the chaotic properties of the system. Without it, the system would not be chaotic. Some properties of Q lead to unexpected results. Surprisingly, due to certain properties of Q, ring collisions contribute to the smallest positive Lyapunov exponents to leading order in density, as is described in chapter 3. The properties of Q also feature in chapter 4, where previously ignored contributions to the Kolmogorov-Sinai entropy are found to be the result of the properties of Q.

$\mathsf{M}_{\gamma_0}(t)$ in equation (1.3) is the product of a sequence of matrices. Let $\mathsf{Z}(t)$ be the $2dN \times 2dN$ matrix which performs the transformations of $\mathcal{Z}(t)$ on all particles. Let L_p be the $2dN \times 2dN$ matrix which performs the transformations of equation (2.22) on the two particles involved in collision p and leaves the rest of the particles untouched. $\mathsf{M}_{\gamma_0}(t)$ is the product of these matrices for the sequence of the collisions $(1, 2, \ldots, p)$ between time t and t_0. Its specific form reads

$$\mathsf{M}_{\gamma_0}(t) = \mathsf{Z}(t - t_p)\cdot\mathsf{L}_p\cdot\mathsf{Z}(t_p - t_{p-1})\mathsf{L}_{p-1}\cdot\cdots\cdot\mathsf{L}_1\cdot\mathsf{Z}(t_1 - t_0) \ . \tag{2.23}$$

2.4 Boltzmann and Enskog equations

A rigorous calculation of the path of every particle is not feasible in a many-particle system with unspecified initial conditions. One has to resort to statistical approximations, for low densities and large particle numbers. These can be formulated in a systematic way. As an introduction, we review how the Stoßzahlansatz is used to derive the Boltzmann and Enskog equations. For higher densities these can be generalised heuristically in the way proposed by Enskog. We will see that this approximation works less well in the calculation presented in chapter 3 than in the standard Enskog equation used for calculating transport coefficients for moderately dense systems.

The Boltzmann and Enskog equations describe the dynamics of hard-sphere and hard-disk systems at, respectively, low and moderate densities. They are equations for the single-particle distribution function, $f(\mathbf{r}, \mathbf{v}, t)$. For a single system, the distribution is peaked at the positions and velocities of the particles, and zero elsewhere,

$$f_{mic}(\mathbf{r}, \mathbf{v}, t) = \sum_{i=1}^{N} \delta(\mathbf{r} - \mathbf{r}_i)\delta(\mathbf{v} - \mathbf{v}_i) \ , \tag{2.24}$$

where $\delta(\mathbf{q})$ represents the product of the Dirac delta functions of the d components of $\mathbf{q}$. Calculating the time evolution of f_{mic} is equivalent to solving the equations of motion and equally impossible.

In order to obtain a practical equation one has to consider smooth distribution functions. This can be viewed in two ways. The distribution function can be interpreted as a density distribution after a course graining in μ space. The distribution function can also be interpreted as an ensemble average of the microscopic distribution function. It is an average distribution function over many typical initial conditions. For detailed derivations of the Boltzmann equation and the fundamental difficulties associated with it, see references [4, 32, 33].

Further, to derive the Boltzmann and Enskog equations, the approximation of the Stoßzahlansatz is necessary.

2.4.1 The BBGKY hierarchy equation

In the derivation of either the Boltzmann or the Enskog equation, one may start from the first Bogoliubov-Born-Green-Kirkwood-Yvon hierarchy equation. This is an exact equation for the rate of change of the one-particle distribution function in terms of the pair-distribution function, $f^{(2)}$. For hard-core interactions the standard form cannot be used, because force is ill-defined. Instead it may be expressed in the form

$$\begin{aligned} &\frac{\partial f(\mathbf{r}, \mathbf{v}, t)}{\partial t} + \mathbf{v} \cdot \nabla_{\mathbf{r}} f(\mathbf{r}, \mathbf{v}, t) + \nabla_{\mathbf{v}} \cdot \mathbf{a}(\mathbf{r}, \mathbf{v}, t) f(\mathbf{r}, \mathbf{v}, t) \\ &= \int_{\hat{\sigma}\cdot(\mathbf{v}-\mathbf{u})\leq 0} d\mathbf{u}\, d\hat{\sigma}\, n a^{d-1} \,|\, \hat{\sigma} \cdot (\mathbf{v} - \mathbf{u})| \\ &\qquad \times \left[f^{(2)}(\mathbf{r}, \mathbf{v}', \mathbf{r} + a\hat{\sigma}, \mathbf{u}', t) - f^{(2)}(\mathbf{r}, \mathbf{v}, \mathbf{r} - a\hat{\sigma}, \mathbf{u}, t) \right] \ , \end{aligned} \tag{2.25}$$

in which $f^{(2)}$ denotes the two-particle distribution function, and $\mathbf{u}$ and $\mathbf{v}$ respectively $\mathbf{u}'$ and $\mathbf{v}'$ are the velocities before the collision with collision normal $\hat{\sigma}$ in the restituting and direct collisions. The second and third terms on the left-hand side of equation (2.25) describe the effects of free flight in position space and the

action of external forces, respectively. The vector $\mathbf{a}(\mathbf{r}, \mathbf{v}, t)$ is the acceleration of a particle due to external forces as a function of position, velocity, and time. The right-hand side expresses the rate of change due to collisions. The integral is over the collision normal and the outgoing velocity of the other particle. The factor $|\,\hat{\sigma} \cdot (\mathbf{v} - \mathbf{u})|$ represents the component of the relative velocity normal to the "collision plane."

2.4.2 The Stoßzahlansatz

In the low-density approximation, Boltzmann's Stoßzahlansatz approximates the pre-collisional pair distribution functions in equation (2.25) by a product of one-particle distributions. In addition, in the Boltzmann equation, both of these are evaluated at the same position $\mathbf{r}$, which is a good approximation if the diameter a is small compared to the mean free path.

The Enskog equation is a heuristic generalisation of the Boltzmann equation, known to give a good approximate description of the dynamics up to moderate densities (about a quarter of close packing). In this equation, it is assumed that the velocities of the colliding particles are still uncorrelated, but there is a spatial correlation equal to that of a system in non-uniform equilibrium with some density field, the same as the actual system. The pair distribution is approximated by the product of two one-particle distribution functions, evaluated at the actual positions of the two particles, and a factor χ_{E}, which is equal to the equilibrium pair-correlation function at contact between the two particles evaluated as a function of the density $n((\mathbf{r}_1 + \mathbf{r}_2)/2)$ at the point halfway between $\mathbf{r}_1$ and $\mathbf{r}_2$. Notice that this approximation is exact for a system in homogeneous equilibrium. The explicit form of the Enskog equation in a system without external fields thus reads

$$\begin{aligned}
&\frac{\partial f(\mathbf{r}, \mathbf{v}, t)}{\partial t} + \mathbf{v} \cdot \nabla_{\mathbf{r}} f(\mathbf{r}, \mathbf{v}, t) \\
&= \int_{\hat{\sigma} \cdot (\mathbf{v} - \mathbf{u}) \leq 0} d\mathbf{u}\, d\hat{\sigma}\, \chi_{\mathrm{E}}(n) n a^{d-1}\, |\,\hat{\sigma} \cdot (\mathbf{v} - \mathbf{u})| \\
&\qquad \times \left[f(\mathbf{r}, \mathbf{v}', t) f(\mathbf{r} + a\hat{\sigma}, \mathbf{u}', t) - f(\mathbf{r}, \mathbf{v}, t) f(\mathbf{r} - a\hat{\sigma}, \mathbf{u}, t) \right] . \qquad (2.26)
\end{aligned}$$

This equation effectively reduces to the Boltzmann equation in the limit $n \to 0$, when the difference in position between the two colliding particles, $r_{ij} = a\hat{\sigma}$, may be ignored, and χ_{E} approaches unity.

The approximation made in the Stoßzahlansatz excludes the possibility that two colliding particles have information about each other from earlier collisions. Predominant corrections from events where such correlations are present are due to so-called ring collisions. For more details on ring collisions, see reference [34]. In a finite system, eventually, every collision will be a correlated collision. The rings, however, are extremely long, and it seems fair to assume that eventually

any remaining correlation becomes negligible. In general, contributions from ring collisions are expected to appear in macroscopic quantities such as transport coefficients in higher orders in the density only. Some more details on ring collisions can be found in chapter 3, where it is discussed how ring collisions can, in fact, affect the low-density limit of some of the Lyapunov exponents.

More details on the Boltzmann equation and Enskog's theory of dense gases may be found in references [32] and [33].

2.4.3 Solutions in equilibrium

In this thesis, only equilibrium systems are studied. In equilibrium the time derivative in equation (2.26) vanishes and, in the absence of external fields, the particles are distributed homogeneously. The equilibrium solution to the Enskog and Boltzmann equations is the Maxwell distribution,

$$f(\mathbf{r},\mathbf{v},t) = n\phi_{\mathrm{M}}(\mathbf{v}_i) = n\left(\frac{2\pi}{m\beta}\right)^{-d/2}\exp\left(-\frac{1}{2}\beta m|\mathbf{v}|^2\right)\,, \tag{2.27}$$

where $\beta = 1/(k_{\mathrm{B}}T)$, and T is the temperature, which is related to the average kinetic energy per particle E through $E = d/(2\beta) = d\,k_{\mathrm{B}}T/2$.

The collision rate for specific collision parameters is proportional to the differential cross section and the component of the relative velocity normal to the collision plane. It is equal to

$$\begin{aligned}\tfrac{1}{2}Np(\mathbf{v},\mathbf{u},\hat{\sigma})d\mathbf{v}d\mathbf{u}d\hat{\sigma} = {} & \tfrac{1}{2}N|\hat{\sigma}\cdot(\mathbf{v}-\mathbf{u})|\chi_{\mathrm{E}}(n)na^{d-1}\phi_{\mathrm{M}}(\mathbf{v})\phi_{\mathrm{M}}(\mathbf{u}) \\ & \times d\mathbf{v}d\mathbf{u}d\hat{\sigma}\ .\end{aligned} \tag{2.28}$$

Note that any integrals are only over the range of $\hat{\sigma}$ where $\hat{\sigma}\cdot(\mathbf{v}_i-\mathbf{v}_j)$ is negative. Often in this thesis the functions to be integrated depend only on the angle θ between $\mathbf{v}_i-\mathbf{v}_j$ and $\hat{\sigma}$. In this case, the integrals over $\hat{\sigma}$ may be transformed into integrals over θ,

$$\int d\hat{\sigma} = \int \sin^{d-2}\theta\, d\theta\ . \tag{2.29}$$

The velocity-dependent collision frequency can be found by integrating the collision rate over the outgoing velocity of the other particle and over the collision normal,

$$\nu(\mathbf{v}) = \int d\mathbf{u}\, d\hat{\sigma}\, \chi_{\mathrm{E}}(n)na^{d-1}|\hat{\sigma}\cdot(\mathbf{v}-\mathbf{u})|\phi_{\mathrm{M}}(\mathbf{u})\ . \tag{2.30}$$

Because the equilibrium distribution is homogeneous and isotropic, the velocity-dependent collision frequency only depends on the absolute value of the velocity,

not on its orientation. After integration over the velocity one finds the average collision frequency for a given particle

$$\bar{\nu} = \int d\mathbf{v}\, \nu(\mathbf{v}) \phi_{\mathrm{M}}(\mathbf{v}) = \frac{2\pi^{(d-1)/2}}{\Gamma\left(\frac{d}{2}\right)} \frac{\chi_{\mathrm{E}}(n) n a^{d-1}}{\sqrt{\beta m}} \ . \tag{2.31}$$

The total collision frequency of the system is equal to $\frac{1}{2} N \bar{\nu}$.

In chapter 4, the distribution of free-flight times is needed. In the low-density limit, the free-flight times of the particles are distributed exponentially and as a function of the particle velocity according to

$$p_\tau(\tau|v) d\tau = \nu(\mathbf{v}) \exp[-\nu(\mathbf{v})\tau] d\tau \ . \tag{2.32}$$

Chapter 3

Goldstone modes in Lyapunov spectra of hard disks

Sections 3.3, 3.4, 3.5, and 3.6 of this chapter are based on Physical Review E **70**, 016207 (2004) [35].

3.1 Introduction

Recently, the largest Lyapunov exponent has been calculated for systems of many freely moving hard spheres [6, 25]. Simulations of this system to calculate the entire spectrum have been carried out by Posch, Hirschl, and Dellago [22, 23, 36]. The behaviour of the smallest positive and corresponding negative exponents in these simulations has received a great deal of attention because of their unexpected properties. For large enough systems, these exponents, at fixed density, temperature, and system shape, are inversely proportional to the system size. The tangent-space eigenvectors associated with these exponents have a wave-like dependence on position.

Eckmann and Gat [27] as well as Taniguchi, Dettmann, and Morriss [28, 29] have made attempts to calculate these exponents by using random-matrix the-

ory. Another approach, based on kinetic theory has been taken by McNamara and Mareschal [30]. In the present chapter, part of the behaviour of the small exponents is explained both qualitatively and quantitatively, also on the basis of kinetic theory. The way in which closure of the equations is obtained differs completely from the approach taken by McNamara and Mareschal.

The composition of this chapter is as follows. Section 3.2 is a short introduction to the results of the simulations by Posch and Hirschl for hard spheres in two dimensions [22]. In section 3.3, the small exponents are shown to be due to the Goldstone mechanism. Starting from the dynamics of hard spheres, described in section 2.2, a set of equations for the Lyapunov modes corresponding to these small exponents are derived in section 3.4. This accomplished by using a generalised Enskog equation. The general form of the solutions is discussed in section 3.5 and the quantitative results derived from them are the subject of section 3.6. Finally, some remarks on the consequences of ring collisions are made in section 3.7.

3.2 Simulations

In principle, $\mathsf{M}_{\gamma_0}(t)$ defined in equation (1.4) can be calculated numerically for finite times for any finite system and the eigenvalues can be determined. Posch and Hirschl [22] have done molecular dynamics simulations to determine the entire Lyapunov spectrum of systems consisting of many hard disks in rectangular boxes with periodic boundary conditions. A spectrum as calculated by Posch and Hirschl is displayed in figure 3.1.

The eigenvectors in tangent space belonging to the large exponents are typically quite localised; only a few particles closely together contribute significantly to a given eigenvector. When the system is large enough compared to the mean free-path length, a step structure appears in the Lyapunov exponents near zero. The heights of the steps are inversely proportional to the size of the box. The tangent-space eigenvector is distributed over all particles, much in the same way as with the zero modes. This is discussed in section 3.3. An example is shown in figure 3.2.

The tangent-space vectors belonging to the six exponents in each step appear, on average and to first approximation, to be linear combinations of the zero modes with a sinusoidal spatial modulation. This is apparent in the example in figure 3.2. The slow modes belonging to a certain wave vector can be separated into two groups, one consisting of four longitudinal modes and the other one of two transverse modes. The transverse modes are found to be linear combinations of sinusoidal spatial modulations of the zero modes resulting from a translation or a Galilei transformation in the direction perpendicular to the wave vector. The longitudinal modes are linear combinations of modulations of the four remaining zero modes. The transverse modes are non-propagating, but the longitudinal modes propagate through the system at constant speed, to first

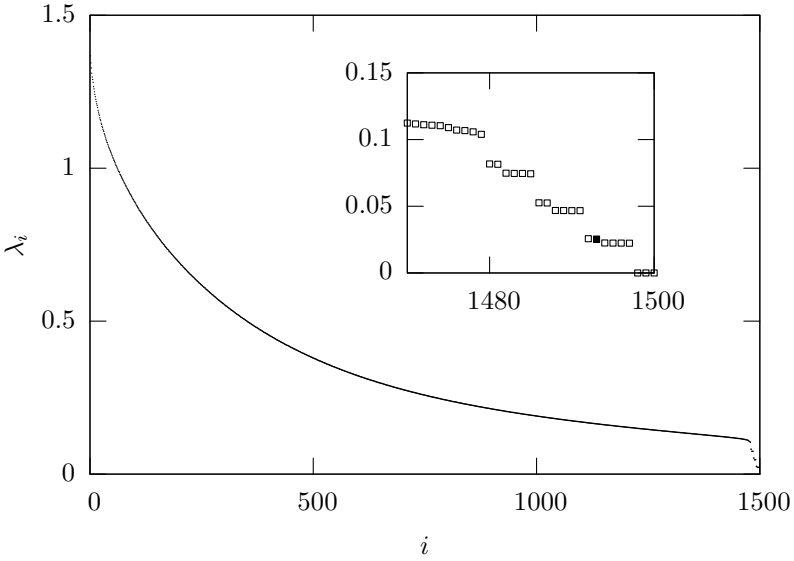

Figure 3.1: The spectrum of Lyapunov exponents from the simulations [22, 23, 37] of 750 hard spheres in two dimensions at density $n = 0.1$ in a rectangular box of dimensions $10\times75\ a^2/n$, with periodic boundary conditions. Only the positive exponents are plotted, since, by the conjugate pairing rule, the negative spectrum is exactly the opposite. The inset shows an enlargement of the bottom right corner.

approximation the same for all longitudinal modes. The Lyapunov exponents belonging to these modes have imaginary components. This behaviour has been confirmed in direct-simulation Monte Carlo simulations performed by Forster and Posch [37]. Taniguchi and Morriss [38] as well as Eckmann et al. [36] have also investigated the behaviour of these modes under reflecting boundary conditions and found similar results. For more details, see references [22, 23].

Besides the simulations in systems of hard disks and spheres, simulations of the spectrum have also been done in systems of particles with soft potentials at various densities. Posch et al. [39, 40] used a Weeks-Chandler-Anderson potential with a finite range to investigate the spectrum for various degrees of softness. Radons and Yang used a Lennard-Jones potential in a one-dimensional system [41, 42]. For low densities such systems behave similarly to hard spheres. At higher densities, the step structure in the spectrum disappears.

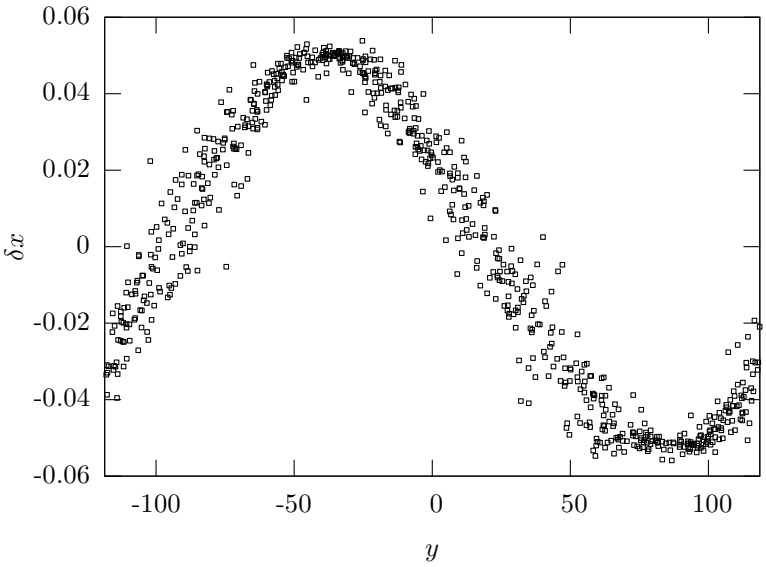

Figure 3.2: The component of $\delta\mathbf{r}_i$ in the short direction, δx, is plotted against the position of the particle in the long direction, y, for the mode corresponding to λ_{1493}, one of the transverse modes in the first step. These data are from the same simulation as the data in figure 3.1. The corresponding exponent is indicated there with a full box.

3.3 Symmetries and Goldstone modes

From the symmetries of the dynamics of systems of many particles, some statements can be made concerning the existence of Lyapunov exponents which are zero. In this chapter, these Lyapunov exponents and their corresponding eigenvectors will be shown to be connected to the collective modes found in the simulations.

3.3.1 Symmetries and zero Lyapunov exponents

Vectors in tangent space which are generated by symmetries of the dynamics of the system do not grow or shrink exponentially. They are eigenvectors with zero Lyapunov exponents and are referred to as the zero modes. For a system of hard spheres under periodic boundary conditions, the symmetries in phase space are uniform translations, Galilei transformations, time translations, and velocity scaling. They correspond to symmetries in tangent space which give rise to the

zero modes. The initial displacements of the zero modes are

$$\delta\gamma_i = (\Delta\mathbf{r}_0, 0) \ , \tag{3.1}$$
$$\delta\gamma_i = (0, \Delta\mathbf{v}_0) \ , \tag{3.2}$$
$$\delta\gamma_i = (\mathbf{v}_i\Delta t_0, 0) \ = (\Delta\mathbf{r}_\mathbf{v}, 0) \ , \tag{3.3}$$
$$\delta\gamma_i = (0, \mathbf{v}_i\Delta\lambda_0) = (0, \Delta\mathbf{v}_\mathbf{v}) \ , \tag{3.4}$$

where $\Delta\mathbf{r}_0$, $\Delta\mathbf{v}_0$, Δt_0, and $\Delta\lambda_0$ are constant vectors and scalars which are independent of the particles. The quantities $\Delta\mathbf{r}_0$ and $\Delta\mathbf{v}_0$ can have components in all d directions of the space. In the case of Galilei transformations and velocity scaling the tangent-space vectors grow linearly, rather than exponentially, with time. Hence the corresponding Lyapunov exponents are zero. These symmetries can be destroyed by boundary conditions. If, for example, the boundary conditions are reflecting the modes associated with uniform translations and Galilei transformations are destroyed.

Soft potentials

In systems with soft potentials, the zero modes resulting from uniform translations and Galilei transformations are still described by equations (3.1) and (3.2). The explicit form of the time-translation mode is different, because of the forces between the particles, but time translation still is an obvious continuous symmetry of the system. The time mode becomes

$$\delta\gamma_i = \left(\mathbf{v}_i\Delta t_0, -\frac{1}{m}\frac{dV(\mathbf{r})}{d\mathbf{r}_i}\Delta t_0\right) \ . \tag{3.5}$$

The velocity scaling mode is associated with velocity scaling, which is associated with energy conservation. In the hard-particle system, the energy mode is proportional to the vector normal to the constant energy surface, the gradient of the energy in the phase space, Γ. One might expect to have the same in the soft-potential system. The energy mode would be expected to be

$$\delta\gamma_i = \left(\frac{1}{m}\frac{dV(\mathbf{r})}{d\mathbf{r}_i}\Delta\lambda_0, \mathbf{v}_i\Delta\lambda_0\right) \ . \tag{3.6}$$

However, this does not work. If, for example, a system is considered with limited-range potentials, points in phase space exist where no potentials overlap. In these points, the mode in equation (3.6) would be equal to the energy-scaling mode in the hard-particle system. As soon as two particles interact, differences appear. But, for given impact parameters, in the soft-potential system, the scattering angle at the rescaled velocity differs from that at the original velocity. In the system with hard-core interaction, this is not the case. After the interaction equation (3.6) is no longer obeyed. The velocity-scaling symmetry is destroyed

by the fact that the potential has a typical energy scale, which cannot be rescaled along with the kinetic energy. The vector in equation (3.6) may be pointing in a direction orthogonal to the constant energy surface, under time-evolution it does not evolve onto itself. The tangent vector in equation (3.6) is not a zero mode.

One might wonder if there is a zero mode related to constant energy at all, since the corresponding symmetry is destroyed. The conjugate pairing rule states that for every positive exponent there is a corresponding negative exponent with the same absolute value. There must therefore be an even number of non-zero Lyapunov exponents. As there is an even number of exponents, we know that there has to be an even number of zero Lyapunov exponents. There must be a sixth (or eighth in three dimensions) zero Lyapunov exponent as well, with a corresponding sixth (or eighth) zero mode.

In systems at low densities, this mode should look similar to the velocity rescaling mode. In order to preserve the scattering angles and prevent exponential growth of the perturbation, a small perturbation must be added. This perturbation just before the collisions must originate from an extra contribution of order n to the velocity perturbation just after the previous collision. This problem may, in fact, have something to do with the disappearace of the step structure in soft-potential systems at high density.

3.3.2 Goldstone modes

The sinusoidal patterns found in the simulations may be explained as Goldstone modes. These occur in systems with a spontaneously broken continuous symmetry. These modes were first introduced by Goldstone [43]. Well-known examples of Goldstone modes are spin waves in ferromagnets, where the rotational symmetry is broken, and phonons in crystals, where translation symmetry is broken by the crystal lattice.

In the present case the symmetries associated with the zero modes are indeed continuous. The tangent space is a linear space and the tangent vector can be chosen to be of any length. In tangent space the system does not move towards a symmetric state, and therefore the symmetries in tangent space which are associated with the zero modes are spontaneously broken.

The symmetry operator and the evolution operator commute. Translation invariance also causes the evolution operator to commute with the translation operator, so that they have a set of common eigenfunctions. These have the general form

$$\delta\gamma_i = f_{\mathbf{k}}(\mathbf{v}_j, \mathbf{r}_{ij}) \exp\left(i\mathbf{k}\cdot\mathbf{r}_i\right) , \tag{3.7}$$

where the eigenvalues of the operator translating each postition over the vector $\mathbf{a}$ are of the form $\exp(i\mathbf{k}\cdot\mathbf{a})$. The Goldstone modes are those eigenmodes that for $k \to 0$ reduce to linear combinations of the zero modes. For non-zero values of k, they contain a sinusoidal modulation in space of the continuous symmetry

which grows or shrinks slowly with time. Spatial propagation, as seen in the simulations for the longitudinal modes, may be accounted for by allowing λ to have an imaginary component. In the usual definition of the Lyapunov exponents, they do not have imaginary components. Here it is useful to allow imaginary components for the purpose of describing the propagation of the longitudinal modes. In the rest of this chapter, a way to calculate the exponents belonging to the Goldstone modes will be discussed.

3.4 Boltzmann and Enskog equations

Except in a rigorous calculation of the path of every particle, starting from the initial conditions, as done in the molecular-dynamics simulations, it is impossible to know the matrix M_{γ_0} in equation (1.4) exactly. The tangent-space eigenvector belonging to a given Lyapunov exponent will in general depend on the initial conditions of all the particles in a much too complicated way to be specified exactly. It is therefore complicated to calculate the tangent-space vector which belongs to any Lyapunov exponent exactly. To find the exponents, one has to resort to statistical approximations, for low densities and large particle numbers. To this end, we start with assumptions similar to the Stoßzahlansatz in the Boltzmann and Enskog equations and derive a generalised Enskog equation from a generalised hierarchy equation.

3.4.1 Generalised Enskog equation in tangent μ space

To describe the dynamics in tangent space, a generalised Boltzmann equation is derived for the single-particle distribution function in both μ space and "tangent μ space," $f(\mathbf{r}, \mathbf{v}, \delta\mathbf{r}, \delta\mathbf{v}, t)$. On integration over the variables in tangent space, the equation and the solutions we are interested in must reduce to equations (2.26) and (2.27) respectively. Note that in this chapter, as opposed to in the rest of this thesis, $\delta\mathbf{r}$ and $\delta\mathbf{v}$ are used to denote d-dimensional tangent vectors. In the rest of this thesis they are dN-dimensional tangent vectors.

For given initial conditions, the eigenvectors of M_{γ_0} in general depend sensitively on the precise values of the collision parameters of all collisions, as generated by the positions and velocities of all particles. The zero modes are exceptions to this. For small k it is to be expected that the Goldstone modes behave in a similar way and are approximately independent of the collision parameters of the various collisions. Under those circumstances one may expect that the $2dN$-dimensional tangent-space vector can be described by a single-particle distribution function that depends smoothly on velocity, position and time, just like the velocity distribution in ordinary μ space. One may start from a generalised hierarchy equation which expresses the rate of change of the single-particle distribution function in μ space and tangent μ space in terms of the two-particle distribution, similarly

to equation (2.25). In the absence of external fields, one has

$$\begin{aligned}
&\frac{\partial f(\mathbf{r},\mathbf{v},\delta\mathbf{r},\delta\mathbf{v},t)}{\partial t} + \mathbf{v}\cdot\nabla_{\mathbf{r}} f(\mathbf{r},\mathbf{v},\delta\mathbf{r},\delta\mathbf{v},t) + \delta\mathbf{v}\cdot\nabla_{\delta\mathbf{r}} f(\mathbf{r},\mathbf{v},\delta\mathbf{r},\delta\mathbf{v},t) \\
&= \int_{\hat{\sigma}\cdot(\mathbf{v}-\mathbf{u})\le 0} d\mathbf{u}\, d\hat{\sigma}\, d\delta\mathbf{u}\, d\delta\tilde{\mathbf{r}}\, n a^{d-1}\, |\,\hat{\sigma}\cdot(\mathbf{v}-\mathbf{u})| \\
&\quad\times\Big[f^{(2)}(\mathbf{r},\mathbf{v}',\delta\mathbf{r}',\delta\mathbf{v}',\mathbf{r}+a\hat{\sigma},\mathbf{u}',\delta\tilde{\mathbf{r}}',\delta\mathbf{u}',t) \\
&\qquad - f^{(2)}(\mathbf{r},\mathbf{v},\delta\mathbf{r},\delta\mathbf{v},\mathbf{r}-a\hat{\sigma},\mathbf{u},\delta\tilde{\mathbf{r}},\delta\mathbf{u},t)\Big] \ , \qquad (3.8)
\end{aligned}$$

where $\delta\mathbf{u}$ and $\delta\mathbf{v}$ are the perturbations of $\mathbf{u}$ and $\mathbf{v}$. The perturbations in the positions of the two particles are denoted by $\delta\mathbf{r}$ and $\delta\tilde{\mathbf{r}}$. The primes are used to denote the velocities and tangent-μ-space vectors of the particles before the collision. The second and third terms on the left-hand side of the equation represent the rate of change of the distribution function due to free flight in μ space and tangent μ space. The right-hand side of the equation describes the rate of change due to collisions.

If in addition one makes the assumption that the distribution function of the tangent space vectors of two particles about to collide, factorises in a similar way as the distribution of their velocities, one ends up with a generalised Enskog equation in tangent μ space, which, in absence of an external field, is of the form

$$\begin{aligned}
&\frac{\partial f(\mathbf{r},\mathbf{v},\delta\mathbf{r},\delta\mathbf{v},t)}{\partial t} + \mathbf{v}\cdot\nabla_{\mathbf{r}} f(\mathbf{r},\mathbf{v},\delta\mathbf{r},\delta\mathbf{v},t) + \delta\mathbf{v}\cdot\nabla_{\delta\mathbf{r}} f(\mathbf{r},\mathbf{v},\delta\mathbf{r},\delta\mathbf{v},t) \\
&= \int_{\hat{\sigma}\cdot(\mathbf{v}-\mathbf{u})\le 0} d\mathbf{u}\, d\hat{\sigma}\, d\delta\mathbf{s}\, d\delta\mathbf{u}\, \chi_{\mathrm{E}}(n) n a^{d-1}\, |\,\hat{\sigma}\cdot(\mathbf{v}-\mathbf{u})| \\
&\quad\times[f(\mathbf{r},\mathbf{v}',\delta\mathbf{r}',\delta\mathbf{v}',t) f(\mathbf{r}+a\hat{\sigma},\mathbf{u}',\delta\mathbf{s}',\delta\mathbf{u}',t) \\
&\qquad - f(\mathbf{r},\mathbf{v},\delta\mathbf{r},\delta\mathbf{v},t) f(\mathbf{r}-a\hat{\sigma},\mathbf{u},\delta\mathbf{s},\delta\mathbf{u},t)] \ . \qquad (3.9)
\end{aligned}$$

If the variables in tangent μ space, $\delta\mathbf{r}$ and $\delta\mathbf{v}$, are integrated over, this equation reduces to equation (2.26).

Because $\delta\mathbf{r}$ and $\delta\mathbf{v}$ are infinitesimal, the dynamics in tangent space are linear in these quantities. Therefore, from equations (2.22) and (3.9) one may obtain closed linear equations for the time evolution of the average first moments $\langle\delta\mathbf{r}\rangle$ and $\langle\delta\mathbf{v}\rangle$. To this end, multiply both sides of equation (3.9) by $\delta\mathbf{r}$ or $\delta\mathbf{v}$ and then integrate over both. The result is a set of equations for the averages,

$$\frac{d}{dt}\delta\mathbf{r}(\mathbf{r},\mathbf{v},t) = -\mathbf{v}\cdot\frac{\partial}{\partial\mathbf{r}}\delta\mathbf{r}(\mathbf{r},\mathbf{v},t) + \delta\mathbf{v}(\mathbf{r},\mathbf{v},t) + \mathsf{C}_{\mathsf{S}}\delta\mathbf{r}(\mathbf{r},\mathbf{v},t) \ , \qquad (3.10)$$

$$\frac{d}{dt}\delta\mathbf{v}(\mathbf{r},\mathbf{v},t) = -\mathbf{v}\cdot\frac{\partial}{\partial\mathbf{r}}\delta\mathbf{v}(\mathbf{r},\mathbf{v},t) + \mathsf{C}_{\mathsf{S}}\delta\mathbf{v}(\mathbf{r},\mathbf{v},t) + \mathsf{C}_{\mathsf{Q}}\delta\mathbf{r}(\mathbf{r},\mathbf{v},t) \ . \qquad (3.11)$$

The functions $\delta\mathbf{r}(\mathbf{r},\mathbf{v},t)$ and $\delta\mathbf{v}(\mathbf{r},\mathbf{v},t)$ are the averages of $\delta\mathbf{r}$ and $\delta\mathbf{v}$ of a particle as a function of its position and velocity, and of time. The linear collision operators C_S and C_Q are associated with the matrices S and Q, and are given by

$$\begin{aligned}\mathsf{C}_\mathsf{S}\,\delta\mathbf{q}(\mathbf{r},\mathbf{v},t) = \int_{\hat\sigma\cdot(\mathbf{v}-\mathbf{u})\le 0} d\mathbf{u}\,d\hat\sigma\,\chi_\mathrm{E}(n)na^{d-1}\,|\,\hat\sigma\cdot(\mathbf{v}-\mathbf{u})|\phi_\mathrm{M}(\mathbf{u}) \\ \times\{\,\delta\mathbf{q}(\mathbf{r},\mathbf{v}',t)+\mathsf{S}\cdot[\,\delta\mathbf{q}(\mathbf{r}+a\hat\sigma,\mathbf{u}',t)-\,\delta\mathbf{q}(\mathbf{r},\mathbf{v}',t)] \\ -\,\delta\mathbf{q}(\mathbf{r},\mathbf{v},t)\}\ , \qquad (3.12)\end{aligned}$$

$$\begin{aligned}\mathsf{C}_\mathsf{Q}\,\delta\mathbf{r}(\mathbf{r},\mathbf{v},t) = \int_{\hat\sigma\cdot(\mathbf{v}-\mathbf{u})\le 0} d\mathbf{u}\,d\hat\sigma\,\chi_\mathrm{E}(n)na^{d-1}\,|\,\hat\sigma\cdot(\mathbf{v}-\mathbf{u})|\phi_\mathrm{M}(\mathbf{u}) \\ \times\mathsf{Q}\cdot[\delta\mathbf{r}(\mathbf{r}+a\hat\sigma,\mathbf{u}',t)-\,\delta\mathbf{r}(\mathbf{r},\mathbf{v}',t)]\ , \qquad (3.13)\end{aligned}$$

where $\delta\mathbf{q}$ denotes either $\delta\mathbf{r}$ or $\delta\mathbf{v}$. In equation (3.12) the first two terms between braces are gain terms. The last term is the loss term. Note that, from equation (2.21), Q depends on the collision parameter and on the velocities of the particles before the collision. This means that in equation (3.13) it depends on $\hat\sigma$, $\mathbf{u}'$, and $\mathbf{v}'$. The collision operators are proportional to the average collision frequency $\bar\nu$, which for dilute systems is proportional to the number density n.

3.4.2 Fourier transform

As the translation operators commute with the collision operators (3.12) and (3.13), solutions to equations (3.10) and (3.11) may be found that are common eigenfunctions of these operators, of the form

$$\delta\mathbf{q}(\mathbf{r},\mathbf{v},t) = \Delta\mathbf{q}(\mathbf{v})\exp(i\mathbf{k}\cdot\mathbf{r}+\lambda t)\ , \qquad (3.14)$$

where $\mathbf{q}$ is either $\mathbf{r}$ or $\mathbf{v}$, and $k_j = 2\pi n_j/L_j$ is the j-th component of the wave vector of the sinusoidal modulation and λ is the corresponding Lyapunov exponent. Among these the Goldstone modes are those solutions that in the limit of vanishing wave number reduce to linear combinations of the zero modes. For these modes to stand out among the continuum of other modes their wavelength has to be large compared to the typical length scale of the mean free path, or

$$k\bar v \ll \bar\nu\ , \qquad (3.15)$$

where $\bar v$ is the average velocity.

On substituting the Fourier transform, equation (3.14), into equations (3.10) and (3.11), they become eigenvalue equations for the Goldstone modes,

$$\lambda\Delta\mathbf{r}(\mathbf{v}) = -i(\mathbf{k}\cdot\mathbf{v})\Delta\mathbf{r}+\Delta\mathbf{v}+\mathsf{B}_\mathsf{S}\Delta\mathbf{r}\ , \qquad (3.16)$$

$$\lambda\Delta\mathbf{v}(\mathbf{v}) = -i(\mathbf{k}\cdot\mathbf{v})\Delta\mathbf{v}+\mathsf{B}_\mathsf{S}\Delta\mathbf{v}+\mathsf{B}_\mathsf{Q}\Delta\mathbf{r}\ . \qquad (3.17)$$

The operators $\mathsf{B_S}$ and $\mathsf{B_Q}$ are the Fourier transforms of the collision operators $\mathsf{C_S}$ and $\mathsf{C_Q}$. They satisfy the equations

$$\mathsf{B_S}\Delta\mathbf{q}(\mathbf{v}) = \int_{\hat{\sigma}\cdot(\mathbf{v}-\mathbf{u})\leq 0} d\mathbf{u}\, d\hat{\sigma}\, \chi_{\mathrm{E}}(n) n a^{d-1}\, |\hat{\sigma}\cdot(\mathbf{v}-\mathbf{u})| \phi_{\mathrm{M}}(\mathbf{u}) \times \{\Delta\mathbf{q}(\mathbf{v}') + \mathsf{S}\cdot[\Delta\mathbf{q}(\mathbf{u}')\exp(-ia\mathbf{k}\cdot\hat{\sigma}) - \Delta\mathbf{q}(\mathbf{v}')] - \Delta\mathbf{q}(\mathbf{v})\} \ , \tag{3.18}$$

$$\mathsf{B_Q}\Delta\mathbf{r}(\mathbf{v}) = \int_{\hat{\sigma}\cdot(\mathbf{v}-\mathbf{u})\leq 0} d\mathbf{u}\, d\hat{\sigma}\, \chi_{\mathrm{E}}(n) n a^{d-1} |\hat{\sigma}\cdot(\mathbf{v}-\mathbf{u})| \phi_{\mathrm{M}}(\mathbf{u}) \times \mathsf{Q}\cdot[\Delta\mathbf{r}(\mathbf{u}')\exp(-ia\mathbf{k}\cdot\hat{\sigma}) - \Delta\mathbf{r}(\mathbf{v}')] \ , \tag{3.19}$$

where $\Delta\mathbf{q}$ can be either $\Delta\mathbf{r}$ or $\Delta\mathbf{v}$. One of these, for instance $\Delta\mathbf{v}$, can be eliminated from the equations. One must solve equation (3.16) for $\Delta\mathbf{v}$ and substitute the result into equation (3.17). This yields an equation for $\Delta\mathbf{r}$,

$$[(\lambda + i\mathbf{k}\cdot\mathbf{v} - \mathsf{B_S})^2 - \mathsf{B_Q}]\Delta\mathbf{r} = 0 \ . \tag{3.20}$$

This equation can be solved by the use of a perturbation expansion in k, provided the mean free path is much smaller than the wavelength, as expressed by equation (3.15).

3.5 Solutions

3.5.1 Perturbation theory

If k is taken to be a small parameter, one may expand the operators and solutions in powers of k, as

$$\mathsf{B_S} = \mathsf{B_S}^{(0)} + k\mathsf{B_S}^{(1)} + k^2\mathsf{B_S}^{(2)} + \dots \ , \tag{3.21}$$

$$\mathsf{B_Q} = \mathsf{B_Q}^{(0)} + k\mathsf{B_Q}^{(1)} + k^2\mathsf{B_Q}^{(2)} + \dots \ , \tag{3.22}$$

$$\Delta\mathbf{r} = \Delta\mathbf{r}^{(0)} + k\Delta\mathbf{r}^{(1)} + k^2\Delta\mathbf{r}^{(2)} + \dots \ , \tag{3.23}$$

The higher order terms of $\Delta\mathbf{r}$, $\Delta\mathbf{r}^{(1)}$ and $\Delta\mathbf{r}^{(2)}$, may be chosen orthogonal to $\Delta\mathbf{r}^{(0)}$. Note that for $k \to 0$, the linear operators $\mathsf{B_S}$ and $\mathsf{B_Q}$ become identical to $\mathsf{C_S}$ and $\mathsf{C_Q}$. When acting on linear combinations of zero modes, $\Delta\mathbf{r}^{(0)}$, the unperturbed operators satisfy the properties

$$\mathsf{B_S}^{(0)}\Delta\mathbf{r}^{(0)} = \mathsf{B_Q}^{(0)}\Delta\mathbf{r}^{(0)} = \langle\Delta\mathbf{r}^{(0)}|\mathsf{B_S}^{(0)} = \langle\Delta\mathbf{r}^{(0)}|\mathsf{B_Q}^{(0)} = 0 \ , \tag{3.24}$$

where $\langle .|. \rangle$ represents the inner product defined by integration against a Maxwell distribution of the velocity, which is the equilibrium distribution. As it turns out, $\mathsf{B}_{\mathsf{Q}}^{(0)}$ has some non-trivial right eigenfunctions with zero eigenvalues, which will have an important effect on the limiting values of Lyapunov exponents in the limit of vanishing density. An example of such an eigenfunction is $\Delta\mathbf{r}(\mathbf{v}) = v_\perp \hat{\mathbf{k}} + v_\parallel \hat{\mathbf{k}}_\perp$, where $v_\perp$ and $v_\parallel$ are the components of $\mathbf{v}$ perpendicular and parallel to $\mathbf{k}$, and $\hat{\mathbf{k}}$ is the unit vector in the direction of $\mathbf{k}$.

In zeroth order equation (3.20) reduces to

$$[(\lambda^{(0)} - \mathsf{B}_{\mathsf{S}}^{(0)})^2 - \mathsf{B}_{\mathsf{Q}}^{(0)}]\Delta\mathbf{r}^{(0)} = 0 \; . \tag{3.25}$$

The relevant solutions to this are the zero modes, with $\lambda^{(0)} = 0$. This means that the Goldstone modes to leading order in k are the zero modes with a sinusoidal modulation, in nice agreement with the findings in references [22, 23].

In linear order, one finds with the aid of equation (3.24)

$$[-\mathsf{B}_{\mathsf{S}}^{(0)}(i\hat{\mathbf{k}}\cdot\mathbf{v} - \mathsf{B}_{\mathsf{S}}^{(1)}) - \mathsf{B}_{\mathsf{Q}}^{(1)}]\Delta\mathbf{r}^{(0)} = -[(\mathsf{B}_{\mathsf{S}}^{(0)})^2 - \mathsf{B}_{\mathsf{Q}}^{(0)}]\Delta\mathbf{r}^{(1)} \; . \tag{3.26}$$

This is an equation for $\Delta\mathbf{r}^{(1)}$. If $\Delta\mathbf{r}$ is taken orthogonal to the space of zero modes, the operator $(\mathsf{B}_{\mathsf{S}}^{(0)})^2 - \mathsf{B}_{\mathsf{Q}}^{(0)}$ becomes invertible. The formal solution of equation (3.26) is

$$\Delta\mathbf{r}^{(1)} = [(\mathsf{B}_{\mathsf{S}}^{(0)})^2 - \mathsf{B}_{\mathsf{Q}}^{(0)}]^{-1}[\mathsf{B}_{\mathsf{S}}^{(0)}(i\hat{\mathbf{k}}\cdot\mathbf{v} - \mathsf{B}_{\mathsf{S}}^{(1)}) + \mathsf{B}_{\mathsf{Q}}^{(1)}]\Delta\mathbf{r}^{(0)} \; . \tag{3.27}$$

This form suggests that $\Delta\mathbf{r}^{(1)}$ is of zeroth order in n, just as $\Delta\mathbf{r}^{(0)}$, but this is actually not the case, because the operator $[(\mathsf{B}_{\mathsf{S}}^{(0)})^2 - \mathsf{B}_{\mathsf{Q}}^{(0)}]^{-1}$ acts on functions with non-vanishing components along the non-trivial right zero eigenfunctions of $\mathsf{B}_{\mathsf{Q}}^{(0)}$. This yields contributions to $\Delta\mathbf{r}^{(1)}$ of order $1/n$. One might wonder whether this could cause a divergence in the limit of vanishing density, but that is not the case because of the restriction imposed on k by equation (3.15).

The second-order equation involves the first-order Lyapunov exponent $\lambda^{(1)}$, the second-order Lyapunov exponent $\lambda^{(2)}$, and the second-order tangent-space vector $\Delta\mathbf{r}^{(2)}$,

$$\begin{aligned}&[\{-\mathsf{B}_{\mathsf{S}}^{(0)}, \lambda^{(2)} - \mathsf{B}_{\mathsf{S}}^{(2)}\}_+ + (\lambda^{(1)} + i\hat{\mathbf{k}}\cdot\mathbf{v} - \mathsf{B}_{\mathsf{S}}^{(1)})^2 - \mathsf{B}_{\mathsf{Q}}^{(2)}]\Delta\mathbf{r}^{(0)} \\ &+ [\{-\mathsf{B}_{\mathsf{S}}^{(0)}, i\hat{\mathbf{k}}\cdot\mathbf{v} - \mathsf{B}_{\mathsf{S}}^{(1)}\}_+ - \mathsf{B}_{\mathsf{Q}}^{(1)}]\Delta\mathbf{r}^{(1)} + [(\mathsf{B}_{\mathsf{S}}^{(0)})^2 - \mathsf{B}_{\mathsf{Q}}^{(0)}]\Delta\mathbf{r}^{(2)} = 0 \; ,\end{aligned} \tag{3.28}$$

where $\{.,.\}_+$ is used to denote the anticommutator of two operators. On taking the inner product with $\Delta\mathbf{r}^{(0)}$, all terms involving $\Delta\mathbf{r}^{(2)}$ vanish as a consequence of equation (3.24). The resulting set of equations reads

$$\begin{aligned}&\langle\Delta\mathbf{r}^{(0)}|[(\lambda^{(1)} + i\hat{\mathbf{k}}\cdot\mathbf{v} - \mathsf{B}_{\mathsf{S}}^{(1)})^2 - \mathsf{B}_{\mathsf{Q}}^{(2)}]|\Delta\mathbf{r}^{(0)}\rangle \\ &+ \langle\Delta\mathbf{r}^{(0)}|[-(i\hat{\mathbf{k}}\cdot\mathbf{v} - \mathsf{B}_{\mathsf{S}}^{(1)})\mathsf{B}_{\mathsf{S}}^{(0)} - \mathsf{B}_{\mathsf{Q}}^{(1)}]|\Delta\mathbf{r}^{(1)}\rangle = 0 \; .\end{aligned} \tag{3.29}$$

As $\Delta\mathbf{r}^{(0)}$ is a linear combination of three independent zero modes, equation (3.29) actually has to be read as a 3×3 matrix equation involving the matrix elements between the various zero modes. In principle all of these are second-order polynomials in $\lambda^{(1)}$. The eigenvalues, as usual, follow from the condition that the determinant of the matrix vanishes as a function of $\lambda^{(1)}$.

3.5.2 General form of the solutions

In order to investigate the general structure of equation (3.29) it is useful to organise the zero modes for $\Delta\mathbf{r}^{(0)}$ as

$$\Delta\mathbf{r}_{\perp}^{(0)} = \hat{\mathbf{k}}_{\perp}; \quad \Delta\mathbf{r}_{\parallel}^{(0)} = \hat{\mathbf{k}}; \quad \Delta\mathbf{r}_{\mathbf{v}}^{(0)} = \sqrt{\frac{\beta m}{2}}\,\mathbf{v}\ , \tag{3.30}$$

where $\beta = 1/(k_{\mathrm{B}}T)$. The first mode consists of a perpendicular displacement, i.e., a spatial translation normal to the wave vector, the second mode to a parallel displacement, and the third one to a time translation.

The first mode is odd in $\hat{\mathbf{k}}_{\perp}$ and the last two even; the first two modes are even in $\mathbf{v}$ and the last one odd. The collision operators B_{S} and B_{Q} as well as the function $\hat{\mathbf{k}} \cdot \mathbf{v}$ are odd in $\hat{\mathbf{k}}_{\perp}$ to every order. The operators $\mathsf{B}_{\mathsf{S}}^{(n)}$ and $\mathsf{B}_{\mathsf{Q}}^{(n)}$ are even in $\mathbf{v}$ for even n and odd for odd n. On the basis of these parity properties, it follows immediately that the structure of equation (3.29), written as a matrix equation on the basis (3.30), is restricted to

$$\begin{aligned}(\lambda^{(1)})^2 \begin{pmatrix} 1 & 0 & 0 \\ 0 & 1 & 0 \\ 0 & 0 & 1 \end{pmatrix} + i\lambda^{(1)} \begin{pmatrix} 0 & 0 & 0 \\ 0 & 0 & x_{\mathbf{v},\parallel} \\ 0 & x_{\parallel,\mathbf{v}} & 0 \end{pmatrix} \\ - \begin{pmatrix} y_{\perp,\perp} & 0 & 0 \\ 0 & y_{\parallel,\parallel} & 0 \\ 0 & 0 & y_{\mathbf{v},\mathbf{v}} \end{pmatrix} = 0\ . \end{aligned} \tag{3.31}$$

The constants x and y are determined by temperature and by the form of the collision operators. From this it becomes clear that the equation can be split into two parts, one for the perpendicular zero mode, the transverse part, and one for the parallel zero mode and the time mode, the longitudinal part. From the general form of the matrices one can derive the general form of the Lyapunov exponents $\lambda = k\lambda^{(1)}$ to be

$$\lambda_{\mathrm{trans}} = \pm k\sqrt{y_{\perp,\perp}}\ , \tag{3.32}$$

$$\lambda_{\mathrm{long}} = \pm k\sqrt{y_1 \pm i\sqrt{y_2}}\ , \tag{3.33}$$

where y_1 and y_2 are functions of $x_{\mathbf{v},\parallel}$, $x_{\parallel,\mathbf{v}}$, $y_{\parallel,\parallel}$, and $y_{\mathbf{v},\mathbf{v}}$. The unnormalised

eigenvectors are

$$\Delta\mathbf{r}^{(0)}_{\text{trans}} = \hat{\mathbf{k}}_{\perp} \ , \tag{3.34}$$

$$\Delta\mathbf{r}^{(0)}_{\text{long}} = \hat{\mathbf{k}} + c\sqrt{\frac{\beta m}{2}}\,\mathbf{v} \ , \tag{3.35}$$

where c is a constant which can be found from the constante in equation (3.31). If $y_{\perp,\perp} > 0$, the Lyapunov exponent of the transverse mode is real and therefore the mode is of the same form as in the simulations reported in references [22, 23, 36]. If $y_2 > 0$, the longitudinal Lyapunov exponents have both real and imaginary components, and these modes also have the form of the longitudinal modes found in the simulations.

3.5.3 Density expansion

In many cases, expressions calculated using the Stoßzahlansatz become exact in the limit of vanishing density, for example in the case of transport coefficients of dilute gases [32]. It is interesting to investigate the behaviour of the Lyapunov exponents in this limit and compare it to the results found in the simulations. In the limit of vanishing density equation (3.29) reduces to

$$\langle\Delta\mathbf{r}^{(0)}|[\lambda^{(1)} + i(\hat{\mathbf{k}}\cdot\mathbf{v})]^2|\Delta\mathbf{r}^{(0)}\rangle - \langle\Delta\mathbf{r}^{(0)}|[i(\hat{\mathbf{k}}\cdot\mathbf{v})\mathsf{B}^{(0)}_{\mathsf{S}} + \mathsf{B}^{(1)}_{\mathsf{Q}}]|\Delta\mathbf{r}^{(1)}\rangle = 0 \ . \tag{3.36}$$

For this equation it is crucial indeed that $\Delta\mathbf{r}^{(1)}$ is of the order of n^{-1}. If there were no non-trivial right eigenfunctions of $\mathsf{B}^{(0)}_{\mathsf{Q}}$ with zero eigenvalue, $\Delta\mathbf{r}^{(1)}$ would be one order of n higher, and the second term would not contribute to the Lyapunov exponents in the limit of vanishing density.

In the following section the actual magnitudes of the two terms in equation (3.36) are discussed further.

3.6 Results and discussion

If only the first term in equation (3.29) is kept, the calculation is fairly simple. From now on we choose $d = 2$. The same calculations can easily be repeated for $d = 3$, but there are far fewer simulation results to compare to. Equation (3.31)

in this approximation becomes

$$(\lambda^{(1)})^2\frac{\beta m}{2}\begin{pmatrix}1&0&0\\0&1&0\\0&0&1\end{pmatrix}+i\lambda^{(1)}\sqrt{\frac{\beta m}{2}}\begin{pmatrix}0&0&0\\0&0&1\\0&1&0\end{pmatrix} - \begin{pmatrix}\frac{1}{2}&0&0\\0&\frac{1}{2}&0\\0&0&1\end{pmatrix}=0\ , \tag{3.37}$$

which is independent of the density. The solutions for the Lyapunov exponents then are

$$\lambda_{\text{trans}} = \pm\frac{k}{\sqrt{\beta m}}\ , \tag{3.38}$$

$$\lambda_{\text{long}} = \pm\frac{1}{2}\sqrt{1\pm i\sqrt{7}}\sqrt{\frac{2}{\beta m}}k \tag{3.39}$$

$$\approx (\pm 0.978 \pm i\ 0.676)\frac{k}{\sqrt{\beta m}}\ . \tag{3.40}$$

The structure of the corresponding eigenvectors is indeed like that found in simulations [22, 23].

To calculate the contribution from the second term in equation (3.29) to the leading order of the Lyapunov exponents, one has to choose a suitable basis in which to express the function $\Delta\mathbf{r}^{(1)}(\mathbf{v})$. The basis must be orthogonal with regard to the chosen inner product $\langle .|. \rangle$. Next, the matrix elements of the operators $\mathsf{B}_{\mathsf{S}}^{(i)}$ and $\mathsf{B}_{\mathsf{Q}}^{(i)}$ must be calculated between elements of the basis.

A simple, but suitable, basis is the set of functions that are products of Hermite polynomials in the components of $\mathbf{v}\sqrt{m\beta/2}$ parallel and perpendicular to the wave vector $\mathbf{k}$. The Hermite polynomials $H_i(x)$ form a complete orthogonal basis with regard to integration against $\exp(-x^2)$, and therefore their products will be orthogonal under the inner product used here. The solution to equation (3.20) can thus be expanded as

$$\Delta\mathbf{r}(\mathbf{v}) = \sum_{l,p,q}\mathbf{e}_l\, c_{l,p,q} H_p(v_\parallel)H_q(v_\perp)\ , \tag{3.41}$$

where l can be either $\perp$ or $\parallel$, $\mathbf{e}_\perp$ is $\hat{\mathbf{k}}_\perp$, and $\mathbf{e}_\parallel$ is $\hat{\mathbf{k}}$.

By truncating all expressions at some finite order in the polynomial expansion, one finds approximate values for $\lambda^{(1)}$. For good convergence one has to go beyond the zeroth- and first-order Hermite polynomials. In the appendix A more details are given on the matrix representations of the truncated operators and on the convergence of the Lyapunov exponents in dependence on the order of truncation.

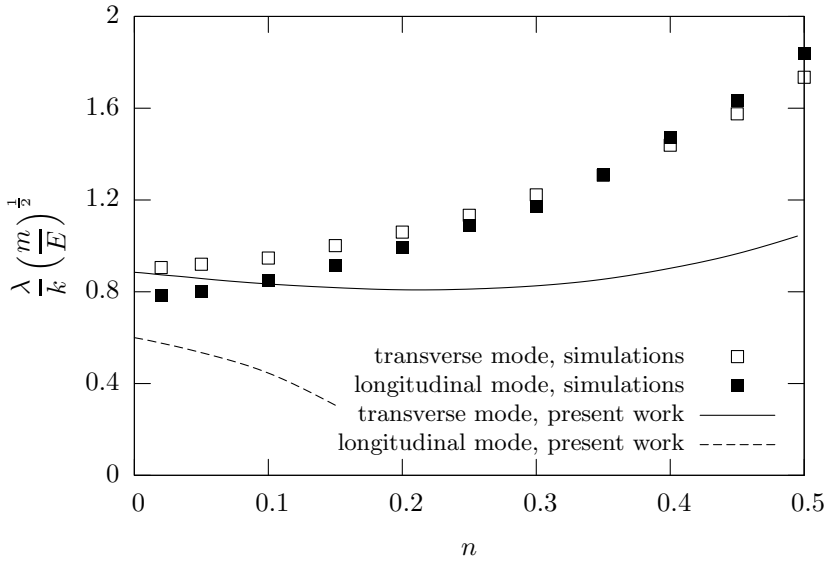

Figure 3.3: The Lyapunov exponents for transverse and longitudinal modes from the simulations [22, 23] compared to the present calculations.

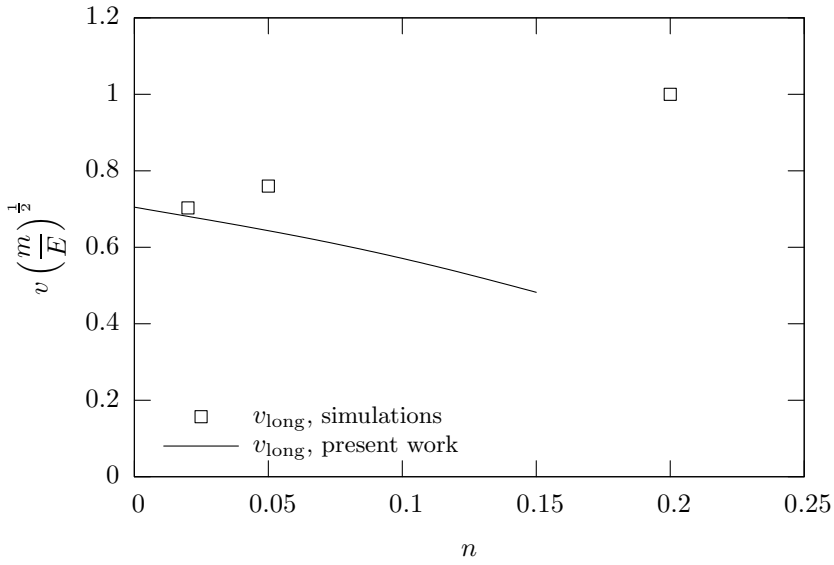

Figure 3.4: The velocities of the longitudinal mode from simulations [22, 23] compared to the present calculations.

In two dimensions, to sixth order in the polynomial expansion, the results in the limit of density going to zero are

$$\lambda_{\text{trans}} = \pm 0.886 \frac{k}{\sqrt{\beta m}} \,, \tag{3.42}$$

$$\lambda_{\text{long}} = \pm 0.607 \frac{k}{\sqrt{\beta m}} \,, \tag{3.43}$$

$$v_{\text{long}} = \pm 0.706 \frac{1}{\sqrt{\beta m}} \,. \tag{3.44}$$

With respect to equations (3.38)–(3.40) the corrections are largest for the Lyapunov exponent of the longitudinal mode.

For low densities the form of the modes is predicted correctly by the calculations; the modes are split into non-propagating transverse and propagating longitudinal modes. For number density $n = \rho a^2 = 0.02$, the Lyapunov exponents from the simulations are

$$\lambda_{\text{trans}} = \pm 0.906 \frac{k}{\sqrt{\beta m}} \,, \tag{3.45}$$

$$\lambda_{\text{long}} = \pm 0.783 \frac{k}{\sqrt{\beta m}} \,, \tag{3.46}$$

$$v_{\text{long}} = \pm 0.703 \frac{1}{\sqrt{\beta m}} \,. \tag{3.47}$$

The calculated Lyapunov exponent of the transverse mode and the propagation speed of the longitudinal mode compare to the values from the simulations, within 2% at $n = 0.02$. The Lyapunov exponent for the longitudinal mode deviates by about 25%.

The results for higher densities are displayed in figure 3.3. With increasing density the calculated values deviate increasingly from the simulation results. For the longitudinal mode the predicted real part of the Lyapunov exponent even drops to zero and the exponent becomes purely imaginary.

The deviations from the simulations can be attributed to contributions from ring terms and possibly other contributions to a generalised B_Q operator that are at most of order n^2. From equation (3.27) one sees that such terms, working on the non-trivial zero eigenfunctions of $\mathsf{B}_\mathsf{Q}^{(0)}$, contribute to the leading order terms in the density expansion of $\Delta\mathbf{r}^{(1)}$, just like $(\mathsf{B}_\mathsf{S}^{(0)})^2$. Therefore they have to be included in the second term in equation (3.36). So in contrast to usual applications of kinetic theory, where ring terms only contribute to higher orders in the density, in the present case they contribute to the leading order. In the present calculation these contributions are not included. Similarly, the ring terms will contribute to higher orders in a density expansion of the Lyapunov exponents. These contributions may be responsible for the discrepancies between simulation

results and Enskog theory for higher densities, which show up in figures 3.3 and 3.4. In section 3.7 the contributions from ring collisions are discussed in more detail. For more details on ring terms in kinetic theory, see reference [34].

It is interesting to compare our results to those by McNamara and Mareschal [30], who also based their work on kinetic-theory calculations. They do not derive equations for the distribution functions, but go directly to hydrodynamic-like equations for the moments. To close these, they make hypotheses to factorise the fluxes. The resulting values for the Lyapunov exponents in the low-density limit are less close to the simulation values than those from our calculations. It is not clear if in this treatment the effects of the non-trivial zero eigenfunctions of $\mathsf{B}_{\mathsf{Q}}^{(0)}$ are accounted for.

Forster and Posch have also done simulations on similar systems with soft potentials [39]. They roughly find a branch again of Lyapunov exponents close to zero, but the sinusoidal structure of the corresponding modes is much less clear. It would be interesting to calculate the Lyapunov exponents with kinetic-theory methods also for this case. It would also be interesting to look at small Lyapunov exponents in non-equilibrium systems. However, in such systems the calculations become more complicated because the stationary velocity distributions are no longer Maxwellian.

3.7 Ring collisions

Ring collisions are sequences of collisions where a number of particles collide with each other, directly or indirectly, more than once. For example, particle one collides with particle two, after which particle two collides with particle three and either two or three is bounced onto particle one. It is also possible for double rings or even more complicated sequences to occur. Some examples are displayed in figures 3.5 and 3.6.

Sequences of collisions of this type are ignored by the Stoßzahlansatz. In order to have a ring collision, either at least three particles must be close together, or one particle must have an outgoing velocity after a collision such that it will collide with a particle that is at a distance of the order of the mean free path.

In a finite system, eventually, every collision will be a ring collision. The rings, however, are extremely long, and the assumption is that any remaining correlations are negligible. Often, ring collisions contribute to macroscopic quantities only in the higher orders in the density. For the transport coefficients, the contributions from ring collisions in two dimensions are of order $n \log n$ compared to the leading order, and in three dimensions of order n. In the case of long time tails, however, ring collisions dominate (see, for example, references [15, 44, 45]).

As described in the previous section, such terms, working on the non-trivial zero eigenfunctions of $\mathsf{B}_{\mathsf{Q}}^{(0)}$, contribute to the leading order terms in the density expansion of $\Delta\mathbf{r}^{(1)}$, just like $(\mathsf{B}_{\mathsf{S}}^{(0)})^2$. Therefore they have to be included in the

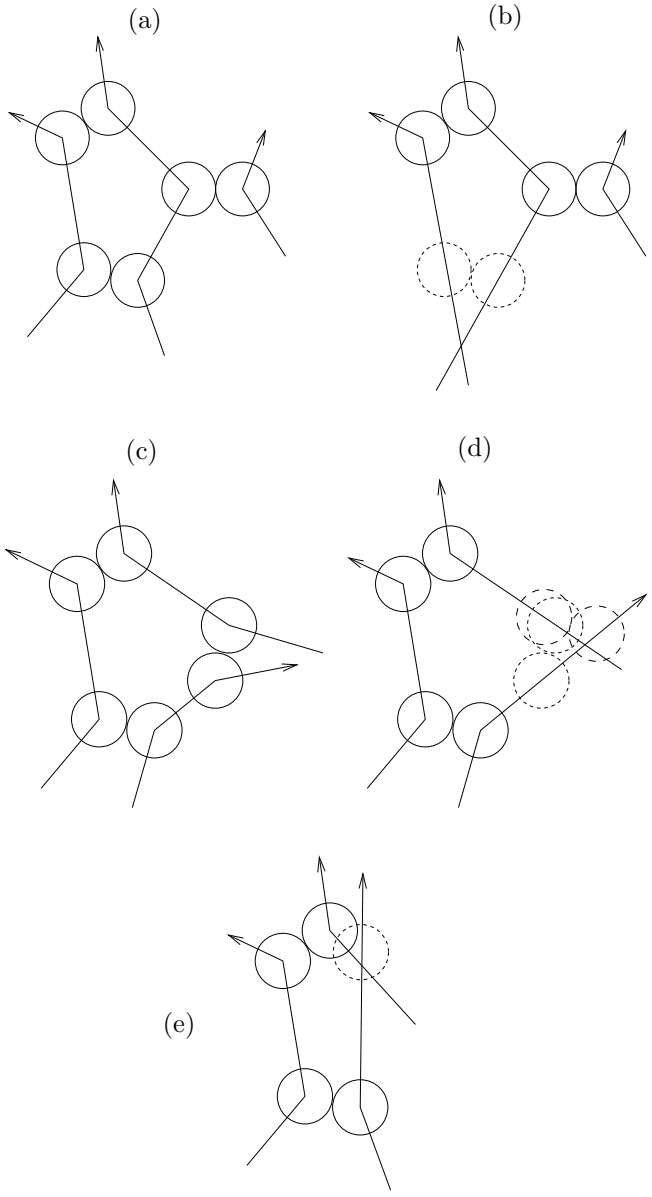

Figure 3.5: The various possibilities for the simplest configurations of ring collisions, three particles with three collisions. Figures (a) and (c) show the real ring collisions, and figures (b), (d), and (e) show the virtual counterparts.

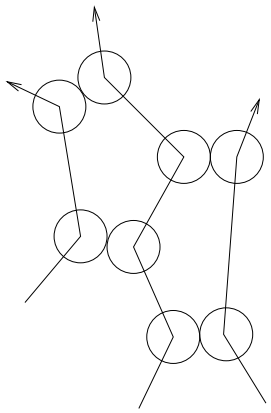

Figure 3.6: An example of a double ring collision involving four collisions and three particles. Such collisions are a factor of n more rare than single rings.

second term in equation (3.36). So in contrast to usual applications of kinetic theory, where ring terms only contribute to higher orders in the density, they contribute to the leading order in the present case.

To find the contributions from ring collisions to the collision operators, the effects of the perturbation expansions of the collision operators working on $\Delta\mathbf{r}$ and $\Delta\mathbf{v}$ must be calculated for a ring collision.

The collision parameters except for the outgoing velocity of one of the particles must be integrated out against the proper probability distributions, just as in the case of the collision operators in equations (3.18) and (3.19). This includes the collision times and the collision normals of all the collisions, as well as the velocities of all but one particle. The collision parameters of the collisions are not independent of each other, since one collision must be configured in such a way as to close the ring. The contributions consist of sums of products of I, S, and Q belonging to various collisions and τ between the collisions, multiplied by the probability of the configuration, and integrated over the collision parameters.

The corrections to B_S can be calculated when it works on $\Delta\mathbf{r}$ or when it works on $\Delta\mathbf{v}$. The results of these calculations differ. It is therefore necessary to write B_S in equations (3.16) and (3.17) as $\tilde{\mathsf{B}}_{\mathsf{S}\mathbf{r}}$ or $\tilde{\mathsf{B}}_{\mathsf{S}\mathbf{v}}$, depending on which part of the tangent space it works on. After this modification equations (3.26) and (3.29)

read,

$$[-\tilde{\mathsf{B}}^{(0)}_{\mathsf{Sv}}(i\hat{\mathbf{k}}\cdot\mathbf{v}-\tilde{\mathsf{B}}^{(1)}_{\mathsf{Sr}})-\tilde{\mathsf{B}}^{(1)}_{\mathsf{Q}}]\Delta\mathbf{r}^{(0)}=-[\tilde{\mathsf{B}}^{(0)}_{\mathsf{Sv}}\tilde{\mathsf{B}}^{(0)}_{\mathsf{Sr}}-\tilde{\mathsf{B}}^{(0)}_{\mathsf{Q}}]\Delta\mathbf{r}^{(1)}\ , \tag{3.48}$$

$$\begin{aligned}\langle\Delta\mathbf{r}^{(0)}|[(\lambda^{(1)}+i\hat{\mathbf{k}}\cdot\mathbf{v}-\tilde{\mathsf{B}}^{(1)}_{\mathsf{Sv}})(\lambda^{(1)}+i\hat{\mathbf{k}}\cdot\mathbf{v}-\tilde{\mathsf{B}}^{(1)}_{\mathsf{Sr}})-\tilde{\mathsf{B}}^{(2)}_{\mathsf{Q}}]|\Delta\mathbf{r}^{(0)}\rangle\\ +\langle\Delta\mathbf{r}^{(0)}|[-(i\hat{\mathbf{k}}\cdot\mathbf{v}-\tilde{\mathsf{B}}^{(1)}_{\mathsf{Sv}})\tilde{\mathsf{B}}^{(0)}_{\mathsf{Sr}}-\tilde{\mathsf{B}}^{(1)}_{\mathsf{Q}}]|\Delta\mathbf{r}^{(1)}\rangle=0\ .\end{aligned} \tag{3.49}$$

Here $\tilde{}$ has been used to indicate collision operators which include both ring collisions and uncorrelated collisions. From symmetries of the collision matrices and the form of this equation, some statements can be made about the sizes and relevance of the contributions from the various collision operators.

3.7.1 Real and virtual ring collisions

Not only have ring collision been ignored by the Stoßzahlansatz, also collision sequences have been allowed in which, at some point in the future or past, two particles pass through each other. Because the particles have already (indirectly) encountered each other before, such an overlap, in the Stoßzahlansatz approximation, cannot lead to a collision. This situation is called a virtual ring collision. To calculate the ring collision contribution to a quantity, one must calculate the contributions from real ring collisions and subtract the contributions from virtual ring collisions. If the contributions from a real collision is equal to the contribution of it's virtual counterpart, this means that the total contribution cancels. In figure 3.5 a few different configurations of ring collisions are shown, along with their virtual counterparts. An example of a double ring collision is show in figure 3.6.

3.7.2 Long collision times

The τ factors could potentially become large, since $\tau\sim 1/n$. This means that a priori there is no reason why long rings would not contribute strongly, even to lower orders in the density than the terms from normal collisions. Simply put, the slow modes could couple strongly to faster growing modes and then back to slow modes through ring collisions. This could, in principle, lead to contributions to the collision operators from the faster growing modes, of order $\bar{\nu}n\log n$. Because of the restrictions of equation (3.15), the Lyapunov exponents calculated in the previous sections for the Goldstone modes can be at most of order n.

In the case of the perturbed collision operators, there are extra factors due to the difference in positions before and after the ring. If the free paths are large, this means that the first and second order in the wave vector corrections are, respectively, one and two orders lower in the density than the zeroth order. This could give rise to large contributions.

3.7.3 Zero modes

The zero modes are exact eigenvectors of the collision matrices, with eigenvalues one. The virtual and real collisions, therefore, work in the same way on the zero modes, but contribute to the collision operators with opposite sign. This means that the contributions from the real ring collisions are cancelled exactly by those from the virtual collisions for any collision operator working on the zero modes, on the right or on the left. This includes collision operators that are of higher order in k.

As a consequence many terms in equations (3.26) and (3.29) cannot yield any leading-order ring-collision contributions to the smallest Lyapunov exponents. Only ring-collision terms in $\mathsf{B}_{\mathsf{Q}}^{(0)}$ on the right-hand side of equation (3.48) may contribute to the lowest order in density.

3.8 Conclusions

In this chapter, it has been demonstrated how Lyapunov exponents close to zero are related to Goldstone modes. The dependence on the wave number was found to be qualitatively consistent with numerical results. The behaviour of the tangent-space eigenvectors was also found correctly. This was achieved through a kinetic-theory approach, in which we used a molecular chaos assumption for the pair-distribution function to derive an equation similar to the Enskog equation. For low densities this reduces effectively to a generalised Boltzmann equation.

The calculated values for the exponents belonging to the transverse modes at low densities are within a few percent of the values found in the simulations [22, 23]. The propagation velocity for the transverse mode is within 1% of the simulation values. The value for the Lyapunov exponent belonging to the longitudinal mode deviates from the simulations by 25%. For increasing densities, the predicted values deviate increasingly from the values found in the simulations. These deviations are probably due to contributions from ring collisions and similar terms. In most applications of the Boltzmann equation such terms produce contributions to the relevant quantities which are of higher order in the density, but in the calculation presented in this chapter they turn out to contribute to the leading order, as a consequence of the non-trivial zero eigenfunctions of one of the collision operators.

Chapter 4

The Kolmogorov-Sinai entropy of dilute hard spheres

4.1 Introduction

The Kolmogorov-Sinai entropy of a dynamical system describes the maximal rate at which the system produces information about its phase-space trajectory. In systems without escape, it equals the sum of all positive Lyapunov exponents. In systems with escape, the Kolmogorov-Sinai entropy also involves the escape rate of trajectories from the system. Because of this it may be connected to transport coefficients [7–10].

In this chapter, again a system consisting of hard, spherical particles is considered at small number density n, in d dimensions ($d = 2, 3$). The Kolmogorov-Sinai entropy is calculated in the low-density approximation with the aid of kinetic theory. It is found to behave as

$$h_{\mathrm{KS}} = N\bar{\nu}A\left[\log(na^d) + B + O(na^d) + O\left(\frac{1}{N}\right)\right] \ . \tag{4.1}$$

The constants A and b have been calculated by van Beijeren et al. [31], but the

results found for B were unsatisfactory when compared to simulation results. In this chapter, a similar, but more satisfactory, calculation of B is presented, and compared to simulation results. The difference is due to the fact that not all components of $\delta\mathbf{v}_i$ are assumed to be multiplied by a factor $\sim 1/n$ at a collision. Contributions to the growth of the stretching factor that were ignored previously are taken into account in the present calculation.

4.2 Kolmogorov-Sinai entropy

In standard terminology, the stretching factor $\Lambda(t)$ is defined as the factor by which the expanding part of tangent space stretches over a time t. This quantity can be used to calculate the Ruelle pressure as well as the sum of the positive Lyapunov exponents, which is equal to the Kolmogorov-Sinai entropy in systems without escape [19, 20, 46]. For long times, the stretching is dominated by the positive Lyapunov exponents, and one has for the Kolmogorov-Sinai entropy

$$h_{\mathrm{KS}} = \lim_{t\to\infty} \frac{1}{t} \log \Lambda(t) \ . \tag{4.2}$$

For long times, the stretching factor can be calculated from the total growth of an arbitrary volume element in dN dimensions. After a few Lyapunov times (defined as the inverse of the smallest positive Lyapunov exponent), the dynamics project the volume element onto the expanding manifold and its subsequent growth is described completely by the stretching factor.

For hard-sphere systems, where the collision times are exactly defined, the stretching factor can be written as the product of stretching factors resulting from each of the different single collisions combined with the subsequent free flights of the two particles involved. In this description, the effects of the free flights of the other particles have already been accounted for at their most recent collisions. On the right-hand side of equation (4.2), the logarithm may be replaced by the sum of logarithms of these stretching factors. The resulting expression may be interpreted as a time average, which in ergodic systems may be replaced by an ensemble average. Hence,

$$h_{\mathrm{KS}} = \frac{N\bar{\nu}}{2} \langle \log \Lambda_i \rangle \ . \tag{4.3}$$

Here Λ_i is the single-collision stretching factor due to collision i. To obtain the Kolmogorov-Sinai entropy, the distribution of single-collision stretching factors must be calculated.

4.2.1 Projection

The growth of a dN-dimensional volume element in $\delta\Gamma$ can be monitored through its projection onto a subspace of $\delta\Gamma$ with at least the same number of dimen-

sions, as long as this projection space is not orthogonal to one of the dN leading eigenvectors of M. In the limit $t \to \infty$, the logarithm of the determinant of the transformation of the projection yields the same Kolmogorov-Sinai entropy as the logarithm of the stretching factor of the actual volume element.

If $(\delta\mathbf{r}_i^{(m)}, \delta\mathbf{v}_i^{(m)})$ are the eigenvectors belonging to the positive exponents, the eigenvectors which belong to their partners under conjugate pairing are equal to $(\delta\mathbf{r}_i^{(m)}, -\delta\mathbf{v}_i^{(m)})$. This means that eigenvectors which have no contributions along either $\delta\mathbf{r}_i$ or $\delta\mathbf{v}_i$ correspond to themselves under conjugate pairing. Such eigenvectors must therefore have Lyapunov exponents which are zero. The spaces spanned by either $\delta\mathbf{r}$ or $\delta\mathbf{v}$ are not orthogonal to any eigenvectors which belong to non-zero Lyapunov exponents. The dN-dimensional vectors whose components belonging to particle i are $\delta\mathbf{r}_i$ and $\delta\mathbf{v}_i$ are denoted by $\delta\mathbf{r}$ and $\delta\mathbf{v}$. In the system described here a convenient choice for the projection space may therefore be either of these spaces. Here, $\delta\mathbf{v}$ is used for this purpose, because it does not change during free flights.

4.2.2 Stretching factor of a single collision

During a free flight, $\delta\mathbf{r}$ grows with $\delta\mathbf{v}$. In previous calculations, it was always assumed that right after a collision $\delta\mathbf{r}_i$ and $\delta\mathbf{v}_i$ were of the same order of magnitude [31]. Under this assumption, in the $\delta\mathbf{r}_i$ just before a collision, the contribution from $\delta\mathbf{r}_i$ just after the previous collision may be neglected compared to $\tau_i\delta\mathbf{v}_i$, where τ_i is the free-flight time of particle i. Note that τ_i is typically of the order of $1/\bar{\nu}$. Of course $\tau_i\delta\mathbf{v}_i$ will be comparable to $\delta\mathbf{r}_i$ after the previous collision if τ_i is short. However this occurs only with a probability proportional to the density and therefore may be neglected.

The assumption that $\delta\mathbf{r}_i$ and $\delta\mathbf{v}_i$ just after a collision are of the same order of magnitude, however, is only true for $d-1$ components of $\delta\mathbf{r}_i - \delta\mathbf{r}_j$, namely the ones normal to $\hat{\mathbf{v}}_{ij}$. The remaining components of $\delta\mathbf{r}_i$ and $\delta\mathbf{r}_j$, along $\hat{\mathbf{v}}_{ij}$ and in the centre-of-mass coordinates, are, after a collision, larger by an order of τ than the corresponding component of $\delta\mathbf{v}_i$, because Q, defined in equation (2.21), does not act on centre-of-mass vectors, nor on perturbations of relative coordinates parallel to the relative velocity. In these directions, the components of $\delta\mathbf{v}$ are still of the same order of magnitude as before the collision, but the corresponding components of $\delta\mathbf{r}_i$ have grown linearly during the preceding free flights. We will show that this phenomenon affects the Kolmogorov-Sinai entropy, even at low density.

The determinant of the transformation of the dN-dimensional volume element projected onto $\delta\mathbf{v}$ depends on $\delta\mathbf{r}$ before the collision. $\delta\mathbf{r}$ may be assumed to depend on $\delta\mathbf{v}$ as

$$\delta\mathbf{r} = \bar{\tau}\mathcal{W} \cdot \delta\mathbf{v} \ , \tag{4.4}$$

with $\bar{\tau} = 1/\bar{\nu}$ the average free-flight time. The matrix $\mathcal{W}$ can be split up into

$d \times d$ matrices between specific particles, W_{ij}. As particles collide and have free flights, W_{ij} changes. The volume element projected onto $\delta\mathbf{v}$ before the collision is mapped to a projection of a volume element after the collision. The determinant of this map depends on $\mathsf{W}_i, \mathsf{W}_j, \mathsf{W}_{ij}$, and W_{ji}, where the second index is omitted if it is the same as the first.

After the collision, $\mathcal{W}$ is changed. The matrix $\mathcal{W}$ after the collision, $\mathcal{W}^*$, can be found by using the dynamics and equation (4.4) to express $\delta\mathbf{r}^*$ just after the collision in terms of $\delta\mathbf{v}^*$, the collision matrices and $\mathcal{W}$. Let $\mathcal{S}$ and $\mathcal{Q}$ be the $dN \times dN$-dimensional matrices which perform the transformations of S and Q on the components of $\delta\mathbf{r}$ and $\delta\mathbf{v}$ along the colliding particles, as described in equations (2.16)–(2.19) and act as the unit operator on the components belonging to all other particles. The transformation can be written as

$$\delta\mathbf{v}' = (\mathcal{I} + \mathcal{S}) \cdot \delta\mathbf{v} + \mathcal{Q} \cdot \delta\mathbf{r} \tag{4.5}$$

$$= (\mathcal{I} + \mathcal{S} + \bar{\tau}\mathcal{Q} \cdot \mathcal{W}) \cdot \delta\mathbf{v} \ , \tag{4.6}$$

$$\delta\mathbf{r}^* = (\mathcal{I} + \mathcal{S}) \cdot \delta\mathbf{r} = \bar{\tau}(\mathcal{I} + \mathcal{S}) \cdot \mathcal{W} \cdot \delta\mathbf{v} \ . \tag{4.7}$$

Here, $\mathcal{I}$ is the $dN \times dN$ identity matrix. This leads to an expression for $\delta\mathbf{r}_i^*$ as a function of $\delta\mathbf{v}_i^*$,

$$\delta\mathbf{r}^* = \hat{\tau}\mathcal{W}^* \cdot \delta\mathbf{v}^* \ , \tag{4.8}$$

where $\mathcal{W}^*$ can be expressed in terms of $\mathcal{W}$ and the collision matrices, as

$$\mathcal{W}^* = (\mathcal{I} + \mathcal{S}) \cdot \mathcal{W} \cdot (\mathcal{I} + \mathcal{S} + \bar{\tau}\mathcal{Q} \cdot \mathcal{W})^{-1} \ . \tag{4.9}$$

Using $(\mathcal{I} + \mathcal{S})^{-1} = \mathcal{I} + \mathcal{S}$, one may write this more conveniently as

$$\mathcal{W}^* = (\mathcal{I} + \mathcal{S}) \cdot [\mathcal{W}^{-1} + \bar{\tau}(\mathcal{I} + \mathcal{S}) \cdot \mathcal{Q}]^{-1} \cdot (\mathcal{I} + \mathcal{S}) \ . \tag{4.10}$$

At low densities, two particles which collide can be assumed to be uncorrelated before the collision (Stoßzahlansatz). This means that all elements of W_{ij} with $i \neq j$ are zero. After the collision there are in general non-zero elements in W_{ij}.

During free flight W_i also changes. Let τ_i be the free-flight time of particle i after the collision. Then, after the free flight,

$$\begin{cases} \mathsf{W}_k' = \mathsf{W}_k^* + \mathbf{1}\bar{\nu}\tau_k & \text{if} \quad k = i, j \ , \\ \mathsf{W}_k' = \mathsf{W}_k^* & \text{if} \quad k \neq i, j \ . \end{cases} \tag{4.11}$$

Note that the change in $\delta\mathbf{r}_k$ with $k \neq i, j$, due to free flights was already taken into account at the last collision of particle k. The matrix $\mathcal{W}$ as it is calculated here describes the connection between $\delta\mathbf{r}_i$ just before the next collision of particle i and $\delta\mathbf{v}_j$ just before the next collision of particle j.

The matrix $(\mathcal{I}+\mathcal{S})\cdot\mathcal{Q}$ is non-negative definite and symmetric. If $\mathcal{W}$ is positive definite, so is its inverse. This means that $\mathcal{W}^{-1}+\bar{\tau}(\mathcal{I}+\mathcal{S})\cdot\mathcal{Q}$ is positive definite, as is its inverse. The coordinate reflection $\mathcal{I}+\mathcal{S}$ is unitary, and therefore the eigenvalues of $(\mathcal{I}+\mathcal{S})\cdot\mathcal{W}^*\cdot(\mathcal{I}+\mathcal{S})$ are the same as those of $\mathcal{W}^*$. Therefore, $\mathcal{W}^*$ is positive definite. By similar reasoning, a symmetric $\mathcal{W}$ is mapped onto a symmetric $\mathcal{W}^*$. Equation (4.11) also maps non-negative definite matrices onto positive definite matrices, and symmetric ones onto symmetric ones. As, without loss of generality, any initial conditions for $\mathcal{W}$ may be chosen, it is possible to choose them such that $\mathcal{W}$ is positive definite and symmetric. This can be done, for example, by choosing the initial $\mathcal{W}$ to be diagonal, with elements equal to 1.

The stretching factor due to one collision can be calculated from the determinant of the transformation of the projection onto the perturbations of the relative and centre-of-mass velocities, $(\delta\mathbf{v}_{ij},\delta\mathbf{V}_{ij})$. From equation (4.6), one finds that this is the determinant of $\mathcal{I}+\bar{\tau}(\mathcal{I}+\mathcal{S})\cdot\mathcal{Q}\cdot\mathcal{W}$.

In the low density limit, and with $\mathsf{W}_{ij}=0$, this is found to be equal to

$$\Lambda = w_{\perp\perp}\left(\frac{2v\bar{\tau}}{a}\right)^{d-1}\cos^{d-3}\theta\ . \tag{4.12}$$

Here, θ is the angle between $\hat{\sigma}$ and $\mathbf{v}$, $\cos\theta=\hat{\sigma}\cdot\hat{\mathbf{v}}$, and $w_{\perp\perp}$ is equal to the determinant of the part of $(\mathsf{W}_i+\mathsf{W}_j)/2$ between vectors that are orthogonal to $\hat{\mathbf{v}}_{ij}$ before the collision. For $d=2$,

$$w_{\perp\perp}=\hat{\mathbf{v}}_{ij\perp}\cdot\frac{\mathsf{W}_i+\mathsf{W}_j}{2}\cdot\hat{\mathbf{v}}_{ij\perp}\ . \tag{4.13}$$

This expression replaces $(\bar{\nu}\tau_+)^{d-1}$, where $\tau_+=(\tau_i+\tau_j)/2$, in previous calculations [31]. In d dimensions, $\hat{\mathbf{v}}_{ij\perp}$ must be replaced by a set of $d-1$ vectors orthogonal to $\hat{\mathbf{v}}_{ij}$. The inner products are replaced by the determinant of the $(d-1)\times(d-1)$ part of $(\mathsf{W}_i+\mathsf{W}_j)/2$ between those vectors.

4.3 Distribution functions

In order to calculate the Kolmogorov-Sinai entropy from equation (4.3), one needs the distribution function of the single-collision stretching factor, as described by equations (4.12) and (4.13). This may be derived from the joint distribution function of the collision parameters τ_i, τ_j, $\mathbf{v}_i$, $\mathbf{v}_j$, θ, and elements of W_i and W_j. In the low-density approximation, the collision parameters are distributed according to the equilibrium solutions of the Boltzmann equation, described in section 2.4.3. The distribution of the particle velocities is the Maxwell distribution. The free-flight times of the particles are distributed exponentially, with the collision frequency $\nu(\mathbf{v})$ depending on the velocity of the particle.

The distribution of $w_{\perp\perp}$ can be found by demanding that the distribution of elements of W_i as a function of $\mathbf{v}_i$ is not changed by collisions and free flights

with parameters distributed according to the solutions of the Boltzmann equation. This yields a complicated non-linear integral equation for the elements of $\mathcal{W}$. This equation involves the distribution of angles between relative velocities of subsequent collisions of a particle with velocity $\mathbf{v}_i$, as well as the velocity dependence of the collision frequency. The latter is only known numerically.

4.3.1 Approximation of the distribution of $w_{\perp\perp}$

If one were to start with some initial distribution function for the elements of W_{ij} and to iterate it using the known distributions of the collision parameters, one would find convergence to the solution of the integral equation. However, even with a simple initial distribution, such iterations will quickly produce distribution functions which can only be calculated numerically. In this section, a mean-field type of approach is used to find an approximate distribution function. We start with a simple distribution with one parameter, which approximates the average distribution. The parameter is then chosen in such a way that the average of the trace of $\mathcal{W}$ remains the same after a collision and free flights. The non-linear terms in the equation for the distribution of the elements of $\mathcal{W}$ are neglected. The equation is iterated a second time to include some of them. We estimate the size of the remaining terms.

In principle it would be possible to use the determinant or some other scalar function of $\mathcal{W}$, instead of the trace. It is however much easier to write down the map of the trace of $\mathcal{W}$ onto the trace of $\mathcal{W}^*$ in equation (4.10) than it is to write down a map of the determinant during free flights. Also, really only the distribution of diagonal elements of $\mathcal{W}$ is needed. Under unitary coordinate transformations, such as rotations and reflections, the trace of a matrix is conserved.

Let $\mathcal{W}_{\mathbf{l}}$ be the matrix $\mathcal{W}$ with all rows and columns removed except for those belonging to the indices specified by the list $\mathbf{l}$, where $\mathbf{l}$ may represent any number of indices. Similarly, let $\mathcal{W}_{(\mathbf{l})}$ be the matrix $\mathcal{W}$ with all rows and columns removed which belong to the indices specified by the list $\mathbf{l}$.

From equation (4.11), the trace of $\mathcal{W}'$ can be found to satisfy

$$\mathrm{Tr}(\mathcal{W}') = \mathrm{Tr}(\mathcal{W})^* + d\bar{\nu}\tau_i + d\bar{\nu}\tau_j \ . \tag{4.14}$$

From equation (4.10), the trace of $\mathcal{W}^*$ can be found as a function of $\mathcal{W}$. As the trace is conserved under the coordinate reflection $(\mathcal{I}+\mathcal{S})\cdot\mathcal{W}\cdot(\mathcal{I}+\mathcal{S})$, one finds

$$\mathrm{Tr}(\mathcal{W}^*) = \sum_k \frac{\det(\mathcal{W}^{-1}+\bar{\tau}(\mathcal{I}+\mathcal{S})\mathcal{Q})_{(k)}}{\det(\mathcal{W}^{-1}+\bar{\tau}(\mathcal{I}1+\mathcal{S})\mathcal{Q})} \ . \tag{4.15}$$

In the low-density limit the mean free time becomes large, and only terms in which the numerator contains the same power of $\bar{\tau}$ as the denominator can contribute. The subdeterminant of $(\mathcal{I}+\mathcal{S})\cdot\mathcal{Q}$ with respect to its zero eigenvectors can be divided out, leaving only the determinant of the remaining part of $\mathcal{W}$, between

vectors on which $\mathcal{Q}$ does not work. As only $(\mathcal{I}+\mathcal{S})\mathcal{Q}$ in equation (4.15) contains the collision normal, in the limit of vanishing density, the trace of $\mathcal{W}^*$ does not depend on θ, but only on $\hat{\mathbf{v}}_{ij}$ and the elements of $\mathcal{W}$.

Let the dN-dimensional basis vectors in which the matrices are expressed be numbered 1 through dN. Let the first dN-dimensional basis vector, ϵ_1, be defined as $\hat{\mathbf{v}}_{ij}$ in the relative coordinates, and the second (in d dimensions the second through d-th), ϵ_2, as $\hat{\mathbf{v}}_{ij\perp}$ in the relative coordinates. $\mathcal{W}^{-1}_{(k)}$ and $\mathcal{W}^{-1}_{(k2)}$ represent the matrix $\mathcal{W}^{-1}$ from which the rows and columns belonging to, respectively, index k and both index k and index 2 are removed. The trace can be rewritten as the sum over fractions of subdeterminants,

$$\mathrm{Tr}(\mathcal{W}^*) = \sum_{k\neq 2} \frac{\det(\mathcal{W}^{-1}_{(k2)})}{\det(\mathcal{W}^{-1}_{(2)})} \ . \tag{4.16}$$

By writing the inverse of the inverse matrix and by working out the determinant of $\mathcal{W}_{\mathbf{l}}$, it is possible to prove by using induction over the number of indices represented by $\mathbf{l}$ that

$$\det \mathcal{W}^{-1}_{(\mathbf{l})} = \det \mathcal{W}_{\mathbf{l}} \det \mathcal{W}^{-1} \ . \tag{4.17}$$

From equations (4.17) and (4.16) one finds, for $d = 2$,

$$\mathrm{Tr}(\mathcal{W}^*) = \sum_{k\neq 2} \frac{\det(\mathcal{W}_{k2})}{\det \mathcal{W}_2} \tag{4.18}$$

$$= \mathrm{Tr}(\mathcal{W}) - \frac{1}{w_{\perp\perp}} \epsilon_2 \cdot \mathcal{W}^2 \cdot \epsilon_2 \ . \tag{4.19}$$

In the d-dimensional case ϵ_2 is replaced by $d-1$ vectors, and equation (4.19) becomes somewhat more complicated.

The change in off-diagonal elements at a collision can be found from a derivation similar to that of the trace elements in equation (4.19). If $p, q \neq 2$, for $d = 2$,

$$\epsilon^*_p \cdot \mathcal{W}^* \epsilon^*_q = \epsilon_p \cdot \mathcal{W} \cdot \epsilon_q - \frac{(\epsilon_p \cdot \mathcal{W} \cdot \epsilon_2)(\epsilon_2 \cdot \mathcal{W} \cdot \epsilon_q)}{\epsilon_2 \cdot \mathcal{W} \cdot \epsilon_2} \ . \tag{4.20}$$

The expression for $d = 3$ is similar. If p or q is equal to 2, the off-diagonal element vanishes. Off-diagonal elements between different particles are not affected by free flights, as is apparent from equation (4.11).

The collisions are most conveniently expressed in the basis which consists of $\hat{\mathbf{v}}_{ij}$ and the $d-1$ vectors $\hat{\mathbf{v}}_{ij\perp}$ orthogonal to it. We therefore also express each W_{ij} in this basis.

Mean-field approximation

Assume that just before a collision, the W_i are equal to their averages and W_{ij} are equal to zero. If the distribution of the angle between the relative velocities of two consecutive collisions is (nearly) isotropic, the two average diagonal elements are (approximately) equal. In this case, the matrix is

$$\mathsf{W}_{ij} = \bar{w}\mathbf{1}\delta_{ij} \ , \tag{4.21}$$

where δ_{ij} is the Kronecker delta function. The initial distribution used in the iteration process is a product of Dirac delta functions at the average value $\bar{w}$ for the diagonal elements and zero for the off-diagonal elements. In a similar way, an exponential distribution function can be used, with average $\bar{w}$, to test the sensitivity to the width of the distribution.

Using equations (4.10) and (4.11) one finds that after the collision and free flight, in the basis consisting of $\hat{\mathbf{v}}_{ij}$ and the $d-1$ vectors orthogonal to it, the values of W_{kl} are changed according to

$$\mathsf{W}'_{kl} = \begin{cases} \begin{pmatrix} (\bar{w}+\bar{\nu}\tau_k) & 0 \\ 0 & (\frac{1}{2}\bar{w}+\bar{\nu}\tau_k)\mathbf{1}_{d-1} \end{pmatrix} & \text{if } k=l=i \vee k=l=j \ , \\ \begin{pmatrix} 0 & 0 \\ 0 & -\frac{1}{2}\bar{w}\mathbf{1}_{d-1} \end{pmatrix} & \text{if } (k,l)=(i,j) \vee (k,l)=(j,i) \ , \\ \bar{w}\,\mathbf{1}\,\delta_{kl} & \text{if } k\neq i,j \vee l \neq i,j \ , \end{cases} \tag{4.22}$$

where $\mathbf{1}_{d-1}$ is used to denote the $(d-1)$-dimensional identity matrix. This equation implies a distribution for the elements of W'_{ij} expressed in the basis belonging to the next collision, which consists of $\hat{\mathbf{v}}'_{ij}$ and the $d-1$ vectors orthogonal to it, $\hat{\mathbf{v}}'_{ij\perp}$. The new distribution of the matrix elements is the distribution of W_{kl} in the coordinates of the next collision, $\mathcal{R}_i \cdot \mathsf{W}'_{kl} \cdot \mathcal{R}_i^T$, where $\mathcal{R}_i$ is the rotation matrix associated with the rotation from the coordinate system using the post-collisional relative velocity of a collision to the system using the pre-collisional relative velocity of the next collision of the same particle. In two dimensions, this matrix is characterised by the angle ϕ_i between the relative velocities at the two collisions,

$$\mathcal{R}_i = \begin{pmatrix} \cos\phi_i & \sin\phi_i \\ -\sin\phi_i & \cos\phi_i \end{pmatrix} \ . \tag{4.23}$$

The distribution of this angle can be denoted by $p_\phi(\phi_i, v_i)$. In three dimensions, the angle ϕ_i is replaced by two angles.

From this approximation a distribution function of $w_{\perp\perp}$ can be found, which depends on $\bar{w}$. At the next collision, for $d = 2$, it is equal to the distribution of

$$w'_{\perp\perp} = \frac{1}{2}\hat{\mathbf{v}}'_{ij} \cdot (\mathsf{W}'_i + \mathsf{W}'_j) \cdot \hat{\mathbf{v}}'_{ij} \tag{4.24}$$

$$= \frac{1}{2}(0,1) \cdot (\mathcal{R}_i \cdot \mathsf{W}'_i \cdot \mathcal{R}_i^T + \mathcal{R}_j \cdot \mathsf{W}'_j \cdot \mathcal{R}_j^T) \cdot (0,1) \tag{4.25}$$

$$= \bar{w}\left[1 - \frac{1}{4}(\cos^2\phi_i + \cos^2\phi_j)\right] + \bar{\nu}\tau_+ \ . \tag{4.26}$$

The distribution of $w_{\perp\perp}$ can be approximated by the distribution of the right-hand side of the equation. In three dimensions, the rotation matrix is more complicated, and so equation (4.26) becomes more complicated. The resulting expressions are not reproduced here.

From equation (4.22) one can find the difference between the areasonable verage traces of $\mathcal{W}'$ and $\mathcal{W}$. In the reasonable approximation that $\langle\cos^2\phi_i\rangle = \frac{1}{2}$,

$$\langle \mathrm{Tr}(\mathcal{W}')\rangle - \mathrm{Tr}(\mathcal{W}) = 2d - (d-1)\bar{w} \ , \tag{4.27}$$

where the notation $\langle . \rangle$ is used to denote an average. As the average trace must not be changed, one finds for $\bar{w}$ the approximation

$$\bar{w}^{(0)} = \frac{2d}{d-1} = \begin{cases} 4 & \text{if } \ d = 2 \ , \\ 3 & \text{if } \ d = 3 \ . \end{cases} \tag{4.28}$$

Note that the result for $\bar{w}$ would have been the same if an initial exponential distribution was used. The resulting distribution function for $w_{\perp\perp}$, however is different in that case. The distribution function implied by equation (4.26) for $w_{\perp\perp}$ at the next collision can be used to estimate the Kolmogorov-Sinai entropy from equations (4.3) and (4.12).

The approximation so far is fairly crude. The non-linearity of equation (4.10) has been partially neglected by using the averages of the off-diagonal elements. In the second term in the calculation of the trace in equation (4.19) only the block diagonal terms, those of the form $\hat{\mathbf{v}}_{\perp ij} \cdot \mathsf{W}_i^2 \cdot \hat{\mathbf{v}}_{\perp ij}$, were involved. In reality, since $\mathcal{W}$ is positive definite, the terms involving off-diagonal elements will produce strictly negative contributions to the average of the trace in equation (4.19).

A better approximation of the average value can be found by iterating the equation for the distribution a second time. The distribution of $\mathcal{R}_i \cdot \mathsf{W}'_{kl} \mathcal{R}_i^T$ can be used to calculate the trace of $\mathcal{W}''$. The colliding particles are independent of each other before the collision, but not independent of the particles they encountered before. These particles, which are not directly involved in the collision, now contribute to the change in the trace, through the second term on the right-hand side of equation (4.19). We find that for $d = 2$ the trace in the low density

approximation satisfies

$$\langle \mathrm{Tr}(\mathcal{W}'')\rangle - \langle \mathrm{Tr}(\mathcal{W}')\rangle = -3\bar{w} + \big\langle \big[2\bar{\nu}^2(\tau_i^2 + 4\tau_i\tau_j + \tau_j^2) + 10\bar{\nu}(\tau_i+\tau_j)\bar{w} + 8\bar{w}^2 - 2\bar{w}\bar{\nu}(\tau_i\cos^2\phi_j + \tau_j\cos^2\phi_i) - \bar{w}^2(\cos^2\phi_i + \cos^2\phi_j)\big] \Big/ \big[2\bar{\nu}(\tau_i+\tau_j) + 4\bar{w} - \cos^2\phi_i - \cos^2\phi_j\big]\big\rangle \ . \quad (4.29)$$

This yields an equation for $\bar{w}$ that is better than equation (4.28).

More iterations would produce more terms and will further reduce the value of $\bar{w}$. A similar but far more complicated expression can be found for $d = 3$ from equations (4.19), (4.22), and the general form of the three-dimensional rotation matrix. The results would be better if the distribution were iterated again, but this would produce expressions of complexity increasing exponentially with the number of iterations. One more iteration would add four angles and four free-flight times to the expression in equation (4.29). The second iteration already produces a reasonable result. Also, after one more iteration, the expression for $w''_{\perp\perp}$ is quite complicated and contains twelve correlated variables, six rotation angles and six free flights. We therefore continue using the distribution of $w'_{\perp\perp}$, but with the value of $\bar{w}$ found from equation (4.29).

The integration over the distribution of ϕ_i, ϕ_j, τ_i, and τ_j can be done numerically. The change in the trace is zero for for $\bar{w}$ equal to

$$\bar{w}_1^{(1)} = \begin{cases} 3.009 & \text{if } \ d = 2 \ , \\ 2.107 & \text{if } \ d = 3 \ . \end{cases} \quad (4.30)$$

If the contributions to the trace from the off-diagonal elements involving the other particles from the previous collisions, through the second term on the right-hand side of equation (4.19), are ignored, the result is changed significantly. In this case,

$$\bar{w}_0^{(1)} = \begin{cases} 3.408 & \text{if } \ d = 2 \ , \\ 2.639 & \text{if } \ d = 3 \ . \end{cases} \quad (4.31)$$

At a collision between i and j, the off-diagonal elements between particles i and k produce significant changes to the diagonal elements of W'_{kk}. It is therefore expected that contributions from particles involved in collisions before the previous collision will also be significant. Also, if the other particle from the previous collision of particle i has collided since, this has an effect on W_i.

Off-diagonal elements from earlier collisions

At a collision between particles q and r, the change in the trace of $\mathcal{W}$, calculated in equation (4.19), is affected by the elements of $\mathcal{W}$ between q or r, and other particles. After a collision between two particles, non-zero off-diagonal elements

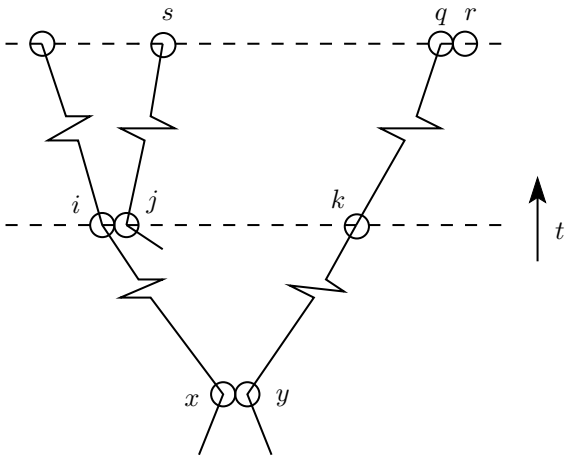

Figure 4.1: At the collision between particles q and r, the off-diagonal elements between q and particle s contribute to the change in the trace, as shown in equation (4.19). These elements date from the collision between particles x and y, in the common history of q and s. At some point in the past, there were elements between a particle i in the history of s and a particle k in the history of q when j, another particle in the history of s, collided with i. After the collision there were elements between j and k, which, through more collisions, eventually lead to elements between s and q. The size of the elements between s and q can be estimated using equations (4.36) and (4.37).

exist between these particles. After a collision between i and j, off-diagonal elements between particles i and k generate off-diagonal elements between j and k, due to the exchange between the $\delta\mathbf{v}_i$ and $\delta\mathbf{v}_j$. If non-zero off-diagonal elements exist between i and k as well as j and l before the collision, after the collision non-zero elements will exist between k and l. A diagrammatic representation of the collision sequence is shown in figure 4.1.

In order to estimate how much such terms contribute to the change in the trace at a collision involving particle k, the typical magnitude of the off-diagonal elements at a collision must be investigated. One may estimate the typical changes in the off-diagonal blocks W_{ik} and W_{jk} at a collision between i and j, by estimating the changes in the trace of the off-diagonal blocks. The typical size of the off-diagonal elements can be characterised by the trace of the off-diagonal block W_{ik}. The diagonal elements of the off-diagonal blocks can be found from equation (4.20). Using the fact that W_{ij} before the collision is zero, one finds, in

two dimensions, for the elements of $\mathcal{W}$ between $\delta\mathbf{r}_i$ and $\delta\mathbf{v}_k$

$$\begin{aligned}\hat{\mathbf{v}}_{ij}\cdot\mathsf{W}'_{ik}\cdot\hat{\mathbf{e}} &= \hat{\mathbf{v}}_{ij}\cdot\mathsf{W}_{ik}\cdot\hat{\mathbf{e}} \\ &\quad - \frac{(\hat{\mathbf{v}}_{ij}\cdot\mathsf{W}_i\cdot\hat{\mathbf{v}}_{ij\perp})[\hat{\mathbf{v}}_{ij\perp}\cdot(\mathsf{W}_{ik}-\mathsf{W}_{jk})\cdot\hat{\mathbf{e}}]}{\hat{\mathbf{v}}_{ij\perp}\cdot(\mathsf{W}_i+\mathsf{W}_j)\cdot\hat{\mathbf{v}}_{ij\perp}} \ , \qquad (4.32)\\ \hat{\mathbf{v}}_{ij\perp}\cdot\mathsf{W}'_{ik}\cdot\hat{\mathbf{e}} &= \frac{1}{2}\hat{\mathbf{v}}_{ij\perp}\cdot(\mathsf{W}_{ik}-\mathsf{W}_{jk})\cdot\hat{\mathbf{e}} \\ &\quad - \frac{[\hat{\mathbf{v}}_{ij\perp}\cdot(\mathsf{W}_i-\mathsf{W}_j)\cdot\hat{\mathbf{v}}_{ij\perp}][\hat{\mathbf{v}}_{ij\perp}\cdot(\mathsf{W}_{ik}-\mathsf{W}_{jk})\cdot\hat{\mathbf{e}}]}{2\hat{\mathbf{v}}_{ij\perp}\cdot(\mathsf{W}_i+\mathsf{W}_j)\cdot\hat{\mathbf{v}}_{ij\perp}} \ . \qquad (4.33)\end{aligned}$$

Here, $\hat{\mathbf{e}}$ can be any vector in two dimensions. If W_{ik} has non-zero elements, then W_{jk} does not, since the particles i and j were uncorrelated before the collision. If W_{ik} has non-zero elements after the collision, both W'_{ik} and W'_{jk} have non-zero elements.

From equation (4.32) the traces after the collision may be found,

$$\begin{aligned}\mathrm{Tr}(\mathsf{W}'_{ik}) &= \frac{1}{2}(\hat{\mathbf{v}}_{\perp ij}\cdot\mathsf{W}_{ik}\cdot\hat{\mathbf{v}}_{\perp ij})\left[1-\frac{\hat{\mathbf{v}}_{\perp ij}\cdot(\mathsf{W}_i-\mathsf{W}_j)\cdot\hat{\mathbf{v}}_{\perp ij}}{\hat{\mathbf{v}}_{\perp ij}\cdot(\mathsf{W}_i+\mathsf{W}_j)\cdot\hat{\mathbf{v}}_{\perp ij}}\right] \\ &\quad + \hat{\mathbf{v}}_{ij}\cdot\mathsf{W}_{ik}\cdot\hat{\mathbf{v}}_{ij} \\ &\quad - (\hat{\mathbf{v}}_{\perp ij}\cdot\mathsf{W}_{ik}\cdot\hat{\mathbf{v}}_{ij})\frac{\hat{\mathbf{v}}_{ij}\cdot\mathsf{W}_i\cdot\hat{\mathbf{v}}_{\perp ij}}{\hat{\mathbf{v}}_{\perp ij}\cdot(\mathsf{W}_i+\mathsf{W}_j)\cdot\hat{\mathbf{v}}_{\perp ij}} \ , \qquad (4.34)\\ \mathrm{Tr}(\mathsf{W}'_{jk}) &= -\frac{1}{2}(\hat{\mathbf{v}}_{\perp ij}\cdot\mathsf{W}_{ik}\cdot\hat{\mathbf{v}}_{\perp ij})\left[1-\frac{\hat{\mathbf{v}}_{\perp ij}\cdot(\mathsf{W}_i-\mathsf{W}_j)\cdot\hat{\mathbf{v}}_{\perp ij}}{\hat{\mathbf{v}}_{\perp ij}\cdot(\mathsf{W}_i+\mathsf{W}_j)\cdot\hat{\mathbf{v}}_{\perp ij}}\right] \\ &\quad - \frac{(\hat{\mathbf{v}}_{ij}\cdot\mathsf{W}_j\cdot\hat{\mathbf{v}}_{ij\perp})(\hat{\mathbf{v}}_{ij\perp}\cdot\mathsf{W}_{ik}\cdot\hat{\mathbf{v}}_{ij})}{\hat{\mathbf{v}}_{\perp ij}\cdot(\mathsf{W}_i+\mathsf{W}_j)\cdot\hat{\mathbf{v}}_{\perp ij}} \ . \qquad (4.35)\end{aligned}$$

It is fair to assume that the off-diagonal elements of W_{ik} tend to be smaller than the diagonal elements. Also, the diagonal elements of $\mathsf{W}_i-\mathsf{W}_j$ are, typically, much smaller than the diagonal elements of $\mathsf{W}_i+\mathsf{W}_j$. The terms with a quotient of these can therefore be neglected in this rough estimation. Further, the d diagonal elements of W_{ik} are typically of the same size. These approximations leave us with the general expressions

$$\mathrm{Tr}(\mathsf{W}'_{ik}) \approx \frac{d+1}{2d}\mathrm{Tr}(\mathsf{W}_{ik}) \ , \qquad (4.36)$$

$$\mathrm{Tr}(\mathsf{W}'_{jk}) \approx \frac{d-1}{2d}\mathrm{Tr}(\mathsf{W}_{ik}) \ . \qquad (4.37)$$

In addition, if both W_{ik} and W_{jl} have non-zero elements, W'_{kl} also has non-zero elements, which are due to the second term on the right-hand side of equation

(4.20). The off-diagonal elements generated in this way are small compared to the elements generated from equations (4.36) and (4.37). In fact, they are smaller than the terms neglected from equations (4.34) and (4.35), because they contain products of the off-diagonal elements which are small compared to the diagonal elements. As they appear quadratically in the change in the trace [see equation (4.19)], despite their quadratically larger number, they may be neglected.

From equations (4.36) and (4.37) an estimate can be made of the contributions to the change in the trace in equation (4.19) from collisions before the previous collision, compared to the contributions from just the previous collisions. The ratio between the total contributions from off-diagonal elements to the change in the trace and the contributions from just the previous collisions is denoted by α.

In every collision in the history, off-diagonal elements are created between the two colliding particles and existing elements are reduced in magnitude and passed on according to equations (4.36) and (4.37). In order to estimate the consequences of W_{qs} at a collision between q and r, one has to find the path from the collision between particles x and y to the present collision between q and r as well as the path from the collision between x and y to the particle s at the time of the collision between q and r, following a sequence of collisions, through which the off-diagonal element between particles q and s is affected. A diagrammatic representation of this is shown in figure 4.1. To this path belongs an approximate reduction of the size of the off-diagonal element, a product of factors of $(d+1)/(2d)$ or $(d-1)/(2d)$ for each collision in the paths. If the path continues with the same particle, there is a factor of $(d+1)/(2d)$. If it switches to the other particle, the factor is $(d-1)/(2d)$.

Every different product with the same number of factors follows a different path of that length, and hence belongs to a different present particle. The product of the two factors of two paths starting from x and y gives the order of magnitude of the off-diagonal element between i and k particles. The square of this factor then gives the relative size of the contribution to the trace at the collision between i and j. If a collision between two particles is now p collisions ago, then, on average, the other part of the future of that collision has also had p collisions. Summing over all the different paths of length p, one finds that the relative contribution from collisions that occurred p collisions before the previous collision can be approximated as

$$\alpha_p \approx \left(\frac{d^2+1}{2d^2}\right)^{2p} . \tag{4.38}$$

Summing over all p gives the estimate

$$\alpha = \sum_p \alpha_p \approx \frac{4d^4}{(3d^2+1)(d^2-1)} . \tag{4.39}$$

The contributions from the previous collisions in equations (4.19) and (4.29)

can be multiplied by α, to find an estimate for the total contribution of all particles with which i and j have a common history. This is an admittedly crude estimate for the contributions, yet should give better results than just neglecting the history before the previous collision. The terms in equation(4.29) that are due to the off-diagonal block between the colliding particles and other particles may be multiplied by α. With this correction it is found that

$$\bar{w}_\alpha^{(1)} = \begin{cases} 2.929 & \text{if } d = 2 \ , \\ 1.947 & \text{if } d = 3 \ . \end{cases} \tag{4.40}$$

The distribution function of $w_{\perp\perp}$ contains an uncertainty in its width, which affects the results of the calculation. When starting from the average, with every next iteration of the equation for the distribution function, the distribution becomes wider. $w_{\perp\perp}$ looks like a sum of several weighted free-flight times for each particle. If one starts from exponentially distributed diagonal elements, rather than simply the averages, the distribution becomes narrower with every iteration. By starting from an exponential distribution, one may estimate the consequences of the width of the distribution of the elements. With an initial exponential distribution, one finds

$$\bar{w}_\alpha^{(1)e} = \begin{cases} 2.426 & \text{if } d = 2 \ , \\ 1.676 & \text{if } d = 3 \ . \end{cases} \tag{4.41}$$

By substituting the distribution function induced by one iteration, together with the average, into equation (4.3) one can now estimate the Kolmogorov-Sinai entropy.

4.4 Results and discussion

As the free-flight times are inversely proportional to the density, $w_{\perp\perp}\bar{\tau}^{d-1}$ will be inversely proportional to n^{d-1}. This leads to a general form for the Kolmogorov-Sinai entropy,

$$h_{\mathrm{KS}} = N\bar{\nu}A[-\log(na^d) + B] \ . \tag{4.42}$$

In earlier calculations [31], the values for A were calculated accurately. The results for B, however, are unsatisfactory. The values of A are easily found from equations (4.3), (4.12), and the dependence of the collision frequency on n,

$$A = \frac{d-1}{2} \ . \tag{4.43}$$

If $w_{\perp\perp}$ is taken to be equal to τ_+, the results for B of reference [31] are reproduced,

$$\tilde{h}_{\mathrm{KS}} = \frac{N\bar{\nu}}{2} \left\langle \log \left[\left(\frac{2v_{ij}\tau_+}{a} \right)^{d-1} \cos^{d-3}\theta \right] \right\rangle \ , \tag{4.44}$$

which yields

$$\tilde{B} \approx \begin{cases} 0.209 & \text{if } d = 2 \ , \\ -0.583 & \text{if } d = 3 \ . \end{cases} \tag{4.45}$$

From molecular dynamics simulations the Kolmogorov-Sinai entropy can be calculated [31, 37]. It is found that

$$h_{\mathrm{KS}}^{\mathrm{s}} = \begin{cases} (0.499 \pm 0.001) N\bar{\nu} \left(-\log n a^d + 1.366 \pm 0.005 \right) & \text{if } d = 2 \ , \\ (1.02 \pm 0.02) N\bar{\nu} \left(-\log n a^d + 0.29 \pm 0.01 \right) & \text{if } d = 3 \ . \end{cases} \tag{4.46}$$

In the calculation presented here, the results of equation (4.44) have to be amended, to become

$$h_{\mathrm{KS}} = \frac{N\bar{\nu}}{2} \left\langle \log \left[w_{\perp\perp} \left(\frac{2 v_{ij} \bar{\tau}}{a} \right)^{d-1} \cos^{d-3} \theta \right] \right\rangle \ . \tag{4.47}$$

From equations (4.26) and (4.30), one finds, after numerical integration, that

$$B_1^{(1)} \approx \begin{cases} 1.592 & \text{if } d = 2 \ , \\ 0.476 & \text{if } d = 3 \ , \end{cases} \tag{4.48}$$

If the contributions from the off-diagonal elements in equation (4.19) are increased by the estimate of the remaining terms, a factor of α, the results change to

$$B_\alpha^{(1)} \approx \begin{cases} 1.572 & \text{if } d = 2 \ , \\ 0.427 & \text{if } d = 3 \ . \end{cases} \tag{4.49}$$

This more closely reproduces the simulation results shown in equation (4.46).

After every extra iteration in the calculation, the distribution becomes wider and therefore the average of the logarithm of $w_{\perp\perp}$ becomes smaller compared to the logarithm of the average. Due to this, cutting off the process after two iterations produces a result for the Kolmogorov-Sinai entropy which is too high. Note that also a wider spread of the off-diagonal elements leads to larger contributions from the off-diagonal terms in equation (4.19), and therefore to a smaller $\bar{w}$, which yields a smaller value for B. Equation (4.48) gives an upper bound for B.

By starting from a wider distribution of diagonal elements, instead of a product of Dirac delta functions, an estimate can be made of the effects of the width of the distribution. From equation (4.41) an estimated lower bound is found,

$$B_\alpha^{(1)e} \approx \begin{cases} 1.370 & \text{if } d = 2 \ , \\ 0.273 & \text{if } d = 3 \ , \end{cases} \tag{4.50}$$

In chapter 6, a more rigorous lower bound will be derived.

From these two estimated bounds, a final estimate of B may be made, including error bounds,

$$B = \begin{cases} 1.47 \pm 0.11 & \text{if } \; d = 2 \; , \\ 0.35 \pm 0.08 & \text{if } \; d = 3 \; . \end{cases} \tag{4.51}$$

The errors could be reduced by using distribution functions for $w_{\perp\perp}$ that have been iterated a larger number of times. The values of the Kolmogorov-Sinai entropy found in the molecular dynamics simulations, equation (4.46), are well within the error bounds of equation (4.51).

4.5 Conclusions

In this chapter, an estimate is presented of the Kolmogorov-Sinai entropy of dilute hard sphere gases in equilibrium, which to leading order is of the form $N\bar{\nu}A(-\log n + B)$. For the first time, B was estimated in a satisfactory way, with results which are consistent with simulation results. It was found that, for $d = 2$, $B = 1.47 \pm 0.11$ and, for $d = 3$, $B = 0.35 \pm 0.08$. The values for B found in the calculation presented here are in good agreement with the results found in molecular dynamics simulations [37]. Also, an upper bound was found for B, that is, $B < 1.592$ if $d = 2$, and $B < 0.476$ if $d = 3$. In chapter 6 a lower bound is derived.

The smaller Lyapunov exponents of this system that are not due to Goldstone modes are proportional to $\bar{\nu}$. They contribute significantly to B in the Kolmogorov-Sinai entropy. The calculation of B presented here shows effects which could therefore affect the behaviour of these exponents in the leading order. A calculation of such effects is presented in chapter 6.

It should be noted that effects such as the ones described here cannot affect the Lyapunov spectrum of the high-dimensional Lorentz gas, calculated in chapter 5, because the scatterers in that system are uniformly convex. But they are generic for the Lyapunov spectra of systems consisting of many particles.

Chapter 5

The dilute d-dimensional Lorentz gas

This chapter is based on Physical Review E **70**, 036209 (2004) [46].

5.1 Introduction

In this thesis, a great deal of attention is given to systems consisting of many moving particles. However, in phase space this corresponds to the motion of a single point particle among a high-dimensional array of scatterers. From this perspective, a system of interacting hard spheres or disks is not all that different from a high-dimensional Lorentz gas, as noted already many years ago by Sinai [47]. In phase space both systems are represented by a point particle moving at constant speed between elastic collisions with hard scatterers. The only, important, difference is that in the high-dimensional Lorentz gas the scatterers are hyper spheres, which have a uniform curvature, whereas for the hard disks or spheres the scatterers are hyper cylinders, which are curved in a few directions only, but flat in all others. In either case the convex shape of the scatterers makes the system strongly chaotic. This similarity between cylindrical scatterers and many-particle systems is explained in more detail in chapter 6.

The difference in the shape of the scatterers has important consequences for

calculations. The scatterers in the Lorentz gas are invariant under rotations in configuration space, which simplifies calculations enormously. Further, the uniform convexity of the Lorentz-gas scatterers, in contrast to the hyper cylinders of the hard-sphere systems, strongly simplifies proofs of ergodic and chaotic properties [48]. It also simplifies the low-density approximation, because it removes the technical problems with the low-density approximation that occur in hard-sphere systems and were described in chapter 4. Yet, it is of interest to perform an explicit calculation of the full Lyapunov spectrum of a high-dimensional dilute Lorentz gas and compare it to the spectra of hard-sphere systems. In addition, the methods used in this chapter may well be amenable to refinements, so as to make them applicable to systems of many moving particles.

In this chapter, the behaviour of a dilute, random, non-overlapping Lorentz gas is studied in an arbitrary number of dimensions d. For large d, this system has many degrees of freedom, while, largely due to the spherical symmetry of the scatterers, it is still possible to do exact calculations. The full Lyapunov spectrum is calculated in the absence of any external fields.

5.2 Dynamics of the Lorentz gas

The system consists of a fixed number of randomly placed, spherical scatterers with radius a at a (small) density n in d dimensions. The discussion is restricted to the case of non-overlapping scatterers, where, a priori, each configuration without overlap among any two scatterers is equally likely. The system is assumed to be large. As long as it is finite, our preferred boundary conditions are periodic ones, but our considerations allow taking the infinite-system limit at fixed density without any problem. A single point particle moves between the scatterers, with speed v, undergoing a specular reflection at each collision. For given scatterer positions, the phase space is represented by the position and velocity of the point particle, $\gamma = (\mathbf{r}, \mathbf{v})$. The tangent space at any point in phase space can be represented by the perturbations in these quantities, $\delta\gamma = (\delta\mathbf{r}, \delta\mathbf{v})$.

Between collisions with the scatterers, the particle moves freely, so $\dot{\mathbf{r}} = \mathbf{v}$ and $\dot{\mathbf{v}} = 0$. At a collision with collision normal $\hat{\sigma}$, the particle is reflected by a scatterer, as shown in figure 5.1, with resulting velocity $\mathbf{v}' = (\mathbf{1} - 2\hat{\sigma}\hat{\sigma}) \cdot \mathbf{v}$. Here $\mathbf{1}$ is the $d \times d$ identity matrix. From equation (1.3) the temporal behaviour of $\delta\gamma$ can be derived. During free flight,

$$\delta\dot{\mathbf{r}} = \delta\mathbf{v} \ , \tag{5.1}$$

$$\delta\dot{\mathbf{v}} = 0 \ . \tag{5.2}$$

At a collision, $\delta\mathbf{v}$ is also reflected. On the tangent trajectory, the perturbation of the pre-collisional position with respect to the reference trajectory leads to a perturbation in the collision normal and the collision time, which shows up in the perturbation of the post-collisional velocity. The perturbation of the collision time

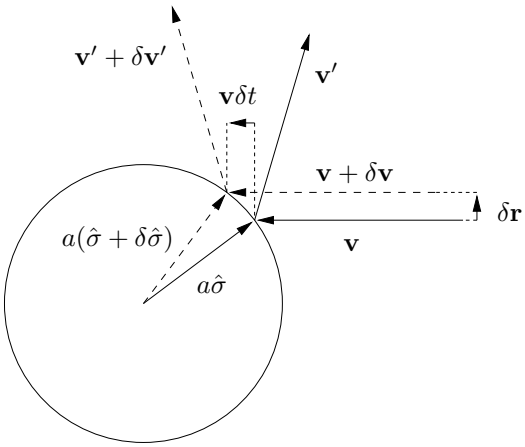

Figure 5.1: Geometry of a collision. The collision normal $\hat{\sigma}$ is the unit vector pointing from the centre of the scatterer to the moving point particle.

also leads to a difference in the post-collisional position (measured at the instant of collision on the tangent trajectory) from the pre-collisional one (measured at the instant of collision on the reference trajectory). As a result, the tangent-space vectors are transformed according to [6, 49]

$$\delta\mathbf{r}' = (\mathbf{1} - 2\hat{\sigma}\hat{\sigma}) \cdot \delta\mathbf{r} \ , \tag{5.3}$$

$$\delta\mathbf{v}' = (\mathbf{1} - 2\hat{\sigma}\hat{\sigma}) \cdot \delta\mathbf{v} + 2\mathsf{Q} \cdot \delta\mathbf{r} \ , \tag{5.4}$$

in which the collision matrix Q is defined by

$$\mathsf{Q} = \frac{1}{a}\left(\mathbf{v}\hat{\sigma} - \hat{\sigma}\mathbf{v} + \frac{\mathbf{v}^2}{\mathbf{v}\cdot\hat{\sigma}}\hat{\sigma}\hat{\sigma} - (\mathbf{v}\cdot\hat{\sigma})\mathbf{1}\right) \ . \tag{5.5}$$

From these equations it follows that, if $\delta\mathbf{r}$ and $\delta\mathbf{v}$ are both parallel to $\mathbf{v}$ before the collision, $\delta\mathbf{r}'$ and $\delta\mathbf{v}'$ are parallel to $\mathbf{v}'$ after the collision and their absolute values are the same as before. These are two linearly independent perturbations, giving rise to two zero Lyapunov exponents. They result from time-translation invariance and from invariance of the trajectories in configuration space under a scaling of the velocity. All other Lyapunov exponents for the Lorentz gas are non-zero. As a consequence of the conjugate pairing rule, $d-1$ of them are positive and the remaining $d-1$ are negative with the same absolute values.

5.3 The largest Lyapunov exponent at low densities

To calculate the non-zero Lyapunov exponents, one needs to consider what happens to an initial perturbation $\delta\gamma(0)$ in tangent space in the limit of infinite time. As an introduction, we first review the calculation of the largest Lyapunov exponent at low scatterer densities.

An initial perturbation which is not parallel to $\mathbf{v}$ generically has a non-vanishing component along the most rapidly growing eigenvector of the time evolution operator in tangent space. Therefore, its evolution for long times will be dominated by the largest Lyapunov exponent. To calculate this time evolution, it suffices to consider the growth of the projection of the growing vector onto a subspace of tangent space. It turns out to be convenient to use the projection onto $\delta\mathbf{v}$ for this.

Define $\delta\mathbf{r}_i$ and $\delta\mathbf{v}_i$ as the tangent-space vectors just after collision i, with collision normal $\hat{\sigma}_i$, occurring a time τ_i after collision $i-1$. Let θ_i be the angle between $\hat{\sigma}$ and the velocity before the collision,

$$\hat{\sigma}_i \cdot \mathbf{v} = -v\cos\theta_i \ . \tag{5.6}$$

Before collision i, one has

$$\delta\mathbf{r}_i^- = \delta\mathbf{r}_{i-1} + \tau_i\delta\mathbf{v}_{i-1} \ , \tag{5.7}$$

where $\delta\mathbf{r}_i^-$ is used to indicate the perturbation in the position just before collision i. From equations (5.4) and (5.5) it follows that, after the $(i-1)$-th collision, $\delta\mathbf{v}_{i-1}$ typically is of the order of $\delta\mathbf{r}_{i-1}v/a$. This is different from the case of hard spheres, where there are many directions on which $\mathcal{Q}$ does not work. In the case of the Lorentz gas there is only one such direction, the one belonging to the time-translation zero mode.

At low densities, the mean free time is of the order of $1/(na^{d-1}v)$. Therefore, to leading order in the density the first term on the right-hand side of equation (5.7) may be neglected in the calculation of the positive Lyapunov exponents. Similarly, in equation (5.4) the first term on the right-hand side becomes negligible at low density, and equations (5.4) and (5.7) may be combined into

$$\delta\mathbf{v}_i = 2\tau_i\mathsf{Q}_i\cdot\delta\mathbf{v}_{i-1} \ . \tag{5.8}$$

The contributions to the Lyapunov exponents of the terms neglected in this approximation are at least one order of n higher than the terms of leading order [18]. In addition, in this approximation, the time-reversal symmetry has been destroyed, hence only the positive Lyapunov exponents can be calculated. However, in the limit of vanishing density, the results for these will be exact.

The action of Q_i on $\delta\mathbf{v}_i$ may be described in the following way. Working on the component along $\mathbf{v}_i$ it yields zero. It multiplies the component normal to $\mathbf{v}$

in the plane through $\mathbf{v}_i$ and $\hat{\sigma}$ with a factor $v/(a\cos\theta_i)$ and rotates the vector component to the direction in this plane normal to $\mathbf{v}_i'$. Finally, it multiplies all other vectors $\delta\mathbf{v}_i$ normal to $\hat{\mathbf{v}}_i$ and $\hat{\sigma}$ with $v\cos\theta_i/a$. Define the unit vector orthogonal to $\mathbf{v}$ in the plane spanned by $\mathbf{v}$ and $\hat{\sigma}$ as

$$\hat{\rho}_i = \frac{(\mathbf{1} - \hat{\mathbf{v}}_i\hat{\mathbf{v}}_i)\cdot\hat{\sigma}_i}{|\sin\theta_i|} \ . \tag{5.9}$$

One may rewrite Q_i as

$$\mathsf{Q}_i = \frac{v}{a}\left(\cos\theta_i(\mathbf{1} - \hat{\mathbf{v}}_i\hat{\mathbf{v}}_i - \hat{\rho}_i\hat{\rho}_i) + \frac{1}{\cos\theta_i}\hat{\rho}_i'\hat{\rho}_i\right) \ . \tag{5.10}$$

Combining this with equations (5.3) and (5.4), one finds that the velocity deviations to leading order in n evolve according to

$$\delta\mathbf{v}_i = \frac{2v\tau_i}{a}\left(\cos\theta_i(\mathbf{1} - \hat{\mathbf{v}}_i\hat{\mathbf{v}}_i - \hat{\rho}_i\hat{\rho}_i) + \frac{1}{\cos\theta_i}\hat{\rho}_i'\hat{\rho}_i\right)\cdot\delta\mathbf{v}_{i-1} \ . \tag{5.11}$$

The largest Lyapunov exponent may now be calculated to leading order in the density as

$$\lambda_1 = \bar{\nu}_d\left\langle\log\frac{|\delta\mathbf{v}_i|}{|\delta\mathbf{v}_{i-1}|}\right\rangle \ , \tag{5.12}$$

where $\bar{\nu}_d$ is the average collision frequency for the system and the brackets indicate an average over the collision sequence, which will be discussed in more detail in section 5.4. The result for the largest exponent in d dimensions will appear as a special case of the calculations presented in the next section.

5.4 Partial stretching factors

The stretching factor is defined as the factor by which the expanding part of tangent space expands with time. This quantity can be used to calculate the Ruelle pressure as well as the sum of the positive Lyapunov exponents, equal to the Kolmogorov-Sinai entropy in systems without escape [19, 20]. In chapter 4, the stretching factor for a system of hard spheres was used to calculate the Kolmogorov-Sinai entropy for that system.

Define the partial stretching factor $\Lambda_S(\mathbf{r},\mathbf{v},t)$ of a p-dimensional subspace S of the $2d$-dimensional tangent space as the factor by which the volume of an infinitesimal p-dimensional hyper cube in this subspace has increased after a time t. Unless S is orthogonal to some eigenvector associated with one of the p largest Lyapunov exponents, the partial stretching factor for long times will be dominated

by the p most unstable directions in tangent space, in other words, by the p largest Lyapunov exponents. Explicitly, one has the identity

$$\sum_{i=1}^{p} \lambda_i = \lim_{t\to\infty} \frac{1}{t} \log \Lambda_S(\mathbf{r}, \mathbf{v}, t) \ . \tag{5.13}$$

As in the case of the largest Lyapunov exponent, where we could consider the long time growth of a basically arbitrary vector in tangent space, we may choose the subspace S in the way that is most convenient to us. And, as before, we choose S as a subspace of the space spanned by velocity deviations perpendicular to $\mathbf{v}$.

The partial stretching factor just after collision N is the product of the partial stretching factors of the collisions 1 through N. These depend on the relative orientations of $\mathbf{v}$, $\hat{\sigma}$, and the image of S. One can write

$$\Lambda_S(\mathbf{r}, \mathbf{v}, t_N) = \prod_{i=1}^{N} \Lambda_p^{(i)}(v, \tau_i, \theta_i, \alpha_i) \ , \tag{5.14}$$

in which α_i is the projection angle of $\hat{\rho}_i$ onto the image of S after the $(i-1)$-th collision. The subspace S can be split into a $(p-1)$-dimensional subspace normal to $\hat{\rho}_i$ and a 1-dimensional subspace spanned by the projection of $\hat{\rho}_i$ onto S. From equation (5.11) one finds that the former contributes a factor of $(\tau_i \cos\theta_i)^{p-1}$ to the partial stretching factor. The projection of $\hat{\rho}_i$ onto the image of S can be split into components perpendicular and parallel to $\hat{\rho}_i$. The former grows with $2v\tau_i \cos\theta_i/a$ and the latter with $2v\tau_i/(a\cos\theta_i)$. The partial stretching factor thus becomes

$$\Lambda_p^{(i)}(v, \tau_i, \theta_i, \alpha_i) = \left(\frac{2v\tau_i}{a}\right)^p \cos^{p-1}\theta_i \sqrt{(\sin\alpha_i \cos\theta_i)^2 + \left(\frac{\cos\alpha_i}{\cos\theta_i}\right)^2} \ . \tag{5.15}$$

From this expression one can calculate the Lyapunov exponents and obtain asymptotic approximations for high dimensionality.

5.4.1 Lyapunov exponents

The sum of the p largest Lyapunov exponents can be calculated by substituting equation (5.14) into equation (5.13),

$$\sum_{i=1}^{p} \lambda_i = \lim_{t_N\to\infty} \frac{1}{t_N} \sum_{i=1}^{N} \log \Lambda_p^{(i)}(v, \tau_i, \theta_i, \alpha_i) \ , \tag{5.16}$$

where t_N is the time at which the N-th collision occurs.

In the low-density limit, the collisions in the Lorentz gas are uncorrelated and therefore the time average in equation (5.16) can be replaced with an ensemble

average,

$$\sum_{i=1}^{p} \lambda_i = \int_0^\infty d\tau \int_0^{\frac{\pi}{2}} d\theta \int_0^{\frac{\pi}{2}} d\alpha \, \nu_p(\tau, \theta, \alpha; v) \log \Lambda_p^{(i)}(v, \tau, \theta, \alpha) \ . \tag{5.17}$$

Here $\nu_p(\tau, \theta, \alpha; v)$ is a probability distribution, describing the probability density per units of time and angle for collisions with the parameters τ, θ, and α at a given velocity v. The index p is attached to remind the reader of the dependence of the distribution of α on the dimensionality of the subset S. A rigorous proof of the theorem used to derive equation (5.17) has been given by Crisanti, Paladin, and Vulpiani [50].

5.4.2 The distribution of free-flight times

To lowest order in the density of scatterers, collisions are uncorrelated; effects of re-collisions appear in the Lyapunov exponents only at higher orders. With increasing d, these higher-density corrections become even smaller, since the probability of a return to a scatterer decreases rapidly. In this approximation, the time of free flight between consecutive collisions is distributed exponentially. In addition, the distribution of the angles θ and α is independent of that of the free-flight time, the direction of the incident velocity and the orientation of the pre-collisional image of S. The probability density for colliding at angle θ is proportional to the differential cross-section. In the distribution of free-flight times it contributes a factor of

$$n a^{d-1} v \, O_{d-1} \sin^{d-2}\theta \cos\theta \, d\theta dt \ . \tag{5.18}$$

Here O_m is the $(m-1)$-dimensional surface area of the m-dimensional unit sphere, i. e.,

$$O_m = \frac{2\,\pi^{\frac{m}{2}}}{\Gamma\left(\frac{m}{2}\right)} \ . \tag{5.19}$$

Finally, the probability distribution of the projection angle α of $\hat{\rho}$ onto the image of S after $i-1$ collisions may be identified with the fraction of the $(d-1)$-dimensional unit sphere that has a projection angle between α and $\alpha + d\alpha$, i.e.,

$$\rho(\alpha) = \begin{cases} \dfrac{O_{d-1-p} O_p}{O_{d-1}} \sin^{d-2-p}\alpha \, \cos^{p-1}\alpha & \text{if } \ p < d-1 \ , \\ \delta(\alpha) & \text{if } \ p = d-1 \ , \end{cases} \tag{5.20}$$

where $\delta(\alpha)$ is the Dirac delta function. Combining equations (5.18) and (5.20) with the exponential distribution of the free-flight times, one finds, for $p < d-1$,

$$\begin{aligned} \nu_p(\tau, \theta, \alpha; v) = {} & 2 n a^{d-1} v \, O_{d-1-p} \, O_p \, \bar{\nu}_d \, \exp(-\bar{\nu}_d \tau) \\ & \times \sin^{d-2}\theta \, \cos\theta \, \sin^{d-2-p}\alpha \, \cos^{p-1}\alpha \ , \end{aligned} \tag{5.21}$$

where the average collision frequency has the explicit form

$$\bar{\nu}_d = \frac{n a^{d-1} v\, O_{d-1}}{d-1} \ . \tag{5.22}$$

Note that $O_{d-1}/(d-1)$ is equal to the volume of the $(d-1)$-dimensional unit sphere, so $a^{d-1}O_{d-1}/(d-1)$ is the total cross-section for a collision with a scatterer.

5.5 The spectrum

Substituting equations (5.15) and (5.21) into equation (5.17) yields an expression for the sum of the p largest Lyapunov exponents,

$$\begin{aligned}\sum_{i=1}^{p} \lambda_i = \int_0^\infty d\tau \int_0^{\frac{\pi}{2}} d\theta\, n a^{d-1} v\, O_{d-1} \bar{\nu}_d \exp(-\bar{\nu}_d \tau) \sin^{d-2}\theta \cos\theta \\ \times \left[p \log\left(\frac{2v\tau}{a}\right) + (p-1)\log\cos\theta \right] \\ + \int_0^{\frac{\pi}{2}} d\theta \int_0^{\frac{\pi}{2}} d\alpha\, n a^{d-1} v\, O_{d-1-p} O_p \sin^{d-2}\theta \cos\theta \sin^{d-2-p}\alpha \cos^{p-1}\alpha \\ \times \log\left[(\sin\alpha\cos\theta)^2 + \left(\frac{\cos\alpha}{\cos\theta}\right)^2 \right] \ . \end{aligned} \tag{5.23}$$

The first integral can easily be carried out analytically. The second integral is more difficult. It can be simplified in special cases, as described in section 5.5.1, or approximated, as described in the remainder of this section.

5.5.1 The Kolmogorov-Sinai entropy

By taking $p = d-1$, one can calculate the sum of all the positive exponents, the Kolmogorov-Sinai (KS) entropy. Since the distribution of α now is a delta function, the second term in equation 5.23 becomes

$$-\int_0^{\frac{\pi}{2}} d\theta\, n a^{d-1} v\, O_{d-1-p} O_p \sin^{d-2}\theta \cos\theta \sin^{d-2-p}\alpha\ \cos^{p-1}\alpha\ \log\ \cos\theta \tag{5.24}$$

Performing the integrals yields

$$\begin{aligned}\sum_{i=1}^{d-1} \lambda_i = \frac{a\bar{\nu}_d}{2v} \Bigg\{ 2(d-1) \left[-\log\left(\frac{n a^d O_{d-1}}{2(d-1)}\right) - \gamma \right] \\ - (d-3)\left[\psi^{(0)}\left(\frac{d+1}{2}\right) + \gamma \right] \Bigg\} \ . \end{aligned} \tag{5.25}$$

Here $\psi^{(i)}(x)$ is the $(i+1)$-th derivative of $\log\Gamma(x)$; $\psi^{(i)}(x) = [\log\Gamma(x)]^{(i+1)}$. This reproduces the results of van Beijeren, Latz, and Dorfman [18–20].

5.5.2 Lower bound

A lower bound for the Lyapunov exponents can be derived by assuming that the minimum growth of the tangent-space vector is realised for every collision. The minimum growth is the growth in the directions perpendicular to $\hat{\sigma}$ and $\mathbf{v}$. This yields

$$\lambda_{d-1} > \lambda_- \ , \tag{5.26}$$

with λ_- defined by

$$\lambda_- = \frac{\bar{\nu}_d}{2}\left[-2\log\Big(\frac{a\bar{\nu}_d}{2v}\Big) - 3\gamma - \psi^{(0)}\left(\frac{d+1}{2}\right)\right] . \tag{5.27}$$

The function $\psi^{(0)}(d+1/2)$ for large d behaves as $\log d$. Therefore, the $\log\bar{\nu}_d$ term dominates the behaviour of λ_-, and λ_- for large d behaves asymptotically as $-\bar{\nu}_d\log\bar{\nu}_d$.

In a system of high dimensionality, the exponents are dominated by the directions perpendicular to $\mathbf{v}$ and $\hat{\sigma}$. They should behave as λ_- with a small correction.

5.5.3 High dimensionality

The integrals in equation (5.23) can be estimated for large d and arbitrary p. For large numbers of dimensions, the distribution of θ is sharply peaked near $\theta = \pi/2$. The argument of the logarithm in the second term of equation (5.23) is therefore dominated by the $1/\cos^2\theta$ term. The range of α where the other term dominates is of the order of $1/d$, and therefore that term can be neglected. This leads to

$$\begin{aligned}\sum_{i=1}^{p}\lambda_i \approx p\lambda_- + \int_0^{\frac{\pi}{2}} d\theta \int_0^{\frac{\pi}{2}} d\alpha\, n a^{d-1} v\, O_{d-1-p} O_p \sin^{d-2}\theta\, \cos\theta \\ \times \sin^{d-2-p}\alpha\, \cos^{p-1}\alpha\, \left(-2\log\cos\theta + \log\cos\alpha\right) \ ,\end{aligned} \tag{5.28}$$

which yields, after performing the integrals,

$$\sum_{i=1}^{p}\lambda_i \approx \frac{\bar{\nu}_d}{2}\left[2\gamma - \psi^{(0)}\left(\frac{d-1}{2}\right) + 2\psi^{(0)}\left(\frac{d+1}{2}\right) + \psi^{(0)}\Big(\frac{p}{2}\Big)\right] + p\lambda_- \ . \tag{5.29}$$

For the largest exponent this means that the behaviour for large d is approximately

$$\lambda_1 \approx \lambda_- + \tfrac{1}{2}\bar{\nu}_d\left(\log d + \gamma - \tfrac{5}{2}\log 2 - \tfrac{1}{2}\right) \ . \tag{5.30}$$

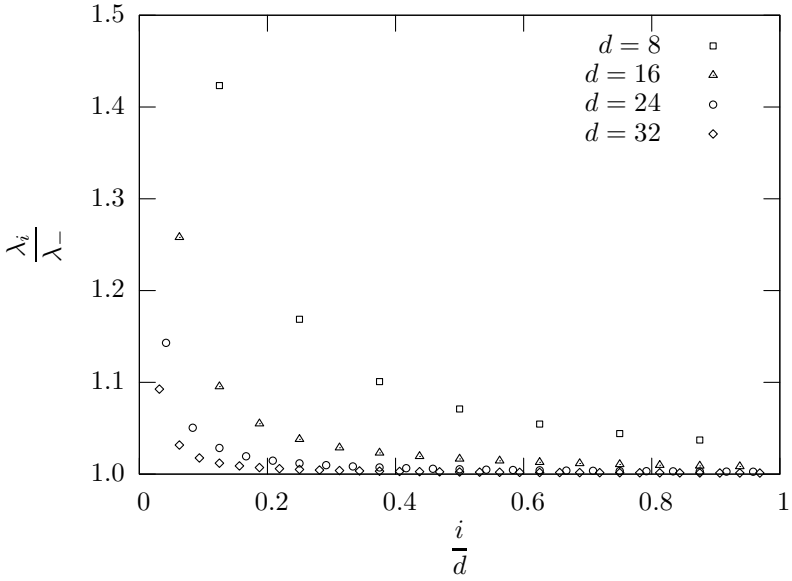

Figure 5.2: The scaled spectrum of positive Lyapunov exponents for several values of the dimensionality d at density $n = 0.01/a^2$.

This behaviour is shown in the uppermost curve in figure 5.3.

The smallest exponent is equal to the Kolmogorov-Sinai entropy minus the sum of the first $d-2$ exponents. In the high-dimensionality limit, the smallest positive exponent behaves as

$$\lambda_{d-1} \approx \lambda_- + \frac{\bar{\nu}_d}{2d} \ . \tag{5.31}$$

This is illustrated in figure 5.5. The p-th exponent can be calculated by subtracting the expression for the sum of the first $p-1$ exponents from that for the first p ones. This results in

$$\lambda_p \approx \lambda_- + \frac{\bar{\nu}_d}{2}\left[\psi^{(0)}\left(\frac{p}{2}\right) - \psi^{(0)}\left(\frac{p-1}{2}\right)\right] \ . \tag{5.32}$$

For the first few exponents, this yields

$$\lambda_2 \approx \lambda_- + \bar{\nu}_d \log 2 \ , \tag{5.33}$$

$$\lambda_3 \approx \lambda_- + \bar{\nu}_d (1 - \log 2) \ , \tag{5.34}$$

$$\lambda_4 \approx \lambda_- + \bar{\nu}_d \left(\log 2 - \tfrac{1}{2}\right) \ . \tag{5.35}$$

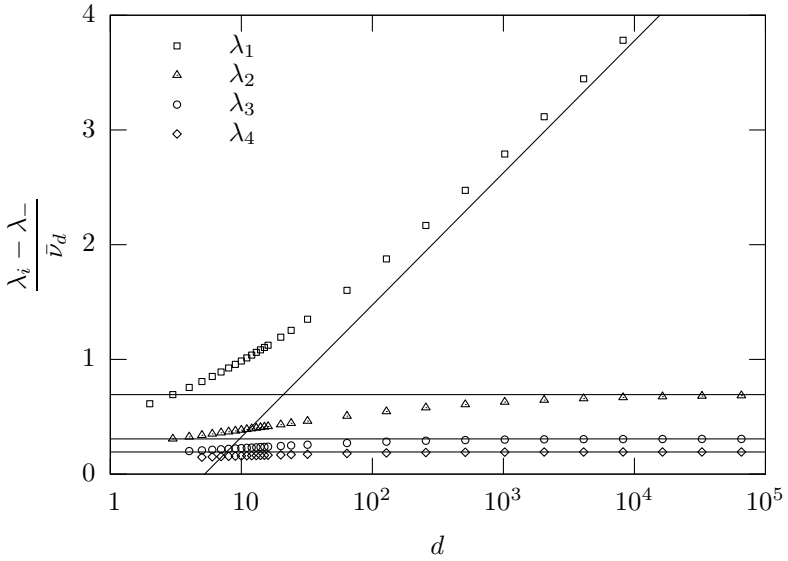

Figure 5.3: The four largest Lyapunov exponents as functions of the dimensionality. Their limiting behaviour is indicated with lines. The second, third, and fourth exponent converge to horizontal lines, as calculated in equations (5.33)–(5.35).

As a consequence of this, for fixed collision frequency, $(\lambda_1 - \lambda_-)/\bar{\nu}_d$ grows logarithmically with dimensionality, whereas $(\lambda_p - \lambda_-)/\bar{\nu}_d$ with $p > 1$ approaches a limit that is independent of d. This too is illustrated in figure 5.3.

5.6 Discussion

The integrals in equation (5.23) can be performed numerically. Several spectra, for various dimensionalities, are plotted in figure 5.2. The results for the largest and smallest exponents are displayed in figures 5.3 – 5.5, along with the limiting behaviours for large dimensionality, which were discussed already in the previous section.

The offset of all Lyapunov exponents, λ_-, depends on both density and dimensionality. For large d, its magnitude is determined primarily by dimensionality, unless density is so low as to satisfy

$$na^d < \frac{O_{d-1}}{d-1} \,. \tag{5.36}$$

It is interesting to compare the Lyapunov spectrum of a high-dimensional Lorentz gas to that of a system of moving hard disks, as computed by Dellago et

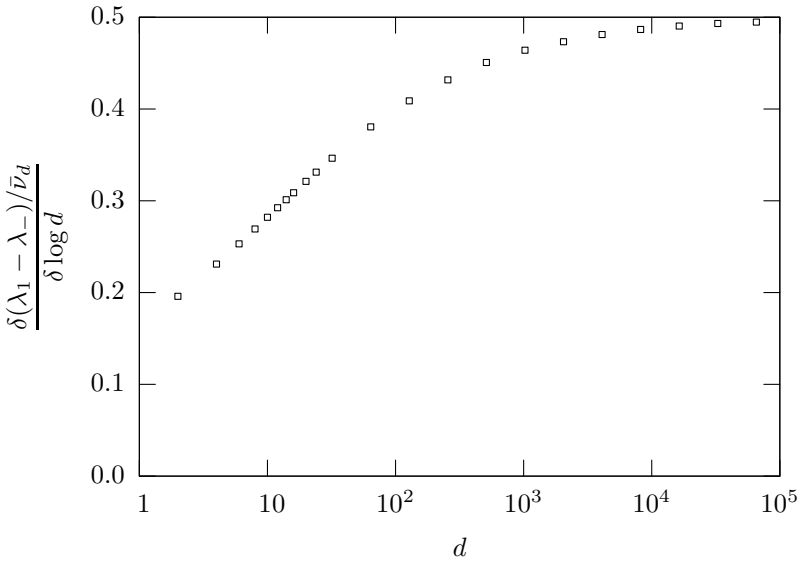

Figure 5.4: The discrete derivative of the largest Lyapunov exponent with respect to $\log d$. The derivative converges to $\frac{1}{2}$, as calculated in equation (5.30).

al. [23]. Figure 3.1 shows such a spectrum for 750 particles in two dimensions at a density of $n = 0.1/a^2$. One immediately notices that the Lorentz gas spectrum is much flatter than that of the hard-disk system. The explanation for this is that for the hard-disk system only a few (four, to be specific) components of the velocity deviation in tangent space are changed at each collision, whereas in the Lorentz gas all components are involved, though some will be increased more than others. A greater similarity may be obtained by replacing the spherical scatterers in the d-dimensional Lorentz gas by randomly oriented hyper cylinders. Indeed our calculations [51] indicate that the spectrum obtained for this system resembles much more that of the hard-disk system, but there remain significant differences due to the randomness of the cylinder orientations (for hard-disk systems the scatterers in phase space are hyper cylinders of specific orientations). In addition, due to the absence of velocities for the scatterers, the d-dimensional Lorentz gas will never exhibit a branch of Goldstone modes with Lyapunov exponents approaching zero as the inverse of system size, such as the ones described for hard disks in chapter 3 and references [22, 28–30, 35, 36, 38, 52].

However, there are also some similarities between the two (positive) spectra: First of all, both become increasingly flat with increasing index (apart from the Goldstone branch for the hard disks). Secondly both become steep near the largest exponent. It is especially remarkable that, for fixed collision frequency,

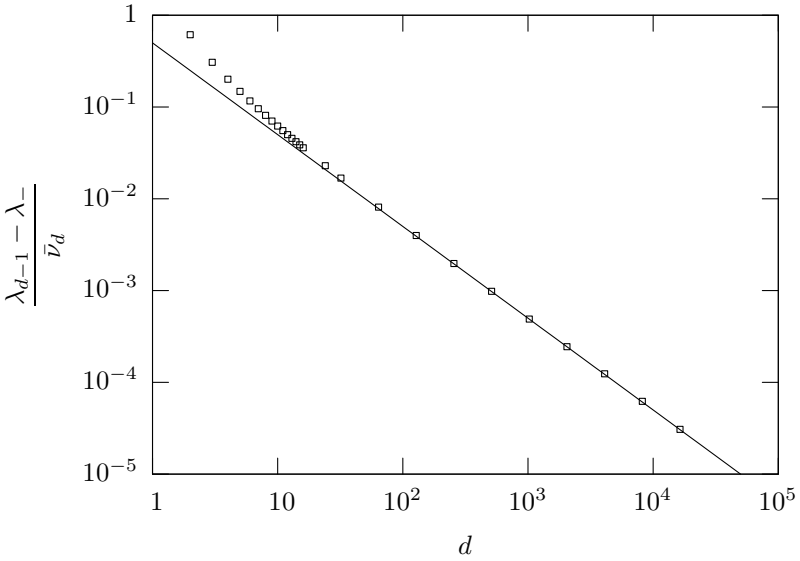

Figure 5.5: The smallest positive Lyapunov exponent as a function of the dimensionality. The values converge to the line $1/(2d)$, calculated in equation (5.31).

the difference between the largest exponent and the next largest one in the Lorentz gas increases logarithmically with the number of degrees of freedom, whereas all the subsequent differences, in the positive half of the spectrum, approach fixed limiting values. Whether something like this also happens for hard disks is not known at present, though there have been conjectures of similar behaviour by Searles et al. [53].

5.7 Conclusions

In this chapter, the full Lyapunov spectrum for the dilute random Lorentz gas in an arbitrary number of dimensions was calculated. Analytical expressions were derived for the behaviour of this spectrum. The spectrum becomes flatter with increasing dimensionality or decreasing density. The separation between the largest and second largest exponent, expressed in units of the collision frequency, increases logarithmically with dimensionality. The smallest exponent itself, however, grows more rapidly with the dimensionality.

In the present case we could take advantage of the property that the partial stretching factor is distributed independently of the subspace being stretched [50]. This is not the case any more for systems of many moving particles, for which the

dynamics are not invariant, on average, under arbitrary rotations in configuration space. In chapter 6 an approach is described which applies parts of the method described in this chapter to many-particle systems.

Chapter 6

Hard disks versus isotropically distributed cylinders

6.1 Introduction

In chapters 2 and 5, it was mentioned already that the dynamics of a collision between two hard particles is equivalent to the dynamics of an elastic collision of a point particle with a cylindrical scatterer in a high-dimensional space. A system consisting of N hard particles in d dimensions can similarly be interpreted as a dN-dimensional space with a point particle bouncing between (hyper-)cylindrical scatterers. As will be shown in section 6.2, the orientations and positions of the scatterers are quite specific.

In chapter 5, the Lyapunov spectrum of the high-dimensional Lorentz gas was calculated. It shows some similarities to the spectrum of many hard particles, but there are also quite a few differences. Some of these differences are due to the shape of the scatterers. The scatterers in the Lorentz gas are spherical, whereas those in many-particle systems are cylindrical. Other differences are due to the positions of the scatterers, or the relative orientations in the case of hard disks. In this chapter, the effects of the shape of the scatterers are investigated. Calcu-

lations on, as well as simulations of systems consisting of isotropically distributed (hyper) cylinders, produce a spectrum much more similar to that of a hard-sphere system than to the spectrum of the Lorentz gas [51].

6.2 Scatterer configurations

Consider the high-dimensional system with (hyper-)cylindrical scatterers that is equivalent to the hard-sphere system. The orientations of the cylinders can be found easily. If two (hyper) cylinders belong to collisions of pairs of different particles, the finite directions of the two (hyper) cylinders are orthogonal. Collisions of the point particle in the high-dimensional space with two specific (hyper) cylinders may be equivalent to two collisions between two pairs of hard spheres which involve a common particle i. In this case, the spherical components, the finite directions, of the two (hyper) cylinders are at an angle. Let the two other particles involved in the two collisions be particles j and l. The d-dimensional planes with which the inclusion of the cylinder pertaining to a collision between particles i and j is a sphere consists of the sets

$$\mathcal{S}_{ij} = \{\mathbf{r} | \mathbf{r}_i = -\mathbf{r}_j \wedge \mathbf{r}_l = 0, \text{ if } l \neq i, j\} \ . \tag{6.1}$$

For any d, the highest possible value for an inner product of unit vectors in $\mathcal{S}_{ij}$ and $\mathcal{S}_{il}$ is $\frac{1}{2}$. Therefore the angle between the two sets is $\pi/3$.

The coordinates of the centre-of-mass constitute d out of the dN dimensions of the original system. If the boundary conditions are periodic or the system is infinite, there is only uniform motion in these directions. This means that perturbations in these coordinates (uniform translations of the system) remain constant. Perturbations of the velocity in these directions (Galilei transformations) lead to a linear growth in the perturbations in the positions. This yields $2d$ linearly independent perturbations which do not grow exponentially, and therefore $2d$ zero Lyapunov exponents, associated with the position and momentum of the centre of mass. There are two more zero Lyapunov exponents, corresponding to a translation in time and a rescaling of the velocity.

After eliminating the centre-of-mass coordinates by setting the centre-of-mass position and momentum to zero, one can describe the system as a point particle with coordinate $\mathbf{r}$ in a $d(N-1)$-dimensional space with periodic boundary conditions and with $N(N-1)/2$ fixed (hyper-)cylindrical scatterers with d spherical dimensions. As energy is conserved, the particle still moves at velocity v, which may be related to the inverse temperature $\beta = 1/(k_{\mathrm{B}}T)$ by

$$v = \sqrt{\frac{(N-1)d}{\beta m}} \ . \tag{6.2}$$

If the system has periodic boundary conditions, there are extra parallel cylinders, corresponding to collisions after at least one of the particles has moved

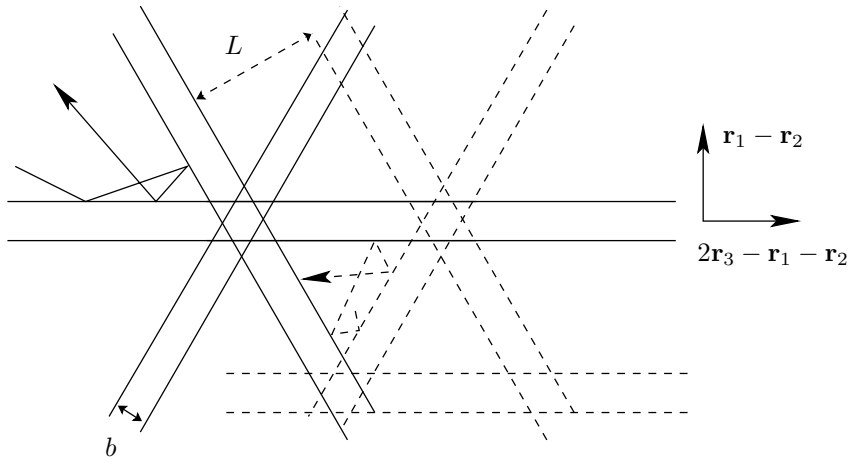

Figure 6.1: The two-dimensional representation of a system consisting of three particles in one dimension. A possible trajectory is shown. If the system is infinite, the particles will soon leave each other's vicinity and never collide again. The axes of the cylinders intersect in one point. If the system has finite size L with periodic boundary conditions, they will encounter each other again. The cylinders belonging to such collisions and a path are indicated with dotted lines.

through the boundaries of the elementary unit cell. In this case the system consists of a $d(N-1)$-dimensional box times $\mathbb{R}^d$ with periodic boundary conditions.

Consider, for example, the simplest non-trivial case: three particles in one dimension. The space has two dimensions and the fixed (hyper) cylinders have one spherical and one infinite dimension. The 2-dimensional representation is displayed in figure 6.1.

The cylinders corresponding to the hard-sphere system are oriented in specific directions. To simplify calculations, it is possible to consider a homogeneous distribution of scatterers, with a distribution of orientations which is isotropic. With such a distribution it may become possible to use the techniques developed in chapter 5 to calculate the Lyapunov spectrum.

6.3 Simulations of the spectrum of isotropically distributed cylinders

In order to investigate the importance of the shape of the scatterers and the distribution of orientations, simulations can be done on a high-dimensional system with homogeneously distributed cylinders with an isotropic distribution of orien-

tations. Cylinders are considered with two spherical directions. This system can be compared to hard disks with the same collision frequency as well as to the Lorentz gas.

6.3.1 Simulation method

The dynamics in phase space were calculated by means of a Monte Carlo method for the location and orientation of the cylinders. Collision parameters were drawn from the relevant distributions, to generate a path in phase space. Each step consists of a short free flight of the point particle, followed by a collision with a cylindrical scatter. The free-flight times are drawn from an exponential distribution of times τ,

$$p(\tau) = \bar{\nu}_N e^{-\bar{\nu}_N \tau} \ , \tag{6.3}$$

where $\bar{\nu}_N$ is the average collision frequency of the point particle with the scatterers. The collision normal is drawn from an isotropic distribution in the $d(N-1)$-dimensional space, such that $\hat{\sigma} \cdot \mathbf{v} < 0$, and accepted with a probability equal to the size of the component along the velocity of the point particle, $-\hat{\sigma} \cdot \hat{\mathbf{v}}$, which is proportional to the collision rate in two dimensions. The orientation of the scatterer is specified by the two vectors in its spherical directions, the collision normal and one other vector, which is drawn from the isotropic distribution as well. This leads to an isotropic distribution of the orientations of the scatterers. For more details on Monte Carlo simulations see reference [54].

At each collision, the dynamics of the point particle are calculated, as well as the transformations of a numbered set of tangent-space vectors. After every step, the tangent-space vectors are reorthonormalised. That is to say, the components of each of the vectors along vectors with higher indices are subtracted and then the vectors are normalised. The scaling factors are equal to the growth of each vector between the last two collisions. For long times, the growth of the i-th vector is dominated by the i-th Lyapunov exponent. The scaling factors are stored and, for each vector, their logarithms are summed. The i-th sum divided by the total elapsed time, for long times, converges to the i-th Lyapunov exponent. For more details on this method for calculating the Lyapunov exponents, see reference [23].

6.3.2 The spectrum

We may compare the spectra of a point particle colliding with homogeneously and isotropically distributed cylinders to the spectra of systems of hard disks with the same collision frequency, energy and dimensionality (with $d = 2$), as well as to the spectrum of the high-dimensional Lorentz gas. Plots of the spectra of the isotropically distributed cylinders at various dimensionalities are shown in figures 6.2 – 6.4 for, respectively, densities $n = 0.1, 0.01$, and 0.0001, along with those of the corresponding hard-disk systems under periodic boundary conditions.

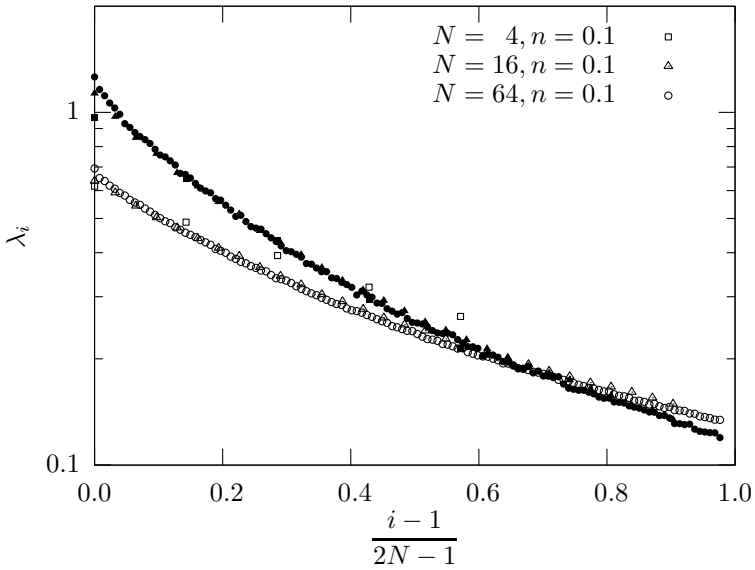

Figure 6.2: The spectra of positive Lyapunov exponents for systems of isotropically distributed (hyper) cylinders with the same collision frequency, energy, and dimensionality as a hard-disk system with density $0.1a^{-2}$ and various particle numbers N. The inverse temperature $\beta = 1$. The open symbols represent the isotropically distributed cylinders and the closed symbols represent the corresponding hard-disk system.

The Lorentz gas spectrum, calculated in chapter 5, is much flatter than that of the hard-disk system. From the figures one can see that the spectrum of a point particle colliding among isotropically distributed cylinders is much more similar to the hard-disk spectrum. This is due to the fact that in the Lorentz gas, all coordinates not associated with zero modes are involved in every collision, and grow with a factor of the order of the free-flight time between two collisions, whereas in the case of the hard disks only eight ($4d$) coordinates are involved in a collision.

For the largest exponents of hard-disk systems it is known that the corresponding perturbation is carried by only a few particles [6]. The vectors belonging to this exponent are changed by the isotropy of the distribution of scatterers. The largest Lyapunov exponents, therefore, are different, compared to the many-particle system, for a system consisting of a point particle colliding with isotropically distributed cylinders.

The tangent-space eigenvectors corresponding to the smaller exponents of hard-disk systems are carried by many particles, and for these modes the similarities to the cylinder system are much greater. The lower Lyapunov exponents

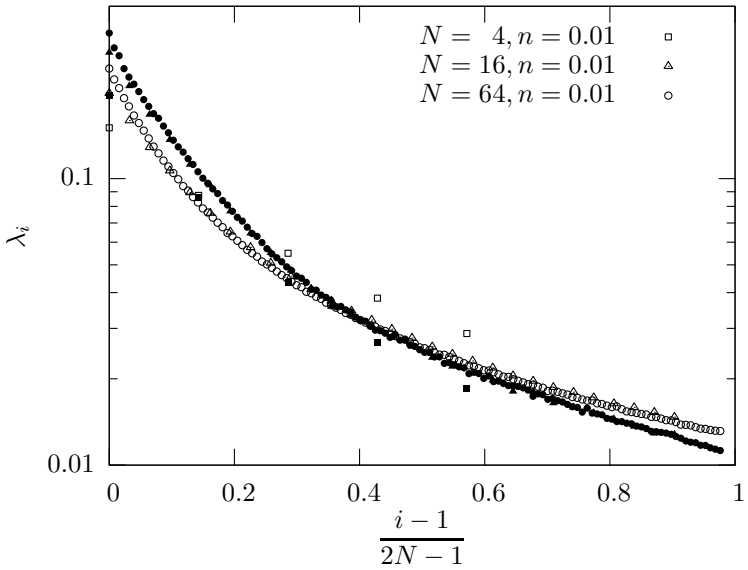

Figure 6.3: The spectra of positive Lyapunov exponents for systems of isotropically distributed (hyper) cylinders that are, similarly to figure 6.2, equivalent to a hard-disk system with density $0.01a^{-2}$ and various particle numbers N.

behave similarly to the exponents of the hard-disk system (apart from the Goldstone modes) and are proportional to $\bar{\nu}$. There is only a difference of a factor of about 1.15 between the smallest exponents in the two systems, which does not depend much on density or particle number. As the cylinders can no longer be associated with two specific particles, Goldstone modes are absent in the cylinder system.

6.4 Isotropic-cylinder approximations for the hard-disk system

The simulation described in the previous section produces a Lyapunov spectrum which is suggestively similar to the spectrum of hard disks. As the system is homogeneous and isotropic, part of the techniques developed in chapter 5 can be applied to calculate the Lyapunov exponents. Rather than working this out we return to the hard-disk system and apply to this some approximation inspired by the isotropic cylinder system

For the largest exponent it is known that the corresponding perturbation is carried by only a few particles [6]. The Lyapunov exponents are strongly affected

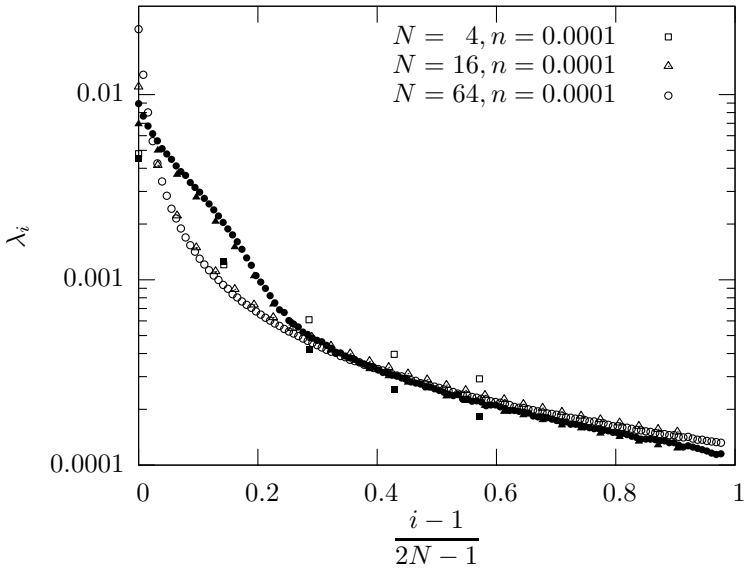

Figure 6.4: The spectra of positive Lyapunov exponents for systems of isotropically distributed (hyper) cylinders that are equivalent, similarly to figure 6.2, to a hard-disk system with density $0.0001a^{-2}$ and various particle numbers N. In the hard-disk spectrum the transition between tangent-space eigenvectors carried by a few particles and those carried by many particles is visible near $(i-1)/(2N-1) \approx 0.25$.

by this, because collisions of particles other than these few do not contribute to the growth of the tangent-space vectors. There is a small probability of large growth, as opposed to a large probability of small growth. In the lower end of the spectrum, the tangent-space vectors are carried by many particles [55]. In this regime, it may be possible to approximate the distribution of scatterers as isotropic.

The properties of the system that give rise to the largest exponents are modified an isotropic scatterer distribution. The values of the largest exponents will therefore be different. For the smaller exponents the approximation should be better. The Goldstone modes, which were discussed in chapter 3, are also removed by the homogeneous distribution of scatterers, as their existence relies on the fact that in the hard-disk system only nearby particles collide. Sometimes, the Lyapunov exponents other than the Goldstone modes are referred to as the "continuum" exponents. This is not entirely accurate, as for finite particle numbers there is no continuum and in the limit of infinite particle numbers the step structure of the Goldstone modes also goes to a continuous line. There is also some discussion of a discontinuity in the spectrum near the largest exponent [53].

In this section, a calculation of the smallest continuum exponents is described which makes use of the stretching factor derived in chapter 4, but which assumes an isotropic distribution of scatterers.

6.4.1 Projection

In chapter 5, the isotropic distribution of scatterers makes it possible to simplify the calculation. Because of it, the probability distribution of the stretching factor is independent of the p-dimensional subspace S which is being stretched.

In the systems described in this chapter, that of isotropically distributed cylinders and that of hard disks, it is important to observe that the choice of the space onto which everything is projected, affects the distribution of the partial stretching factors. In equation (4.11) it is shown how diagonal elements of $\mathcal{W}$ grow linearly during free flights. In the calculations of the stretching factor in hard-disk systems in chapter 4, $w_{\perp\perp}$ is, essentially, calculated as a weighted sum over a sequence of free flights. In the case of truly isotropically distributed cylinders, the (partial) stretching factors are different from those in the equivalent hard-disk system. However, in that case, $w_{\perp\perp}$ can be replaced with a similar expression.

Terms in the sum in $w_{\perp\perp}$ occur in the partial stretching factors of several collisions. Also, the relative size of their contributions is affected by the relative orientation of $\hat{\mathbf{v}}_{ij}$ belonging to the two collisions. Suppose one such term contains a long free-flight time. In the phase-space direction belonging to this particle, the stretching is large, and this affects the orientation of the growing manifold. At future collisions of the particle, $w_{\perp\perp}$ will again contain large terms due to this free-flight time. This introduces a correlation between the orientation of the manifold and the partial stretching factor. In the projection onto $\delta\mathbf{v}$, the distribution of partial stretching factors depends on the orientation of the stretched space S, even in the case of fully isotropically distributed cylinders.

If an approximation is to be made in the hard-disk system which does not exhibit this problem, the standard choice of projection on $\delta\mathbf{v}$, which was used in chapter 4, is inadequate. Instead, as is done in this section, the dynamics must be projected onto $\delta\mathbf{r}$. In this representation, the correlations through the sums of collision times are removed. However, the isotropic distribution of orientations is still an approximation, as there is correlation between free-flight times and other collision parameters from different collisions through the particle velocity.

6.4.2 The partial stretching factors for hard spheres at low densities

The stretching of a p-dimensional subspace of the space of $\delta\mathbf{r}$, due to a collision between particles i and j, depends on the subspace itself and on $\mathcal{W}$ at the collision. There are $2d$ coordinates involved in the collision projected on $\delta\mathbf{r}$, d for each particle. The tangent-space dynamics are described in chapter 2. In the

relative coordinates, the collision transforms the tangent-space vectors as in an elastic collision with a d-dimensional, fixed, spherical scatterer. Q works on $d-1$ directions of the relative coordinates orthogonal to $\hat{\mathbf{v}}_{ij}$. The stretching in those directions was calculated in chapter 5 from equation (5.11).

Let $\hat{\rho}$ represent the vector, in d dimensions, which is orthogonal to $\hat{\mathbf{v}}_{ij}$ and in the plane spanned by $\hat{\sigma}$ and $\hat{\mathbf{v}}_{ij}$. In the direction of $\delta\mathbf{r}_{ij}$ parallel to $\hat{\rho}$, the partial stretching factor of the projection on $\delta\mathbf{r}$ after a collision and subsequent free flights is, in leading order in the density, $2v\tau_+/(a\cos\theta)$, where τ_+ is the same as in chapter 4, that is, $\tau_+ = (\tau_i+\tau_j)/2$. In $d-2$ directions orthogonal to $\hat{\rho}$ and $\hat{\mathbf{v}}_{ij}$, the partial stretching factor is $2v\tau_+\cos\theta/a$. There are $d+1$ coordinates involved in the collision on which $\mathcal{Q}$ does not work, the centre-of-mass coordinates and the relative coordinates parallel to $\hat{\mathbf{v}}_{ij}$. In these directions, the linear stretching due to the free flights must be calculated and incorporated into the partial stretching factor. Meanwhile, for all other particles, $\delta\mathbf{r}$ grows linearly as well. This can be accounted for later, at their next collision.

The distribution of this stretching is complicated if the distribution of the elements of $\mathcal{W}$ is hard to obtain. In a simple calculation, the expressions for $\mathcal{W}'$ and $\mathcal{W}^*$ in the mean-field approximation of section 4.3.1 can be used [see equations (4.21) and (4.22)]. In this case, $\mathcal{W}$ is approximated by $\bar{\mathcal{W}} = \mathcal{I}\bar{w}$. With this simple form of $\mathcal{W}'$ and $\mathcal{W}^*$, the partial stretching factors in the remaining $d+1$ directions can be calculated. For the $d-1$ directions of the centre-of-mass coordinates orthogonal to $\hat{\mathbf{v}}_{ij}$, the eigenvalues of $\mathcal{W}'$ are $\bar{w}+\bar{\nu}\tau_+$, yielding a partial stretching factor of $(\bar{w}+\bar{\nu}\tau_+)/\bar{w}$. Similarly, for the remaining two directions, those parallel to $\hat{\mathbf{v}}_{ij}$, one finds $(\bar{w}+\bar{\nu}\tau_i)/\bar{w}$ and $(\bar{w}+\bar{\nu}\tau_j)/\bar{w}$.

In the directions of particles not involved in the collision, nothing is changed. In the coordinates parallel to $\hat{\mathbf{v}}_{ij}$,

$$\hat{\mathbf{v}}'_{ij}\cdot\delta\mathbf{r}'_i = \left(1+\frac{\bar{\nu}\tau_i}{\bar{w}}\right)\hat{\mathbf{v}}_{ij}\cdot\delta\mathbf{r}_i\ . \tag{6.4}$$

In the relative coordinates, Q acts on vectors orthogonal to $\hat{\mathbf{v}}'_{ij}$,

$$\begin{aligned}(\mathbf{1}-\hat{\mathbf{v}}'_{ij}\hat{\mathbf{v}}'_{ij})\cdot\delta\mathbf{r}'_{ij} = \frac{2v\tau_+}{a}\left[\cos\theta(\mathbf{1}-\hat{\mathbf{v}}'_{ij}\hat{\mathbf{v}}_{ij}-\hat{\rho}'\hat{\rho})+\frac{1}{\cos\theta}\hat{\rho}'\hat{\rho}\right]\cdot\delta\mathbf{r}_{ij}\\ +\frac{\bar{\nu}(\tau_i-\tau_j)}{2\bar{w}}(\mathbf{1}-\hat{\mathbf{v}}'_{ij}\hat{\mathbf{v}}_{ij})\cdot\delta\mathbf{R}_{ij}\ .\end{aligned} \tag{6.5}$$

In the centre-of-mass coordinates orthogonal to $\hat{\mathbf{v}}'_{ij}$,

$$\begin{aligned}(\mathbf{1}-\hat{\mathbf{v}}'_{ij}\hat{\mathbf{v}}'_{ij})\cdot\delta\mathbf{R}'_{ij} = \left(1+\frac{\bar{\nu}\tau_+}{\bar{w}}\right)(\mathbf{1}-\hat{\mathbf{v}}'_{ij}\hat{\mathbf{v}}_{ij})\cdot\delta\mathbf{R}_{ij}\\ +\frac{\bar{\nu}(\tau_i-\tau_j)}{2\bar{w}}(\mathbf{1}-\hat{\mathbf{v}}'_{ij}\hat{\mathbf{v}}_{ij})\cdot\delta\mathbf{r}_{ij}\ .\end{aligned} \tag{6.6}$$

The eigenvalues of the transformation, the growth factors, may be numbered g_l, with l between 1 and $2d$. They can be found from equations (6.4) – (6.6). More

simply put, the following growth factors occur:

$$g_l = \begin{cases} \dfrac{2v\tau_+}{a\cos\theta} & \text{if } \; l = 1 \; , \\ \dfrac{2v\tau_+\cos\theta}{a} & \text{if } \; 1 < l \leq d-1 \; , \\ 1 + \dfrac{\bar{\nu}\tau_i}{\bar{w}} & \text{if } \; l = d \; , \\ 1 + \dfrac{\bar{\nu}\tau_+}{\bar{w}} & \text{if } \; d < l \leq 2d-1 \; , \\ 1 + \dfrac{\bar{\nu}\tau_j}{\bar{w}} & \text{if } \; l = 2d \; . \end{cases} \tag{6.7}$$

From these growth factors, the partial stretching factor can be calculated.

6.4.3 Lower bound of the Kolmogorov-Sinai entropy

In principle, the choice of projection does not affect the Kolmogorov-Sinai entropy. Also, since no partial stretching factors are considered in the calculation, only the stretching factor, there is no need for any isotropic approximation. From equations (6.7) and (4.30) or (4.40) the stretching factor can be calculated. With equation (4.3) the Kolmogorov-Sinai entropy becomes,

$$h_{\mathrm{KS}} = \frac{N\bar{\nu}}{2} \left\langle \log \left[\prod_{l=1}^{2d} g_l \right] \right\rangle \; . \tag{6.8}$$

The approximation of $\mathcal{W}^{-1}$ by $1/\bar{\mathcal{W}}$ affects the Kolmogorov-Sinai entropy. After numerical integration, using the estimate for $\bar{w}$ in equation (4.40), this yields for the constant B the approximate values

$$B_{\alpha\mathbf{r}}^{(1)} \approx \begin{cases} 0.98 & \text{if } \; d = 2 \; , \\ 0.13 & \text{if } \; d = 3 \; . \end{cases} \tag{6.9}$$

The estimation is quite rough, compared to the results of equation (4.51). Note that here, unlike in the calculation in chapter 4, a wider spread of the elements of $\mathcal{W}$, or a lower value of $\bar{w}$, leads to a larger value for B. The result for $\bar{w}$ in equation (4.30) does not include the estimate of the terms from collisions before the previous collision in the calculation of $\bar{w}$ through α. As the results of equation (4.30) are an upper bound for $\bar{w}$, a lower bound for B can be found from them, or

$$B > \begin{cases} 0.96 & \text{if } \; d = 2 \; , \\ 0.09 & \text{if } \; d = 3 \; . \end{cases} \tag{6.10}$$

6.4.4 The smallest exponents

Despite the crudeness of the approximations made in this section to calculate the (partial) stretching factors, it is possible to use the results to estimate the smallest continuum Lyapunov exponents.

Any $[d(N-1)-2]$-dimensional subspace $S_{d(N-1)-2}$ of the $[d(N-1)-1]$-dimensional subspace $S_{d(N-1)-1}$ of $[\delta\mathbf{r}_i]$ orthogonal to the zero modes can be characterised by a single vector, $\hat{\mathbf{g}}$. This is the vector orthogonal to $S_{d(N-1)-2}$ and the zero modes. The assumption made in this section is that this vector, which is the eigenvector belonging to the smallest positive (continuum) exponent has significant components along the directions $\delta\mathbf{r}_i$ and $\delta\mathbf{v}_i$ of many particles, and is more or less isotropically distributed in phase space, which permits the isotropic approximation mentioned before. Also, these components do not depend on the velocities of the particles.

The smallest continuum exponent can be calculated from equation (5.13), the partial stretching factor of $S_{d(N-1)-2}$ at a collision, and the stretching factor. Following the derivation in section 5.4 for the hard-disk system, one obtains

$$\lambda_{d(N-1)-2} = \frac{N\bar{\nu}}{2}\left\langle \log\Lambda^{(p)} - \log\Lambda^{(p)}_{d(N-1)-2}\right\rangle \ , \tag{6.11}$$

where p is the index of the collision, $\Lambda^{(p)}$ is the stretching factor due to collision p, and $\Lambda^{(p)}_{d(N-1)-2}$ is the partial stretching factor of $S_{d(N-1)-2}$ due to collision p.

The difference of the two logarithms in equation (6.11) can be expressed in terms of the components of $\hat{\mathbf{g}}$ along the growing directions, denoted as $\sin\phi_l$, with l the index of the growth factor. If $\sin\phi_l$ is small for all l, $\langle\sin^2\phi_l\rangle = 1/(dN)$, one finds

$$\lambda_{d(N-1)-2} \approx \frac{N\bar{\nu}}{2}\left\langle -\log\left(\prod_{l=1}^{2d}\sqrt{\cos^2\phi_l + \frac{1}{g_l^2}\sin^2\phi_l}\right)\right\rangle \ . \tag{6.12}$$

If $\hat{\mathbf{g}}$ has components along many particles, then $\sin\phi_l$ is small, and the logarithm can be expanded around unity argument, to yield

$$\lambda_{d(N-1)-2} \approx \frac{N\bar{\nu}}{4}\left\langle \sum_{l=1}^{2d}\left(1-\frac{1}{g_l^2}\right)\sin^2\phi_l\right\rangle \ . \tag{6.13}$$

With the assumptions made about the distribution of ϕ_l, one then finds

$$\lambda_{d(N-1)-2} \approx \frac{\bar{\nu}}{4d}\sum_{l=1}^{2d}\left(1-\left\langle\frac{1}{g_l^2}\right\rangle\right) \ . \tag{6.14}$$

The $d-1$ directions in which the growth factor is of order $1/n$ contribute an amount $\bar{\nu}/(4d)$ to the smallest exponents. The growth factors due to the free

flights, of order 2, contribute smaller amounts. If the growth factors had been calculated from the projection on $\delta\mathbf{v}$, the isotropic approximation would have been worse, and only the growth in the $d-1$ directions on which $\mathcal{Q}$ works would have been found. The other terms in the smallest exponents would have been absent.

Combining equation (6.14) with equations (4.40) and (6.7), after numerical integration over the growth factors to calculate the averages, yields estimates for the leading order of the smallest continuum exponent, at low densities,

$$\lambda_{d(N-1)-2} \approx \begin{cases} 0.26\,\bar{\nu} & \text{if } \; d = 2\ , \\ 0.32\,\bar{\nu} & \text{if } \; d = 3\ . \end{cases} \tag{6.15}$$

These expressions are similar to the lowest continuum exponent found in simulations of hard disks and hard spheres, which are also proportional to $\hat{\nu}$. For large particle numbers and low densities, the smallest continuum exponents are equal to [37]

$$\lambda_{d(N-1)-2} = \begin{cases} 0.31\,\bar{\nu} & \text{if } \; d = 2\ , \\ 0.39\,\bar{\nu} & \text{if } \; d = 3\ . \end{cases} \tag{6.16}$$

The prefactors found in the estimation based on the mean-field and isotropic approximations differ from the simulation results by less than 20 %.

6.5 Conclusions

In this chapter, in section 6.3, Monte Carlo simulations of the spectrum of the isotropically distributed cylinders were discussed. The lower three quarters of the positive Lyapunov exponents were found be similar to the exponents of hard disks as a function of the (effective) density. The dependence on the number of dimensions (particles) is also the same for the lower end of the spectrum. The larger exponents behave differently, as was to be expected.

Further, in section 6.4, an estimate of the smallest continuum exponent was discussed. In this calculation, the collective property of the eigenvector belonging to the smallest exponent was used. This is less severe than assuming a completely isotropic distribution of scatterer orientations, but the results are the same to leading order. Based on the calculations presented in chapter 4, an approximation for the partial stretching factor was made. The results of this calculation resemble the simulation results for hard disks. The smallest continuum exponents depend on the collision frequency $\bar{\nu}$ in the correct way. The prefactor deviates from the simulation results by about 20%. The $\sim \bar{\nu}$ behaviour of the smallest continuum exponents is entirely due to the fact that at a collision the tangent-space vectors only grow in a few directions.

Both calculations discussed in this chapter indicate that the lower end of the continuum spectrum is predominantly determined by the shape of the scatterers, and not so much by the scatterer orientations. With better approximations of the partial stretching factor, it should be possible to use the method developed in chapter 5 with an isotropic distribution of scatterer orientations to calculate the lower three quarters of the continuum Lyapunov spectrum of hard disks and spheres.

Appendix A

Polynomial expansion of the generalised Enskog equation

A.1 Expansion in Hermite polynomials of the tangent-space collision operators

In order to solve equation (3.29), one must write the operators in equations (3.18) and (3.19) as matrices with elements defined as inner products of these operators between the basis functions described in equation (3.41). From now on we take $d = 2$, but the same calculations can easily be done for three dimensions. We only show results for basis functions of up to linear order in $\mathbf{v}$. In equation (3.41) p and q can be equal to 0 or 1. In fact, one has to include higher powers to find good approximations for the solutions to the original equations. In this appendix basis functions with up to sixth power in $\mathbf{v}$ are used.

If the first component is the component parallel to $\mathbf{k}$, the basis is ordered as $(1,0)$, $(0,1)$, $(\sqrt{\beta m/2}\, v_\parallel, 0)$, $(0, \sqrt{\beta m/2}\, v_\parallel)$, $(\sqrt{\beta m/2}\, v_\perp, 0)$, $(0, \sqrt{\beta m/2}\, v_\perp)$. All coefficients are given to leading order in n. In this notation the zero modes are

$$\Delta\mathbf{r}_1^{(0)} = \begin{cases} (1,0,0,0,0,0)\ , \\ (0,1,0,0,0,0)\ , \\ (0,0,\frac{1}{2}\sqrt{2},0,0,\frac{1}{2}\sqrt{2})\ . \end{cases} \tag{A.1}$$

Here, the subscript 1 indicates that basis functions up to first order in $\mathbf{v}$ have been included. From equations (3.26) and (3.29) it follows that the operator B_S, specified in equation (3.18), is only needed up to first order in k. One finds for the matrix elements of B_S in the expansion of equation (3.21)

$$\mathsf{B}^{(0)}_{\mathsf{S},1} = \sqrt{\frac{2}{\beta m}}\,\frac{3\sqrt{2\pi}}{8}\,na \qquad \begin{pmatrix} 0 & 0 & 0 & 0 & 0 & 0 \\ 0 & 0 & 0 & 0 & 0 & 0 \\ 0 & 0 & -1 & 0 & 0 & 1 \\ 0 & 0 & 0 & -3 & 1 & 0 \\ 0 & 0 & 0 & 1 & -3 & 0 \\ 0 & 0 & 1 & 0 & 0 & -1 \end{pmatrix}, \tag{A.2}$$

$$\mathsf{B}^{(1)}_{\mathsf{S},1} = \sqrt{\frac{2}{m\beta}}\,\frac{\sqrt{2}\,\pi i}{16}\,na^2 \qquad \begin{pmatrix} 0 & 0 & 3 & 0 & 0 & 1 \\ 0 & 0 & 0 & 1 & 1 & 0 \\ 3 & 0 & 0 & 0 & 0 & 0 \\ 0 & 1 & 0 & 0 & 0 & 0 \\ 0 & 1 & 0 & 0 & 0 & 0 \\ 1 & 0 & 0 & 0 & 0 & 0 \end{pmatrix}. \tag{A.3}$$

The first three contributions to B_Q as expanded in equations (3.19) and (3.22) have similar matrix representations of the form

$$\mathsf{B}^{(0)}_{\mathsf{Q},1} = \frac{2}{\beta m}\,2\pi\,n \qquad \begin{pmatrix} 0 & 0 & 0 & 0 & 0 & 0 \\ 0 & 0 & 0 & 0 & 0 & 0 \\ 0 & 0 & 0 & 0 & 0 & 0 \\ 0 & 0 & 0 & -1 & 1 & 0 \\ 0 & 0 & 0 & 1 & -1 & 0 \\ 0 & 0 & 0 & 0 & 0 & 0 \end{pmatrix}, \tag{A.4}$$

$$\mathsf{B}^{(1)}_{\mathsf{Q},1} = \frac{2}{\beta m}\,\frac{\sqrt{\pi}\,i}{8}\,na \qquad \begin{pmatrix} 0 & 0 & 1 & 0 & 0 & -1 \\ 0 & 0 & 0 & -5 & 7 & 0 \\ 1 & 0 & 0 & 0 & 0 & 0 \\ 0 & -5 & 0 & 0 & 0 & 0 \\ 0 & 7 & 0 & 0 & 0 & 0 \\ -1 & 0 & 0 & 0 & 0 & 0 \end{pmatrix}, \tag{A.5}$$

$$\mathsf{B}^{(2)}_{\mathsf{Q},1} = \frac{2}{\beta m}\,\frac{\pi}{8}\,na^2 \qquad \begin{pmatrix} -2 & 0 & 0 & 0 & 0 & 0 \\ 0 & 2 & 0 & 0 & 0 & 0 \\ 0 & 0 & -1 & 0 & 0 & 0 \\ 0 & 0 & 0 & 5 & -4 & 0 \\ 0 & 0 & 0 & -4 & 3 & 0 \\ 0 & 0 & 0 & 0 & 0 & 1 \end{pmatrix}. \tag{A.6}$$

The operators $i\hat{\mathbf{k}}\cdot\mathbf{v}$ and $-(\hat{\mathbf{k}}\cdot\mathbf{v})^2$ can also be written in this way. One finds

$$i\hat{\mathbf{k}}\cdot\mathbf{v} = -\sqrt{\frac{1}{\beta m}} \begin{pmatrix} 0 & 0 & i & 0 & 0 & 0 \\ 0 & 0 & 0 & i & 0 & 0 \\ i & 0 & 0 & 0 & 0 & 0 \\ 0 & i & 0 & 0 & 0 & 0 \\ 0 & 0 & 0 & 0 & 0 & 0 \\ 0 & 0 & 0 & 0 & 0 & 0 \end{pmatrix}, \tag{A.7}$$

$$-(\hat{\mathbf{k}}\cdot\mathbf{v})^2 = -\frac{1}{\beta m} \begin{pmatrix} 1 & 0 & 0 & 0 & 0 & 0 \\ 0 & 1 & 0 & 0 & 0 & 0 \\ 0 & 0 & 3 & 0 & 0 & 0 \\ 0 & 0 & 0 & 3 & 0 & 0 \\ 0 & 0 & 0 & 0 & 1 & 0 \\ 0 & 0 & 0 & 0 & 0 & 1 \end{pmatrix}. \tag{A.8}$$

A.2 Solutions to the generalised Boltzmann equation

With these matrices and equation (3.26) the vectors for $\Delta\mathbf{r}^{(1)}$ may be expressed in terms of $\Delta\mathbf{r}^{(0)}$ up to first order in the polynomial expansion in $\mathbf{v}$. With the orthogonality relation between $\Delta\mathbf{r}^{(1)}$ and $\Delta\mathbf{r}^{(0)}$, mentioned in section 3.5.1, this yields

$$\Delta\mathbf{r}_1^{(1)} = -\frac{2i}{9na\sqrt{\pi}} \begin{pmatrix} 0 & 0 & 0 & 0 & 0 & 0 \\ 0 & 0 & 0 & 0 & 0 & 0 \\ 1 & 0 & 0 & 0 & 0 & 0 \\ 0 & 1 & 0 & 0 & 0 & 0 \\ 0 & 1 & 0 & 0 & 0 & 0 \\ -1 & 0 & 0 & 0 & 0 & 0 \end{pmatrix} \cdot \Delta\mathbf{r}_1^{(0)} . \tag{A.9}$$

The matrices expressing the collision operators in the basis of Hermite polynomials can be used to find the 3×3 matrices in equations (3.29) and (3.31). The equation to leading order in n then becomes

$$\det \begin{pmatrix} -\frac{7}{18} + \left(\lambda_1^{(1)}\sqrt{\frac{\beta m}{2}}\right)^2 & 0 & 0 \\ 0 & -\frac{7}{18} + \left(\lambda_1^{(1)}\sqrt{\frac{\beta m}{2}}\right)^2 & i\lambda_1^{(1)}\sqrt{\frac{\beta m}{2}} \\ 0 & i\lambda_1^{(1)}\sqrt{\frac{\beta m}{2}} & -1 + \left(\lambda_1^{(1)}\sqrt{\frac{\beta m}{2}}\right)^2 \end{pmatrix} = 0 . \tag{A.10}$$

n	transverse $\lambda_n^{(1)}\sqrt{\frac{\beta m}{2}}$	longitudinal $\lambda_n^{(1)}\sqrt{\frac{\beta m}{2}}$
1	± 0.62361	$\pm 0.639552 \pm 0.463231\, i$
2	± 0.62361	$\pm 0.422807 \pm 0.499026\, i$
3	± 0.626194	$\pm 0.424806 \pm 0.499105\, i$
4	± 0.626194	$\pm 0.428599 \pm 0.498952\, i$
5	± 0.626254	$\pm 0.428645 \pm 0.498954\, i$
6	± 0.626254	$\pm 0.429104 \pm 0.498953\, i$

Table A.1: The Lyapunov exponents and the propagation velocities for the longitudinal mode calculated using products of Hermite polynomials in $\mathbf{v}$ up to different orders.

Here, the indices of the matrix on the left-hand side are ordered according to $(\Delta\mathbf{r}_\perp^{(0)}, \Delta\mathbf{r}_\parallel^{(0)}, \Delta\mathbf{r}_\mathbf{v}^{(0)})$. The matrix can be factorised into two parts. One part describes the transverse mode and produces an equation for $(\lambda^{(1)})^2$, with the solution

$$\lambda_1^{(1)}\sqrt{\frac{\beta m}{2}} = \pm\frac{1}{6}\sqrt{14} \approx \pm 0.62361\ . \tag{A.11}$$

The remaining part produces a quadratic equation in $(\lambda^{(1)})^2$, yielding the longitudinal mode. The solutions for $\lambda^{(1)}$ are

$$\lambda_1^{(1)}\sqrt{\frac{\beta m}{2}} = \pm\frac{1}{6}\sqrt{\left(7 \pm i\sqrt{455}\right)} \approx \pm 0.639552 \pm 0.493231\, i\ . \tag{A.12}$$

The same calculation can be done with larger subsets of the basis. The results are shown in Table A.1.

Using functions up to an odd power in $\mathbf{v}$ is different from using functions up to an even power, because the odd-powered functions contribute more to different matrix elements than the even-powered functions. To see whether the solutions have converged, one must therefore raise the power by steps of 2. The error in the results using up to sixth powers in $\mathbf{v}$ can be estimated by comparing the results for powers in $\mathbf{v}$ up to four. The error in the solutions when using up to the sixth power in $\mathbf{v}$ in the basis functions appears not to be much larger than a promille.

Bibliography

[1] F. Cecconi, D. del Castillo-Negrete, M. Falcioni, and A. Vulpiani, The origin of diffusion: the case of non chaotic systems, Physica D **180**, 129 (2003).

[2] G. Gallavotti and E. G. D. Cohen, Dynamical ensembles in stationary states, J. Stat. Phys. **80**, 931 (1995).

[3] G. Gallavotti and E. G. D. Cohen, Dynamical ensembles in nonequilibrium statistical mechanics, Phys. Rev. Lett. **74**, 2694 (1995).

[4] J. R. Dorfman, *An Introduction to Chaos in Nonequilibrium Statistical Mechanics* (Cambridge University Press, Cambridge, 1999).

[5] E. Ott, *Chaos in Dynamical Systems* (Cambridge University Press, Cambridge, 1993).

[6] R. van Zon, *Chaos in dilute hard sphere gases in and out of equilibrium*, PhD thesis, Utrecht University (2000).

[7] P. Gaspard and G. Nicolis, Transport properties, Lyapunov exponents and entropy per unit time, Phys. Rev. Lett. **65**, 1693 (1990).

[8] P. Gaspard and F. Baras, Dynamical chaos underlying diffusion in the Lorentz gas, in M. Maréschal and B. Holian, editors, *Microscopic Simulations of Complex Hydrodynamic Phenomena*, page 301 (Plenum, New York, 1992).

[9] R. J. Dorfman and P. Gaspard, Chaotic scattering theory of transport and reaction-rate coefficients, Phys. Rev. E **51**, 28 (1995).

[10] R. J. Dorfman and P. Gaspard, Chaotic scattering theory, thermodynamic formalism, and transport coefficients, Phys. Rev. E **52**, 3525 (1995).

[11] H. van Beijeren, J. R. Dorfman, E. G. D. Cohen, H. A. Posch, and C. Dellago, Lyapunov exponents from kinetic theory for a dilute, field-driven Lorentz gas, Phys. Rev. Lett. **77**, 1974 (1996).

[12] A. Latz, H. van Beijeren, and J. R. Dorfman, Lyapunov spectrum and the conjugate pairing rule for a thermostated random Lorentz gas: Kinetic theory, Phys. Rev. Lett. **78**, 207 (1997).

[13] C. Dellago and H. A. Posch, Lyapunov spectrum and the conjugate pairing rule for a thermostated random Lorentz gas: Numerical simulations, Phys. Rev. Lett. **78**, 211 (1997).

[14] C. Appert and M. H. Ernst, Chaos properties and localization in Lorentz lattice gases, Phys. Rev. E **56**, 5106 (1997).

[15] D. Panja, J. R. Dorfman, and H. van Beijeren, Long-time-tail effects on Lyapunov exponents of a random, two-dimensional field-driven Lorentz gas, J. Stat. Phys. **100**, 279 (2000).

[16] C. Dellago, H. van Beijeren, D. Panja, and J. R. Dorfman, Field dependent collision frequency of the two-dimensional driven random Lorentz gas, Phys. Rev. E **64**, 036217 (2001).

[17] O. Mülken and H. van Beijeren, Thermodynamic formalism for field driven Lorentz gases, Phys. Rev. E **69**, 046203 (2004).

[18] H. van Beijeren, A. Latz, and J. R. Dorfman, Chaotic properties of dilute two- and three-dimensional random Lorentz gases: Equilibrium systems, Phys. Rev. E **57**, 4077 (1998).

[19] H. van Beijeren and J. R. Dorfman, Lyapunov exponents and KS entropy for the Lorentz gas at low densities, Phys. Rev. Lett. **74**, 4412 (1995).

[20] H. van Beijeren and J. R. Dorfman, A note on the Ruelle pressure for a dilute disordered Sinai billiard, J. Stat. Phys. **108**, 767 (2002).

[21] H. van Beijeren, Lyapunov exponents of the Lorentz gas with soft potentials, in preparation.

[22] H. A. Posch and R. Hirschl, Simulations of billiards and of hard body fluids, in D. Szasz, editor, *Hard Ball Systems and the Lorentz Gas*, volume 101 of *Encyclopedia of Mathematical Sciences* (Springer-Verlag, New York, 2000).

[23] C. Dellago and H. A. Posch, Kolmogorov-Sinai entropy and Lyapunov spectra of a hard-sphere gas, Physica A **68**, 240 (1997).

[24] R. van Zon and H. van Beijeren, Front propagation techniques to calculate the largest Lyapunov exponent of dilute hard disk gases, J. Stat. Phys. **109**, 641 (2002).

[25] R. van Zon, H. van Beijeren, and C. Dellago, Largest Lyapunov exponent for many particle systems at low densities, Phys. Rev. Lett. **80**, 2035 (1998).

[26] R. van Zon, H. van Beijeren, and J. R. Dorfman, Kinetic theory of dynamical systems, in J. Karkheck, editor, *Proceedings of the 1998 NATO-ASI "Dynamics: Models and Kinetic Methods for Non-equilibrium Many-Body Systems"*, page 131 (Kluwer, Dordrecht, 2000).

[27] J.-P. Eckmann and O. Gat, Hydrodynamic Lyapunov modes in translation-invariant systems, J. Stat. Phys. **98**, 775 (2000).

[28] T. Taniguchi, C. P. Dettmann, and G. P. Morriss, Lyapunov spectra of periodic orbits for a many-particle system, Phys. Rev. E **68**, 747 (2003).

[29] T. Taniguchi and G. P. Morriss, Master equation approach to the conjugate pairing rule of Lyapunov spectra for many-particle thermostatted systems, Phys. Rev. E **66**, 066203 (2002).

[30] S. McNamara and M. Mareschal, On the origin of the hydrodynamic Lyapunov modes, Phys. Rev. E **63**, 051103 (2001).

[31] H. van Beijeren, J. R. Dorfman, H. A. Posch, and C. Dellago, The Kolmogorov-Sinai entropy for dilute gases in equilibrium, Phys. Rev. E **56**, 5272 (1997).

[32] S. Chapman and T. Cowling, *The Mathematical Theory of Non-uniform Gases* (Cambridge University Press, 1970).

[33] J. O. Hirshfelder, C. F. Curtis, and R. B. Bird, *Molecular Theory of Gases and Liquids* (Wiley, New York, 1954).

[34] J. V. Sengers, D. T. Gillespie, and J. J. Perez-Esandi, Three-particle collision effects in the transport properties of a gas of hard spheres, Physica A **90**, 365 (1978).

[35] A. S. de Wijn and H. van Beijeren, Goldstone modes in Lyapunov spectra of hard sphere systems, Phys. Rev. E **70**, 016207 (2004).

[36] J.-P. Eckmann, C. Forster, H. A. Posch, and E. Zabey, Lyapunov modes in hard-disk systems, nlin.CD/0404007.

[37] C. Forster and H. A. Posch, private communication.

[38] T. Taniguchi and G. P. Morriss, Boundary effects in the stepwise structure of the Lyapunov spectra for quasi-one-dimensional systems, Phys. Rev. E **68**, 026218 (2003).

[39] W. G. Hoover, H. A. Posch, C. Forster, C. Dellago, and M. Zhou, Lyapunov modes of two-dimensional many-body systems; soft disks, hard disks, and rotors, J. Stat. Phys. **109**, 765 (2002).

[40] C. Forster and H. A. Posch, Lyapunov modes in soft-disk systems, nlin.CD/0409019.

[41] H. L. Yang and G. Radons, Lyapunov instabilities of Lennard-Jones fluids, nlin.CD/0404027.

[42] G. Radons and H. L. Yang, Static and dynamic correlations in many-particle Lyapunov vectors, nlin.CD/0404028.

[43] J. Goldstone, Field theories with 'superconductor' solutions, Nuovo Cimento **19**, 154 (1961).

[44] M. H. Ernst and G. A. van Velzen, Long-time tails in lattice Lorentz gases, J. Stat. Phys. **57**, 455 (1989).

[45] S. P. Das and M. H. Ernst, Long-time tails in a Lorentz gas, Physica A **153**, 67 (1988).

[46] A. S. de Wijn and H. van Beijeren, The Lyapunov spectrum of the many-dimensional dilute random Lorentz gas, Phys. Rev. E **70**, 036209 (2004).

[47] Y. G. Sinai, Gibbs measures in ergodic theory, Russian Mathematical Surveys **27**, 21 (1972), reprinted in Y. G. Sinai, editor, *Dynamical Systems, a Collection of Papers* (World Scientific, Singapore, 1991).

[48] N. Simányi and D. Szász, Hard ball systems are completely hyperbolic, Annals of Mathematics **149**, 35 (1999).

[49] C. Dellago, H. A. Posch, and W. G. Hoover, Lyapunov instability in a system of hard disks in equilibrium and nonequilibrium steady states, Phys. Rev. E **53**, 1485 (1996).

[50] A. Cristanti, G. Paladin, and A. Vulpiani, *Products of Random Matrices in Statistical Physics* (Springer-Verlag, New York, 1993).

[51] A. S. de Wijn and H. van Beijeren, in preparation.

[52] T. Taniguchi and G. P. Morriss, Time-oscillating Lyapunov modes and autocorrelation functions for quasi-one-dimensional systems, nlin.CD/0404052.

[53] D. J. Searles, D. J. Evans, and D. J. Isbister, The number dependence of the maximum Lyapunov exponent, Physica A **240**, 96 (1997).

[54] G. T. Barkema and M. E. J. Newman, *Monte Carlo Methods in Statistical Physics* (Oxford University Press, Oxford, 1999).

[55] T. Taniguchi and G. P. Morriss, Localized behavior in the Lyapunov vectors for quasi-one-dimensional many-hard-disk systems, Phys. Rev. E **68**, 046203 (2003).

Samenvatting

Statistische mechanica is de tak van de theoretische natuurkunde die macroscopische eigenschappen beschrijft van systemen die uit veel deeltjes bestaan aan de hand van microscopische eigenschappen. Aan het eind van de negentiende eeuw werd door onder anderen Boltzmann, Maxwell en Gibbs de basis gelegd voor de statistische mechanica van systemen in evenwicht. Een belangrijk begrip uit de statistische mechanica is de Boltzmann-factor waarmee een kans kan worden toegekend aan elke evenwichtstoestand. Met het gereedschap van de statistische mechanica van evenwichtssystemen kunnen praktische berekeningen worden uitgevoerd voor een heel scala van systemen. Voor systemen uit evenwicht zijn veel minder van dit soort methoden beschikbaar.

Volgens de tweede hoofdwet van de thermodynamica neemt de entropie, een maat voor de wanorde van een systeem, toe. Veel-deeltjessystemen produceren entropie terwijl ze naar een evenwichtstoestand toe bewegen en gaan niet uit zichzelf terug naar een situatie uit evenwicht. In beginsel is elk klassiek fysisch systeem echter omkeerbaar. De omkeerbare microscopische dynamica heeft onomkeer macroscopisch gedrag tot gevolg, voor bijna alle beginvoorwaarden. Vaak is het echter niet haalbaar een fysisch systeem direct als microscopisch dynamisch systeem te behandelen omdat het grote aantal vrijheidsgraden berekeningen veel te gecompliceerd maakt. In de statistische mechanica wordt een verband gelegd tussen de dynamische, microscopische beschrijving van een systeem en de statistische, macroscopische beschrijving.

Ludwig Boltzmann leidde aan het eind van de negentiende eeuw de naar hem genoemde vergelijking af. De Boltzmann-vergelijking beschrijft de tijdsevolutie van de kansverdeling van deeltjes in plaats en snelheid. Ondanks de volledig omkeerbare, microscopische dynamica volgt uit de Boltzmann-vergelijking onomkeerbaar macroscopisch gedrag. In de afleiding van zijn vergelijking maakte Boltzmann gebruik van een aanname over de wanorde van systemen die uit veel deeltjes bestaan, de Stoßzahlansatz. Deze komt neer op een aanname over de begintoestand en het gedrag van het microscopische, dynamische systeem.

Dynamische eigenschappen, zoals ergodiciteit en chaos, zijn van invloed op het onomkeerbare macroscopische gedrag. De verbanden tussen dynamische sys-

temen en de statistische mechanica van niet-evenwichtssystemen zijn een bron van verhitte discussie, omdat ons begrip ervan nog zeer onvolledig is.

Chaos

Bij een meting is altijd sprake van een beperkte resolutie. Dit betekent dat van een fysisch systeem nooit de precieze begintoestand bekend is. Het systeem start in een beginpunt en beweegt vervolgens door de faseruimte, de ruimte van alle mogelijke toestanden. Voor veel systemen heeft onzekerheid in de beginvoorwaarden tot gevolg dat alleen voor beperkte tijd zinvolle voorspellingen gedaan kunnen worden over hun evolutie. Een kleine onzekerheid in het beginpunt leidt na verloop van tijd tot een grote onzekerheid in het pad van het systeem door de faseruimte. Het traject van een knikker die met een aantal andere knikkers botst is moeilijk nauwkeurig te voorspellen, omdat een klein verschil in de richting van de beginsnelheid grote gevolgen heeft voor het verdere verloop. Een systeem met zulke gevoeligheid voor beginvoorwaarden noemen we chaotisch.

Beschouw bijvoorbeeld een eenvoudig dynamisch systeem met twee vrijheidsgraden, het tweedimensionale Lorentz-gas. Dit bestaat uit een verzameling vaste, bolvormige verstrooiers, waartussen een puntdeeltje beweegt dat elastisch met de verstrooiers botst. De faseruimte van dit systeem heeft vier dimensies, twee voor de positie en twee voor de snelheid. Twee verschillende paden met iets verschillende beginvoorwaarden zijn weergegeven in figuur 1.2. De paden divergeren exponentieel.

Het chaotische gedrag wordt gekwantificeerd door de Lyapunov-exponenten. Deze geven de mogelijke snelheden waarmee een infinitesimaal verschil in beginvoorwaarden exponentieel kan groeien of krimpen. De ruimte van mogelijke infinitesimale verstoringen van punten in de faseruimte wordt de raakruimte genoemd. Een systeem heeft evenveel Lyapunov-exponenten als de bijbehorende faseruimte dimensies heeft. Deze Lyapunov-exponenten kunnen allemaal verschillend zijn, maar vaak zijn een klein aantal exponenten aan elkaar gelijk. Ze worden vaak genummerd op volgorde van grootte. De verzameling van Lyapunov-exponenten van een systeem heet het Lyapunov-spectrum. Als een systeem minstens een positieve Lyapunov-exponent heeft, wordt het chaotisch genoemd. Voor meer informatie over chaos en dynamische systemen, zie referentie [5].

Als een chaotisch systeem waarvan de toestand met een vaste resolutie kan worden bepaald langere tijd wordt geobserveerd, dan wordt steeds meer bekend over de beginvoorwaarden. Twee punten in de faseruimte die eerst niet van elkaar konden worden onderscheiden, zijn na verloop van tijd verder van elkaar verwijderd, zodat meer informatie kan worden verkregen over de begintoestand door een systeem langer te observeren. De maximale snelheid waarmee informatie over het systeem toeneemt, wordt de Kolmogorov-Sinai-entropie genoemd. Voor ge-

sloten systemen is deze gelijk aan de som van de positieve Lyapunov-exponenten. Voor open systemen kan de Kolmogorov-Sinai-entropie daarboven vaak gerelateerd worden aan transportcoëfficiënten [7–10].

Veel systemen bezitten een aantal Lyapunov-exponenten die nul zijn. Deze horen bij eenvoudige verstoringen die niet exponentieel groeien, zoals uniforme translaties, of Galilei-transformaties, die alleen lineair toenemen. Zulke verstoringen worden "zero modes" genoemd en kunnen altijd geassocieerd worden met symmetrieën zoals bijvoorbeeld translatiesymmetrie, Galilei-invariantie, tijdstranslatie-invariantie of energieherschaling.

Veel deeltjes en veel vrijheidsgraden

Het eerder genoemde Lorentz-gas wordt vaak gebruikt voor het bestuderen van systemen uit evenwicht. Het Lorentz-gas is een dynamisch systeem dat door het lage aantal vrijheidsgraden en de eenvoudige vorm van de verstrooiers toch hanteerbaar is. Ook met allerlei toevoegingen, zoals krachtvelden of extra potentialen, is het veelal mogelijk om berekeningen uit te voeren [11, 15–17, 21]. De verstrooiers kunnen in een regelmatig rooster worden geplaatst, of op willekeurige posities. Een essentieel verschil tussen veel-deeltjessystemen en het Lorentz-gas is het aantal tijdsafhankelijke vrijheidsgraden.

Een veel-deeltjessysteem heeft een groot aantal Lyapunov-exponenten, in tegenstelling tot het Lorentz-gas, dat in twee dimensies slechts een en in drie dimensies twee positieve exponenten heeft. Het totaal aantal Lyapunov-exponenten van een veel-deeltjessysteem is evenredig met het aantal deeltjes. Op het Lyapunov-spectrum van veel-deeltjessystemen zijn effecten van invloed die nooit kunnen voorkomen in de spectra van laagdimensionale systemen. Om het chaotische gedrag van systemen met veel vrijheidsgraden uit evenwicht te begrijpen is het van essentieel belang een volledig begrip te verkrijgen van de effecten die van invloed zijn op veel-deeltjessystemen in evenwicht. In dit proefschrift worden berekeningen beschreven aan drie verschillende systemen in evenwicht met veel vrijheidsgraden.

Alle drie de systemen hebben een harde potentiaal. Dat wil zeggen, ze bestaan uit harde deeltjes die elastisch met elkaar of met harde sferische of cilindrische verstrooiers botsen. De dynamica van zulke botsingen is veel eenvoudiger dan de dynamica van zachte potentialen. Bovendien sluiten deze potentialen simultane interacties tussen drie deeltjes uit. Dit maakt berekeningen veel eenvoudiger. Voor lage dichtheden komt het gedrag van systemen met harde potentialen redelijk overeen met dat van systemen met zachte potentialen.

In hoofdstuk 2 wordt, als voorbereiding op de rest van het proefschrift, de dynamica van de harde interactie uitgewerkt. Ook wordt de Boltzmann-vergelijking afgeleid voor systemen van harde bollen.

Bewegende harde bollen

In hoofdstukken 3 en 4 worden systemen behandeld van veel vrije, elastisch botsende, harde bollen in twee en drie dimensies. Eerder werden berekeningen gedaan aan de grootste Lyapunov-exponenten van zulke systemen [6, 25]. Uit die berekeningen, en uit simulaties [55], blijkt dat de verstoringen die horen bij de grootste Lyapunov-exponenten gedragen worden door een klein aantal deeltjes. In de rest van het spectrum worden de verstoringen juist door meer deeltjes gedragen.

Uit simulaties van zulke systemen met verschillende randvoorwaarden is gebleken dat het Lyapunov-spectrum in het gebied van de kleine exponenten interessant gedrag vertoont [22, 23, 36]. Er is de laatste jaren daarom veel aandacht geweest voor deze exponenten. De kleinste exponenten in absolute waarde vertonen een stapstructuur als gevolg van ontaarding. Bij vaste dichtheid, temperatuur en vorm zijn de kleinste positieve en negatieve exponenten omgekeerd evenredig met de grootte van het systeem, voor voldoende grote systemen. De bijbehorende verstoringen hebben een zeer suggestieve golfvormige afhankelijkheid van de plaats. Ze komen, per golfvector, voor in groepen van zes in twee dimensies en acht in drie dimensies. Per golfvector kunnen ze weer worden onderscheiden in twee respectievelijk vier transversale modes en vier longitudinale modes.

In hoofdstuk 3 [35] wordt beschreven hoe deze exponenten gezien kunnen worden als Goldstone-modes. Goldstone-modes doen zich voor wanneer een continue symmetrie, zoals bijvoorbeeld een van de symmetrieën die geassocieerd worden met de zero modes, spontaan wordt gebroken. Vanuit dit uitgangspunt worden deze exponenten in hoofdstuk 3 benaderd via kinetische theorie. Daarvoor wordt een gegeneraliseerde Boltzmann-vergelijking afgeleid, die niet alleen de plaats en snelheid van een deeltje bevat, maar ook de verstoring hiervan op een baan met infinitesimaal verschillende beginvoorwaarden. De oplossingen hiervan geven de kleinste exponenten en de bijbehorende verstoringen.

Het blijkt echter dat de Stoßzahlansatz in dit geval niet volstaat, zelfs niet in de limiet dat de dichtheid naar nul gaat. Voor de Lyapunov-exponent van de transversale mode en de voortplantingssnelheid van de longitudinale mode zijn de resultaten van de Boltzmann-vergelijking goed in de limiet van lage dichtheid, maar voor de Lyapunov-exponent van de longitudinale mode wijkt de uitkomst 25% af van de resultaten uit simulaties. Dit is erg verrassend, aangezien voor de berekening van veel grootheden, zoals bijvoorbeeld transportcoëfficiënten, de Boltzmann-vergelijking volstaat in leidende orde. De reden waarom in dit geval de door de Stoßzahlansatz verwaarloosde effecten van ringbotsingen kunnen bijdragen wordt beschreven in sectie 3.7. Het zou zeker interessant zijn om de berekeningen van de exponenten die bij de Goldstone-modes horen uit te breiden door deze effecten mee te nemen, maar de vraag is of dit haalbaar is.

In hoofdstuk 4 wordt de Kolmogorov-Sinai-entropie van het zelfde systeem berekend. In eerdere berekeningen [31] was de leidende, logaritmische, term in de dichtheidsontwikkeling al berekend. De constante termen die daar nog bij

komen, en waar geen verdere benaderingen voor nodig leken, kwamen echter niet overeen met de resultaten uit simulaties. Zowel in de eerdere berekening als in de berekening in hoofdstuk 4 wordt gebruik gemaakt van de "stretching factor." Deze geeft de totale exponentiële oprekking van de raakruimte voor lange tijden.

In de berekening wordt duidelijk waar de problemen met de constante termen vandaan komen. In de lage-dichtheidsbenadering uit referentie [31] wordt een gedeelte van de voorgeschiedenis van de deeltjes verwaarloosd. In hoofdstuk 4 wordt uitgelegd hoe dit probleem technisch opgelost kan worden. De resultaten van de berekening komen dan ook beter overeen met de simulaties.

Hoogdimensionaal Lorentz-gas

Het kleine aantal vrijheidsgraden is niet de enige eigenschap die het Lorentz-gas zo handelbaar maakt. Ook de sferische vorm van de verstrooiers maakt veel berekeningen eenvoudiger. Zo voorkomt die bijvoorbeeld de problemen met de benadering voor lage dichtheid, die voor harde-bollengassen moeilijkheden oplevert met de constante termen in de Kolmogorov-Sinai-entropie. Gezien de zeer technische berekeningen van hoofdstuk 4 is dit een zeer plezierige eigenschap van het Lorentz-gas. Ondanks de verschillen met veel-deeltjessystemen, is het interessant om het Lorentz-gas in een situatie te beschouwen waarin het veel vrijheidsgraden heeft die elkaar beïnvloeden. De faseruimte van veel-deeltjessystemen kan beschreven worden als een hoogdimensionale ruimte met daarin cilindervormige verstrooiers met specifieke posities en oriëntaties. Vanuit het oogpunt van dynamische systemen lijken het hoogdimensionale Lorentz-gas en systemen van veel deeltjes veel op elkaar.

In hoofdstuk 5 [46] wordt het volledige Lyapunov-spectrum van een random, homogeen Lorentz-gas bij lage dichtheid in een willekeurig aantal dimensies berekend. In deze berekening wordt hier een "partial stretching factor" ingevoerd. Deze geeft de oprekking aan van een p-dimensionaal oppervlakje in de raakruimte. Voor lange tijden wordt deze oprekking gedomineerd door de p grootste Lyapunov-exponenten. Dankzij de homogeniteit en de isotropie van de verdeling van de verstrooiers is het mogelijk om bij lage dichtheid uit de "partial stretching factors" de Lyapunov-exponenten te berekenen.

De resultaten van deze berekening kunnen worden vergeleken met de Lyapunov-spectra van veel-deeltjessystemen. Beide spectra zijn steiler bij de grootste exponent en vlakken af in de buurt van de kleinste exponent. Het spectrum van het Lorentz-gas wordt echter vlakker naarmate het aantal dimensies toeneemt, terwijl de spectra van veel-deeltjessystemen dezelfde vorm houden. Dit is het gevolg van de vorm van de verstrooiers. Het is ook interessant om op te merken dat de grootste exponent in gedrag kwalitatief verschilt van de op een na grootste. Verder kunnen de Goldstone-modes die in hoofdstuk 3 worden beschreven, niet voorkomen in het Lorentz-gas, door de homogeniteit van de faseruimte.

Cilindrische verstrooiers

Het is zinvol om een systeem te onderzoeken dat ergens tussen de twee systemen inzit, zodat de technieken die voor het Lorentz-gas geschikt zijn gedeeltelijk bruikbaar blijven, terwijl de dynamica toch meer weg heeft van die van een harde-bollensysteem. In hoofdstuk 6 worden daarom systemen onderzocht met cilindrische verstrooiers die homogeen en isotroop zijn verdeeld. Deze zijn wel onderhevig aan de problemen die worden beschreven in hoofdstuk 4.

Uit de gedane simulaties van zulke systemen blijkt dat de Lyapunov-spectra van homogeen en isotroop verdeelde (hyper)cilinders veel meer lijken op die van harde bollen dan de spectra van het hoogdimensionale Lorentz-gas. Omdat de verstoringen die bij de grootste exponenten horen in harde-bollensystemen slechts door een beperkt aantal deeltjes worden gedragen, is er bij de grootste exponenten wel een duidelijk kwalitatief verschil tussen de twee systemen. Voor de kleinere exponenten, met uitzondering van die van de Goldstone-modes, die bij de cilinders niet voorkomen, is het verschil louter kwantitatief, niet meer dan 15%.

Met deze informatie wordt het erg interessant om een hybride berekening uit te voeren die gebruik maakt van "partial stretching factors." Deze worden afgeleid uit de "stretching factor" berekend in hoofdstuk 4. Daarbij wordt voor het bereken van de Lyapunov-exponenten op grond van de "partial stretching factors" een isotrope benadering gebruikt. Een opzet van deze berekening wordt in hoofdstuk 6 gegeven. Daar worden de kleinste Lyapunov-exponenten van een dergelijk systeem geschat en vergeleken met de corresponderende exponenten van het equivalente harde-bollensysteem. Beide hangen op dezelfde manier af van de botsingsfrequentie, met een voorfactor die niet meer dan 20% verschilt.

Conclusies

De berekeningen die in dit proefschrift worden beschreven versterken alle het begrip van chaos in systemen met meerdere vrijheidsgraden. Vooral in hoofdstuk 3 en 5 worden nieuwe technieken ontwikkeld om de Lyapunov-exponenten van zulke systemen analytisch uit te rekenen. In hoofdstuk 4 worden vooral technische problemen met eerdere berekeningen opgelost. De simulaties en berekeningen in hoofdstuk 6 verschaffen inzicht in de vorm van het onderste stuk van de "continuum"-spectra van veel-deeltjessystemen. Het zou interessant zijn om de benadering uit hoofdstuk 6 toe te passen op het hele onderste gedeelte van het Lyapunov-spectrum van harde bollen, in plaats van alleen op de kleinste exponenten.

Een ander interessant aspect van het spectrum van harde bollen is een overgang tussen exponenten waarvan de verstoringen door weinig deeltjes worden gedragen en die waarvan de verstoring door veel deeltjes wordt gedragen. Hoe deze overgang precies tot stand komt en hoe de exponenten boven de overgang zich gedragen is, behalve voor de grootste, nog niet duidelijk.

Dankwoord

Allereerst wil ik graag mijn promotor, Henk van Beijeren, bedanken, zonder wiens begeleiding en ondersteuning dit proefschrift nooit tot stand was gekomen. Zijn zorgvuldige manier van werken en kritische houding zijn erg belangrijk geweest voor de kwaliteit van het onderzoek dat in dit proefschrift wordt beschreven. I would like to thank Bob Dorfman, Harald Posch, and Christina Forster. Ik heb bovendien veel gehad aan de persoonlijke en wetenschappelijke adviezen van Gerard Barkema en Mathieu Ernst. Ook bedank ik Hans Weda en Wessel Dankers voor hun praktische hulp bij het schrijven van mijn proefschrift.

Op het persoonlijke vlak dank ik veel aan mijn ouders, Harold en Anna, mijn broer, Alfred, en mijn vriend, Guus. Zij hebben me met raad en daad bijgestaan.

Tenslotte hebben mijn vrienden en (ex-)collega's voor de nodige afleiding gezorgd. Mede dankzij de gezellige sfeer op het Instituut voor Theoretische Fysica bestaat tussen die twee groepen een flinke overlap.

Curriculum Vitae

De auteur van dit proefschrift is geboren op 28 september 1979 in De Bilt. Tussen 1990 en 1996 ging zij naar het Stedelijk Gymnasium Johan van Oldenbarnevelt in Amersfoort. In 1995 en 1996 werd ze, na deelname aan de Nationale Natuurkunde Olympiade, uitgezonden naar de Internationale Natuurkunde Olympiade in Canberra en Oslo, waar ze een eervolle vermelding en een bronzen medaille won.

In 1996 begon ze aan de studies Natuurkunde en Wiskunde aan de Universiteit Utrecht. Op 29 augustus 1997 haalde ze voor beide het propedeutisch examen, cum laude. Tijdens haar studie heeft ze als student-assistent gewerkt bij de eerstejaars werkcolleges, het eerstejaars practicum en het derdejaars vak Voortgezette Klassieke Mechanica. Na een scriptie te hebben geschreven over Randall-Sundrum Compactificatie bij Prof. Dr. E. P. Verlinde in het Spinoza Instituut, legde ze op 17 april 2000 haar doctoraal examen Theoretische Natuurkunde af.

Daarna, op 1 juni 2000, begon ze als onderzoeker in opleiding in dienst van de Stichting voor Fundamenteel Onderzoek der Materie (FOM), onder begeleiding van Prof. Dr. Henk van Beijeren in het Instituut voor Theoretische Fysica in Utrecht. Op 16 augustus 2001 haalde ze haar doctoraal examen Wiskunde. In het kader van haar onderwijstaak heeft ze bij de werkcolleges van een aantal vakken geassisteerd, namelijk Voortgezette Klassieke Mechanica, Thermische en Statistische Fysica 2, Theorie van de Vaste Stof en Mechanica 2.

De auteur heeft tijdens haar promotieonderzoek deelgenomen aan conferenties en zomerscholen in onder andere Wenen, Altenberg, Dresden, Polen, Brussel, Rutgers University en College Park. Ze heeft voordrachten gegeven in onder andere Dresden, Wenen, Brussel en Lyon.